

Biodegradable amphiphilic PEG-PCL-PEI triblock
copolymers designed for the self-assembly of
multifunctional gene carriers

Dissertation

zur

Erlangung des Doktorgrades

der Naturwissenschaften

(Dr. rer. nat.)

dem Fachbereich Pharmazie (FB 16)

der Philipps-Universität Marburg

(Hochschulkenziffer 1180)

vorgelegt von

Dipl.-Chem. Thomas Karlheinz Endres

aus Dettelbach

Marburg/Lahn, 2012

Erstgutachter:
Zweitgutachter:

Prof. Dr. Thomas Kissel
Prof. Dr. Andreas Greiner

Tag der Einreichung:
Tag der mündlichen Prüfung:

16.10.2012
07.12.2012

Die vorliegende Arbeit entstand auf Anregung und unter Leitung von

Prof. Dr. Thomas Kissel

am Institut für Pharmazeutische Technologie und Biopharmazie der
Philipps-Universität Marburg.

Contents

I	Gene therapy	9
1	Motivation	9
2	Carriers	9
3	Permanent and transient gene therapy approaches	11
4	Hurdles for <i>in vivo</i> usage	13
4.1	Systemic hurdles	13
4.1.1	Administration	13
4.1.2	Targeting	13
4.1.3	Endothelium	13
4.1.4	Immune response and “stealth” properties	14
4.2	Cellular hurdles	15
4.2.1	Cell membrane	15
4.2.2	Endosome	16
4.2.3	Cytosol	17
4.3	Issues arising from cationic surface charge	17
4.3.1	Carrier loading via electrostatic interaction	17
4.3.2	Colloidal stability	18
4.3.3	Cell uptake and cytotoxicity	19
4.3.4	Balance of positive charges	19
5	Evolution of non-viral delivery systems	19
5.1	Homopolymers	20
5.2	Hydrophilic modification	23
5.3	Hydrophobic modification leading to amphiphilic block copolymers	23
5.3.1	Employed hydrophobic polymers	27
5.3.2	Self organisation	27
5.4	Multifunctional carriers	29
5.4.1	“Theranostics”	29
5.4.2	Fluorescence resonance energy transfer (FRET)	30
5.4.3	Stimuli responsive systems	31
6	Aims and objectives	32

II Self-assembled biodegradable amphiphilic PEG-PCL-IPEI triblock copolymers at the borderline between micelles and nanoparticles designed for drug and gene delivery	35
Abstract	36
1 Introduction	37
2 Materials and methods	38
2.1 Reagents and chemicals	38
2.2 Synthesis	39
2.3 Basic polymer characterisation	40
2.3.1 NMR	40
2.3.2 FT-IR	40
2.3.3 Gel permeation chromatography (GPC)	40
2.3.4 Differential scanning calorimetry (DSC)	40
2.3.5 Cu ²⁺ -assay	41
2.3.6 Critical micelle concentration (CMC)	41
2.4 Assembly of nano-carriers from triblock copolymers	41
2.5 Characterisation of nano-carriers	42
2.5.1 Size and ζ -potential	42
2.5.2 Fixed aqueous layer thickness (FALT)	42
2.5.3 Atomic force microscope (AFM)	42
2.5.4 Cryogenic scanning electron microscope (cryoSEM)	43
2.5.5 Structure elucidation via ¹ H NMR spectroscopy	43
2.5.6 Analysis of colloidal stability	43
2.5.7 Cytotoxicity in HeLa-Luc cells (MTT assay)	44
3 Results	44
3.1 Synthesis and characterisation	44
3.2 Carrier size and assembly mechanism	50
3.3 PEG shell thickness measurements	52
3.4 Structure elucidation using ¹ H NMR techniques	54
3.5 Analysis of stability	57
3.6 Cytotoxicity assay	60
4 Discussion	61
5 Conclusions	66

Acknowledgments	67
III Optimising the self-assembly of siRNA loaded PEG-PCL-IPEI nano-carriers employing different preparation techniques	68
Abstract	69
1 Introduction	70
2 Materials and methods	71
2.1 Reagents and chemicals	71
2.2 Polymer synthesis and characterisation	72
2.3 Cu ²⁺ -assay	72
2.4 Assembly of unloaded nano-carriers	72
2.5 Carrier loading by different techniques	73
2.6 Cryogenic transmission electron microscopy (cryoTEM)	73
2.7 Size and ζ -potential	73
2.8 Stability	74
2.9 RNase assay in presence of heparin	74
2.10 RT-PCR	75
2.11 Response surface design	75
2.12 Statistics	75
3 Results and discussion	76
3.1 Aggregation behaviour as a function of N/P	76
3.2 Different loading techniques	78
3.3 Comparison of classical pipetting and microfluidic mixing	79
3.4 Statistical analysis of the microfluidic mixing technique	85
4 Conclusions	89
Acknowledgments	90
IV Lyophilised ready-to-use formulations of PEG-PCL-PEI nano-carriers for siRNA delivery	91
Abstract	92

1	Introduction	93
2	Materials and methods	94
3	Results and discussion	95
4	Conclusions	100

V	Amphiphilic and biodegradable PEG-PCL-PEI triblock-copolymers for dual delivery of siRNA and quantum dots: <i>in vitro</i> and <i>in vivo</i> investigation of a FRET capable carrier system	101
----------	---	------------

	Abstract	102
--	-----------------	------------

1	Introduction	103
----------	---------------------	------------

2	Material and methods	105
----------	-----------------------------	------------

2.1	Reagents and chemicals	105
-----	----------------------------------	-----

2.2	Polymer synthesis and characterisation	105
-----	--	-----

2.3	Assembly of nano-carriers	106
-----	-------------------------------------	-----

2.4	QD loading of nano-carriers	106
-----	---------------------------------------	-----

2.5	Complexation of nano-carriers with siRNA	106
-----	--	-----

2.6	Size measurements	107
-----	-----------------------------	-----

2.7	<i>In vitro</i> experiments	107
-----	---------------------------------------	-----

2.7.1	Cellular uptake	107
-------	---------------------------	-----

2.7.2	Transfection efficiency	107
-------	-----------------------------------	-----

2.7.3	Confocal laser scanning microscopy	108
-------	--	-----

2.8	<i>In vivo</i> experiments	108
-----	--------------------------------------	-----

2.9	Fluorescence spectra	109
-----	--------------------------------	-----

2.10	SYBR TM Gold assay	110
------	---	-----

3	Results and discussion	110
----------	-------------------------------	------------

4	Conclusions	120
----------	--------------------	------------

VI Summary	122
Zusammenfassung	125
VII Perspectives	131
Ausblick	132
References	134
<i>Appendices</i>	150
List of figures	152
List of tables	153
List of commonly used abbreviations	154
List of publications	157
In a nutshell	158
Übersicht	159
<i>Curriculum vitæ</i>	162
Danksagung	163
Erklärung	164

Part I

Gene therapy

1 Motivation

A broad group of acquired or inherited fatal diseases such as immunodeficiency syndromes, cystic fibrosis or some types of cancer are ultimately caused by gene defects and to date the vast majority of those can only be treated in a symptomatic manner. The idea of “simply” replacing defective or adding missing genes has been around for a couple of decades, but it finally found serious attention with the information explosion in DNA technology as well as the ability to transfer and express genes in mammalian cells [1]. Gene therapy, introducing nucleic acids into cells, is supposed to provide serious benefit by directly influencing genetic material as compared to conventional non-causal therapies. Genes that are missing owing to a genetic mutation could be complemented to supply a vital protein. Unwanted genes could be blocked by the introduction of a counteracting one. Distinct cells may be selectively destroyed via suicide strategies [2]. Furthermore, antisense routes offer the opportunity to selectively down-regulate the expression of specific genes on the translational level by sequence specific interaction with messenger RNA (mRNA). Especially in cancer treatment novel therapeutic scopes, exhibiting high selectivity plus low toxicity, are urgently needed to so replace/support classical chemo-therapeutics and radiation therapy.

2 Carriers

Due to their inability to enter negatively charged cells and due to enzymatic degradation, nucleic acids require formulations for a successful gene therapy approach. Therefore, the idea of gene carriers is conceptually simple: So-called vectors are responsible for packaging, protection and cell internalisation of genetic drugs.

Generally, two different carrier approaches have been utilised, namely viral and non-viral ones. Viruses have evolved efficient mechanisms to enter cell and nucleus and therefore impress by their cell specificity and their efficiency to internalise genetic material into host cells. Researchers tried to “tame” viruses for exploiting

their properties. However, in recent years, a rethinking occurred, mainly due to severe safety concerns (such as high immunogenicity after repeated administration or potential oncogenicity due to insertional mutagenesis). Non-viral vectors, using cationic polymers and lipids, are generally regarded as superior in terms of safety and furthermore offer virtually unlimited loading capacity [3]. Cationic polymers such as polyethyleneimine (PEI) are the ideal candidates to serve as nucleic acid carriers, due to their ability to condense nucleic acids to nano-scaled complexes. Electrostatic interaction of polycationic carrier polymers and polyanionic nucleic acids lead to the formation of complexes, often referred to as “polyplexes”. Those protect the genetic cargo from nuclease-induced degradation and enable cell interaction (Figure I.1). Cationic polymers are comparatively easy to manufacture on an industry level (and in good manufacturing practice) with tailored chemical functionalities and versatile physicochemical properties. Nevertheless, limited transfection efficiency commonly remains a major drawback of many non-viral approaches. Another important challenge will be to reduce the toxicity induced by cationic charges. Although remarkable advances have been made *in vitro*, *in vivo* applications are still scarce [1]. Nevertheless, polymeric delivery systems do have the potential to surpass their viral counterparts, if those limitations could be overcome. Perhaps novel chemical design strategies along with a better understanding in structure activity relationships may help to overcome those issues.

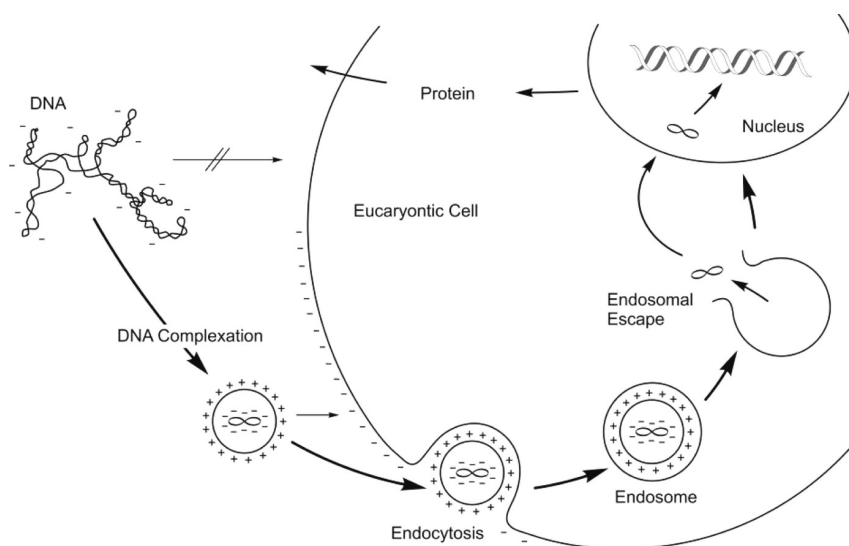


Figure I.1: Vector mediated internalization of DNA [4]

3 Permanent and transient gene therapy approaches

Originally gene therapy was designed to treat inherited diseases, such as the deficiency of a specific gene. Therefore, it was the goal to deliver plasmid DNA (pDNA) into the nucleus of a defective cell to express the resulting transgene. Depending on the vector, DNA either integrates into the host genome or exists as an episomal vector. Therefore, the resulting transfection can either be permanent or transient [1]. Stable lifelong expression, on one hand, has the potential to ultimately “cure” inherited diseases caused by a monogenic defect (e.g. in case of cystic fibrosis, haemophilia or familial hypercholesterolemia [3]). On the other hand, altering the host genome causes safety concerns: in case of intolerance or side effects there is no possibility of intervention and also re-administration is barely feasible. By contrast, transient gene therapy lasts for a couple of days or weeks (depending on the rate of cell division) and the dose can be adjusted more easily. Additionally, for acquired diseases like infection or cancer, permanently altering the patient’s genome is often not desirable and drugaction is therefore supposed to be a transient one. [5]

The discovery of RNA interference (RNAi) techniques enabled a new scope of transient gene therapy at the post-transcriptional messenger RNA (mRNA) level. This involves the delivery of short (21-25 base pairs) nucleic acid fragments, e.g. small interfering RNA (siRNA) instead of high molecular weight DNA plasmids (up to 100 000 base pairs). This new therapeutic pathway allows to temporarily down-regulate the expression of virtually any gene of interest by administration of tailor made synthetic oligonucleotides. Whereas pDNA needs to be introduced into the nucleus, the site of action for siRNA is the cytosol. There, siRNA is loaded into the so-called “RNA-induced silencing complex” (RISC) (Figure I.2). After cleavage of one strand, the residual one guides the RISC to its complementary sequence of mRNA and endonuclease enzymes of the RISC sequence-specifically cleave a distinct mRNA region. The degraded mRNA is subsequently no longer available for translation, leading to a transient down-regulation of the corresponding protein (knock-down). [6]

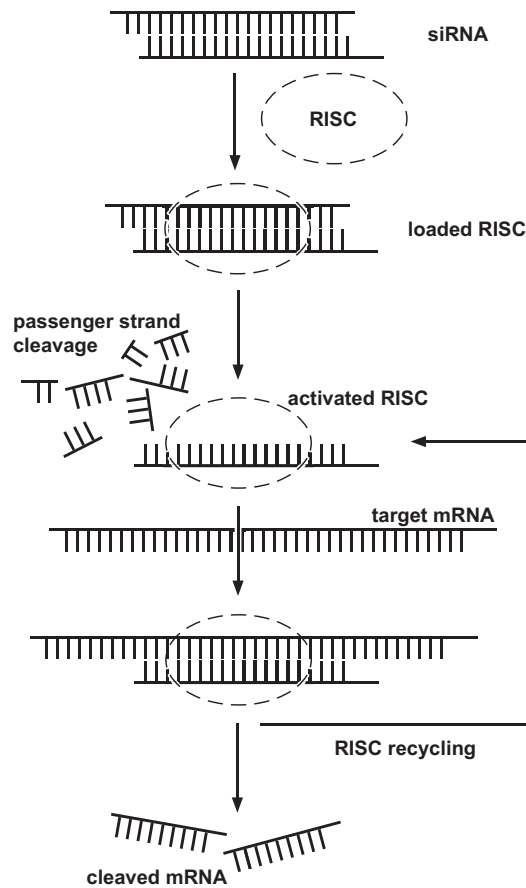


Figure I.2: Steps in the RNAi process: siRNA gets loaded onto the RISC, followed by the formation of an activated RISC containing only one siRNA guide strand. The activated RISC is subsequently guided to its complementary mRNA sequence. After region specific mRNA cleavage, RISC gets recycled to carry out additional silencing loops.

DNA and siRNA generally share many common properties: They are both double stranded nucleic acids with a negatively charged phosphodiester backbone. As the packaging of cationic non-viral delivery systems is based on electrostatic interaction, delivery of DNA or siRNA is generally feasible using quite similar vectors. However, there may be a need to adapt carrier properties to fulfil the needs of the respective payload. As compared to DNA, siRNA shows a longer persistence length, making it a stiffer molecule. Hence, despite the lower molecular weight, siRNA is generally harder to condense by cationic agents [6]. This may lead to undesirable large and unstable complexes and makes colloidal stability of carriers even more important. Furthermore, the ribose functionalities make RNA more susceptible to hydrolysis and degradation by serum nucleases than DNA (containing deoxyribose residues) [6]. This further exacerbates the need of an intelligently designed protective carrier for delivery of siRNA.

4 Hurdles for *in vivo* usage

Despite the tremendous promises of gene therapy, there are (especially *in vivo*) numerous obstacles to overcome for a successful therapeutic application.

4.1 Systemic hurdles

4.1.1 Administration

The first question that has to be addressed when dealing with nucleic acid drugs is a suitable way of administration. On one hand, this can be done by loco-regional administration, such as direct tissue injection or by inhalation for treating airway diseases. For the latter the respiratory mucus layer represents an additional barrier [4]. In case of direct injection into a tumour, the low extent of diffusion throughout the tissue limits the applicability. On the other hand, systemic delivery by intravenous injection represents a more desirable approach, in turn presenting further issues.

4.1.2 Targeting

Once systemically administered, therapeutics undesirably tend to accumulate in tissues and organs such as lung, liver, spleen or kidney. Therefore, to enable therapeutic levels of transgene expression and to avoid side effects, carriers have to be taken up by the target tissue in a selective way. Ultimately, the ideal vector is supposed to be cell type specific, which can be achieved, up to a certain degree, via targeting ligands. Utilising receptor mediated uptake mechanisms has the potential to dramatically decrease nonspecific interaction with healthy cells and body tissues plus increasing drug concentrations at the target site. One promising example is the folic acid receptor; whereas there are high expression levels in some types of cancer cells, expression is comparatively low in normal tissue [7, 8]. Transferrin [9, 10] or epidermal growth factor (EGF) [11] represent other potent ligands which have been widely employed for tumour targeting.

4.1.3 Endothelium

But even in absence of homing ligands, there is a chance for nano-scaled delivery systems to passively accumulate in solid tumours. Whereas the endothelial membrane is quite tight in most regions of the human body (except some organs such as liver, spleen or bone-marrow), cancer tissues often result in a leaky vasculature together with an impaired lymphatic drainage (Figure I.3) [3]. This may lead to a capture

of long-circulating carriers in the tumour interstitium, which is often referred to as the so-called enhanced permeation and retention (EPR) effect [12, 13, 14]. On one hand using this technique represents a way to pass the endothelial barrier. On the other hand, irregular distribution of carriers throughout the cancer tissue along with a diminished concentration towards the mass of the tumour [3] remains a major problem. Therefore, using actively targeted vector systems with additional benefit from the EPR effect appears to be a promising strategy [13].

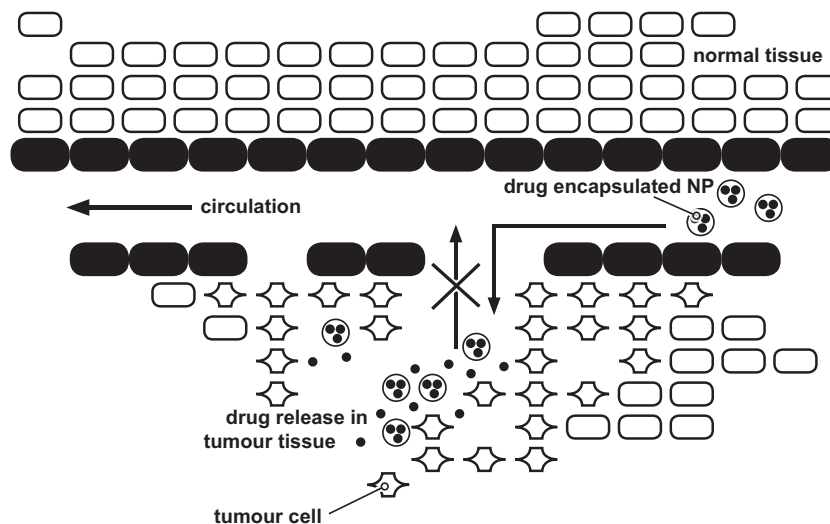


Figure I.3: Schematic illustration of the EPR effect

4.1.4 Immune response and “stealth” properties

The host immune response represents yet another hurdle in gene therapy. Even though non-viral delivery systems do not stimulate any antigen-dependent immunity as compared to viral approaches, unspecific activation of the host immune system becomes an issue for *in vivo* administration. Once systemically administered via intravenous injection, the mammalian immune system has developed effective strategies to eliminate non-innate invaders. This clearance process is mediated by interaction of carriers with components in the blood serum. Opsonin molecules (e.g. immunoglobulins or the C-reactive protein) are adsorbed onto the carrier’s surface, which renders them recognisable to the complement system. Tagged materials are subsequently cleared from the circulation e.g. via phagocytosis by macrophages (e.g. Kupffer cells in the liver) [15].

Modification of the carrier surface to hinder the adsorption of opsonins is a feasible method to diminish unspecific immune response. In this context surface chemistry, charge, structure and hydrophobicity are known to play an important role [15]. Hydrophobic surfaces are generally thought to be more prone to the opsonisation

process and a rapid removal of hydrophobic particles from the bloodstream as compared to their hydrophilic counterparts was previously demonstrated by Illum *et al.* [16]. Apart from that an unexpected increase of proinflammatory signalling was reported [17, 4]. Polyethylene glycol (PEG), covalently attached or adsorbed onto the carrier surface, is commonly employed for hydrophilic modification of carrier systems. PEGylated surfaces generally show reduced toxicity as well as prolonged circulation times *in vivo* [18, 19]. PEG's so-called "stealth" effect is owed to unique solution properties and molecular conformation in aqueous medium [15]. Hydrogen bonds between ether oxygens and water hydrogens lead to a hydrophilic water-like structure with highly mobile and flexible PEG polymer chains. Resulting surfaces are believed to repel approaching proteins due to a reduced interface. Covalent attachment of PEG, which typically involves the formation of block copolymers, was proven to be more effective in shielding the PEI charges than absorption of PEG onto the carrier surface [20]. Length and density of attached PEG chains were shown to have an effect on "stealth" properties [21, 22], whereas minimal chain-length between 1500-3000 Da is generally accepted as a prerequisite for the formation of a protective hydrogenated shell [15].

4.2 Cellular hurdles

Carriers that have survived degradation and clearance in the blood stream and have passed the endothelial of a target tissue, finally reach the cell membrane. But this is only half the way to successful gene therapy, as additional hurdles on the cellular level are to be overcome.

4.2.1 Cell membrane

Complexes with suitable surface properties were shown to be capable of traversing the cell membrane [3]. A size of approximately 150 nm [6] and a positive surface charge are generally accepted as prerequisites for cell interaction. Untargeted carriers bind electrostatically to the cell membrane and are typically internalised via passive (adsorptive) endocytosis. Alternatively, as mentioned above, ligand-decorated carriers are capable of active receptor mediated endocytosis; ligands specifically bind to receptors on the surface of distinct cells, which triggers an internalisation signal. Receptor and ligand are then clustered into coated pits and enter the cell very effectively [23].

4.2.2 Endosome

Independent from the mechanism of endocytosis, carriers are subsequently located in vesicular structures, so-called endosomes. Those invariably follow the same pathway leading from the early to the late endosome, ultimately ending up in the lysosomal compartment. In the course of this cellular trafficking an influx of protons leads to a decrease in pH from 7 to approximately 5. The resulting ion gradient in turn leads to an influx of chloride ions, thereby increasing the osmolality inside the endosome/lysosome. A subsequent influx of water finally results in overpressure and rupture of the lysosomal membrane [24]. However, prior to this, due to prevailing aggressive nucleases and decreasing pH values, nucleic acids inside the endosome are typically digested and therefore need to be protected and previously released into the cytosol in order to be effective [3]. The prime importance of endosomal protection for gene delivery efficiency was demonstrated by addition of chloroquine, which represses endosomal degradation and therefore leads to increased transfection efficiency [24].

Viruses have developed effective ways to escape from the endosome. For non-viral approaches one potential way of escape, which has been hypothesised for polyamine carriers with different degrees of protonation (such as PEI or some dendrimers), is commonly referred to as the “proton sponge” effect (Figure I.4). Carrier’s amine functionalities accept inflowing protons due to a buffering capacity in the respective pH-range. This leads to stable pH values and hinders nucleic acid degradation. An influx of chloride ions and water into the buffered endosome finally facilitates nucleic acid release through overpressure induced rupture of the vesicular membrane [24, 25]. However, apart from the proton sponge hypothesis, alternative ways of endosomal escape via electrostatic induced membrane fusion [26, 27] or disruption [28, 6] have been discussed in literature.

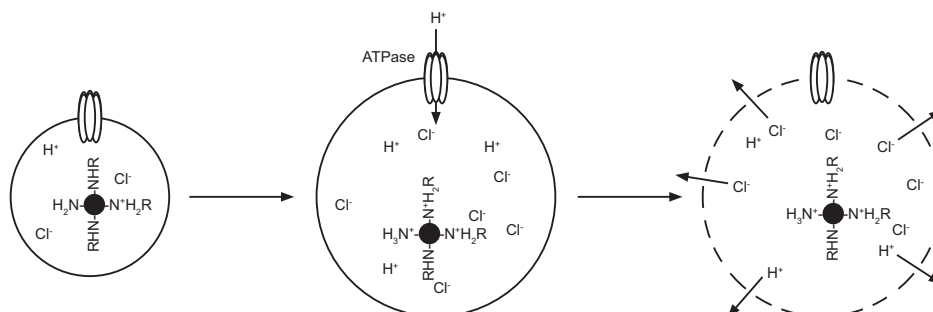


Figure I.4: Schematic illustration of the proton sponge mechanism: functionalities on the carrier accept protons streaming into the endosomal vesicle. An influx of chloride counter ions and water cause swelling and ultimately rupture of the endosomal membrane.

4.2.3 Cytosol

After release from the endosome, nucleic acids are located in the cytosol. In some cases nucleic acid and gene carrier are already disassembled at the time of endosomal release, for others the carrier complex is still intact [6]. In any case the cytosol is an destructive place for nucleic acids; the mobility of large molecules is extremely low and prevailing cytoplasmic nucleases favour digestion. For siRNA the cytosol is already the site of action. DNA, however, has to be transported into the nucleus to facilitate transgene expression. As transport into the nucleus typically occurs upon cell division, DNA has to be stable until the next disassembly during the next cell cycle. For RNA and DNA approaches, the carrier has to be tailor made in a way that provides sufficient protection via tight complexation. By contrast, the electrostatic interaction between nucleic acid and polycation must not be too strong, as this may lead to insufficient unpacking at the appropriate stage. Therefore, in order to be effective, a balance of complexation strength has to be adjusted to enable protection and release of genetic material at the right time [3, 6].

4.3 Issues arising from cationic surface charge

Whereas for the majority of non-viral delivery systems positive charges are absolutely necessary for complexation and delivery, they do have a downside regarding non-specific interaction and toxicity.

4.3.1 Carrier loading via electrostatic interaction

As stated previously, aside from encapsulation approaches, loading of most non-viral delivery systems is generally an electrostatically driven process and the cationic charge is therefore a prerequisite for interaction with nucleic acids. With surprising accuracy the complexation process of non-viral carrier and nucleic acid can be described by the classical DLVO (Derjaguin, Landau, Verwey, Overbeek) theory, with according implications on colloidal stability [29]. Upon carrier loading, the ratio of positively charged nitrogens (e.g. from PEI amine-functionalities) and negatively charged phosphates (from the backbone of nucleic acids), which is commonly referred to as the N/P ratio, is one of the most crucial factors for carrier stability, performance and toxicity. Figure I.5 exemplarily shows the charge of a PEI-based delivery system (manufactured in the course of this thesis) as a function of N/P. Despite various conditions upon complex preparation, complex formation is mainly driven by electrostatic interaction.

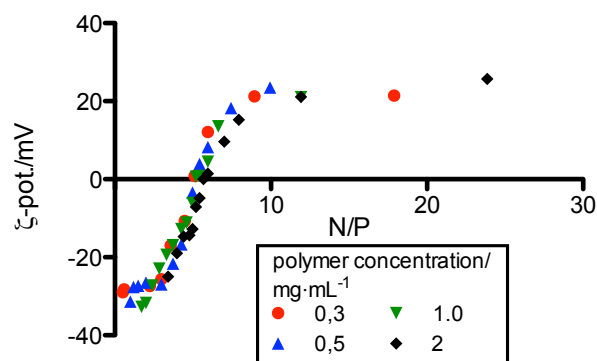


Figure I.5: Charge (ζ -potential determined via LDA) of cationic carrier (PEG500-PCL10k-PEI2500) upon complexation with siRNA ($100 \mu\text{M}$ solution) as a function of N/P. Despite changing polymer concentrations used for complexation, resulting carriers are mainly controlled by their electrostatic interaction. (Data collected from various experiments in the course of this thesis)

4.3.2 Colloidal stability

By design unloaded carriers bear a positive surface charge (with a ζ -potential of up to 50 mV), which (according to the DLVO theory) contributes to overall colloidal stability. Upon addition of negatively charged nucleic acids, there is a decline in surface charge (Figure I.5), which generally favours aggregation. This is one of the reasons why the N/P is typically chosen in a way that results in an excess positive surface charge (in most cases N/P-ratios of approximately 5 are employed [30]). However, carriers not only need to be stable in a sample vial, but also inside a medium of high ionic strength (such as blood serum). In such an environment salt ions and anionic proteins tend to shield the stabilising cationic functionalities of like-charged carriers. Therefore, exclusively charge-stabilised unmodified carriers exhibit tremendous problems, rendering them unlikely for *in vivo* application. First of all interaction with negatively charged serum components (e.g. albumin or fibronectin), erythrocytes or tissue membranes may occur. This was demonstrated recently for carrier-interaction with albumin, leading to the formation of large aggregates with inverted surface charge [3]. Those are known to be excluded from cellular internalisation altogether [6]. Additionally, unspecific interaction dramatically decreases circulation time [15] and ultimately leads to blockage of blood vessels accompanied by embolism (first of all in the lung). Actually, a direct correlation between the number of accessible surface charges and the amount of complement activation has been claimed [31]. Alternatively, apart from Coulomb repulsion, there is the opportunity of steric shielding via surface modification (e.g. by attachment of PEG moieties) to increase physical stability. This is believed to be the favourable

technique under physiological salt and polyelectrolyte concentrations. However, this may in turn have an adverse effect on cell uptake [32].

4.3.3 Cell uptake and cytotoxicity

Cationic surface charge increases the interaction with negatively charged cell membranes. Hence, one way to improve cell uptake may be to increase the carrier surface charge (as already mentioned above, another way may be utilising targeting ligands). At the same time, however, this will inevitably increase unwanted interactions with blood components and tissue membranes in an unspecific manner. As a result membrane damage and cell necrosis lead to increased toxicity both on cellular and systemic level [33].

4.3.4 Balance of positive charges

Consequently, colloidal stability and cell uptake ability on the one hand and toxicity and lack of specificity on the other hand have to be balanced. Targeting ligands and “stealth” properties through shielding moieties may help to conquer this dilemma. A thoroughly adjusted N/P ratio may further contribute to tailor the surface charge: lower N/P ratios generally lead to a decrease in toxicity due to decreased surface charges (similarly this may lead to a reduced efficiency as well). Furthermore, at lower N/P ratios less potentially toxic polymer is required to administer the same therapeutic amount of nucleic acid, which is also reducing overall toxicity. In the end a compromise between stability, efficiency and toxicity has to be found, typically ending up with a slightly positive surface charge in the order of a few mV.

5 Evolution of non-viral delivery systems

A major benefit of using unit-by-unit constructed cationic polymers as non-viral gene delivery vehicles is the possibility of straightforward modification using the tools of organic chemistry. Hence, from the beginning of non-viral gene delivery in the 1990s, constant evolution resulted in increasingly sophisticated delivery systems to tackle the above-described challenges in the course of the delivery process and meet the special needs of various host systems. The overall goal must be to manufacture delivery systems with “virus-like” high efficiency, specificity and low safety risks [3].

5.1 Homopolymers

Early gene vehicles were basically assembled from positively charged homopolymers. So far, various macromolecules such as PEI, poly(lysine), chitosan, poly((2-dimethylamino)ethyl methacrylate) (pDMAEMA) or several polysaccharides have been used for complexation of nucleic acids. Apart from that, amine bearing dendrimers, such as poly(amidoamine) (PAMAM) have been reported (Figure I.6). Positive charges typically arise from protonation of primary and secondary amines. These amine functionalities trigger complexation with nucleic acids, are capable of accepting protons for buffering the endosome, and additionally are strong nucleophiles, which can also be further employed for coupling of targeting ligands or functional groups. Tertiary amines (e.g. included in branched PEIs) are less nucleophilic, but may be helpful for further buffering the endosomal compartment after endocytosis [34].

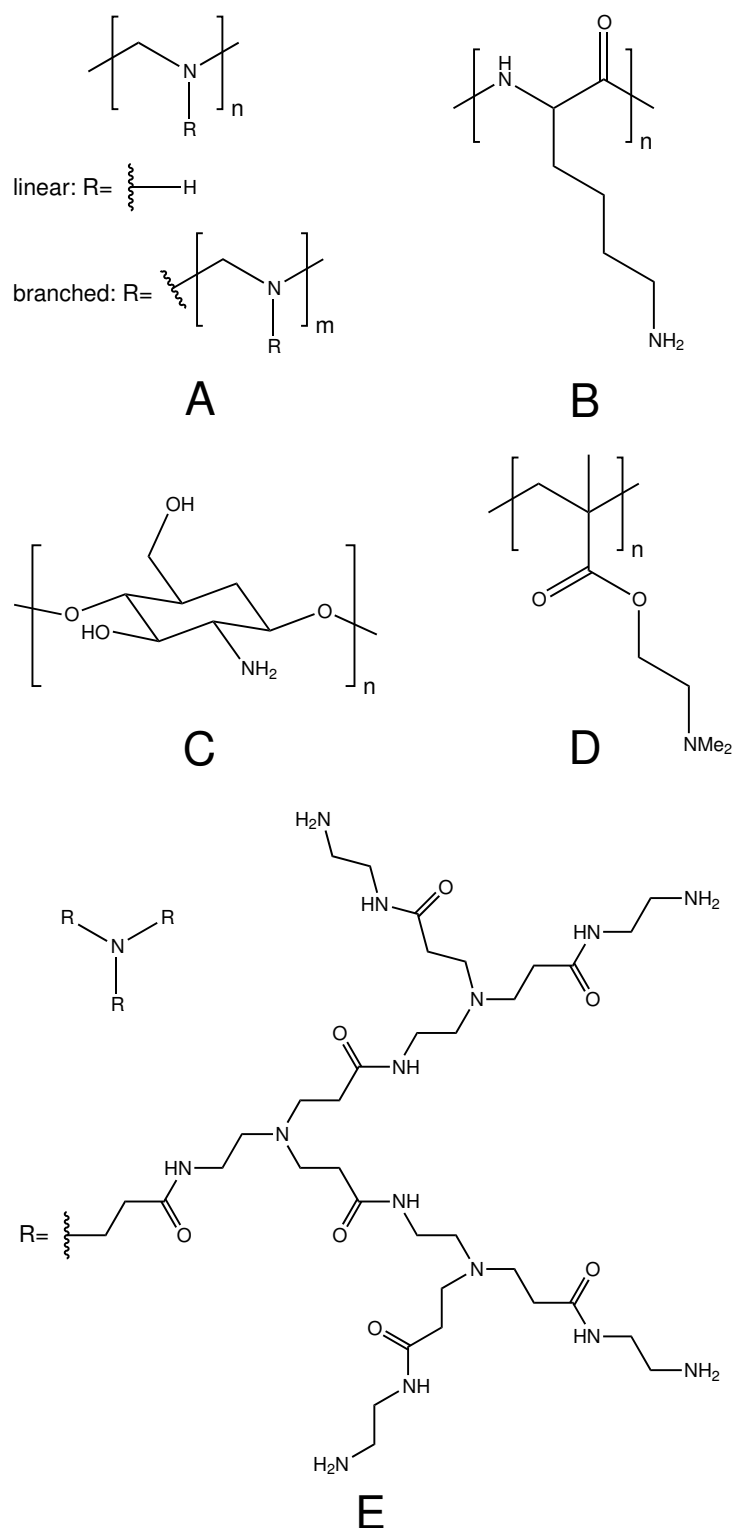


Figure I.6: Structures of commonly used homopolymer gene delivery vehicles A: poly(ethyleneimine); B: poly(lysine); C: chitosan; D: poly((2-dimethylamino)ethyl methacrylate); E: poly(amidoamine) (generation 3)

Among different types of macromolecules used for gene delivery, PEI surely is regarded to play the most important role. The polyamine has been introduced roughly

two decades ago and even today PEI is one of the most frequently employed non-viral gene delivery vehicles [30]. A high density of protonable amino groups results in a remarkable charge density, leading to very effective condensation of nucleic acids. Among non-viral carriers, PEI based systems are paramount effective, possibly due to the formation of homogeneous, nano-scaled and spherical nucleic acid-complexes bearing a high surface charge. Those are well-suited for cell internalisation and offer effective protection of nucleic acids from degradation [3]. Amino groups in different protonation states are furthermore believed to be particularly effective regarding the above mentioned endosomal buffering capacity [4].

PEI exists in a linear (lPEI) as well as in a (hyper)branched architecture (bPEI) and both have been successfully employed as gene vectors. bPEI is generally reported to exhibit stronger complexation affinity towards nucleic acids, leading to smaller complexes. Furthermore, probably due to the additional tertiary amines offering buffering capacity over a wider pH range, a pronounced proton sponge capability was hypothesised for the branched species [3, 4]. However, regarding the potency of branched and linear forms, there is some controversy in literature; several studies revealed that “polyplexes” formed from lPEI are more effective than their branched counterparts [35, 36, 37, 38, 39]. According to that, the higher transfection efficiency of lPEI was hypothesised to arise from differences in intracellular trafficking [35] or altered stability under salt conditions [39]. Besides transfection efficiency, branched and linear forms differ in terms of toxicity, typically increasing with increasing degree of branching [6]. However, various PEI based systems reported in literature are somewhat difficult to compare, as complex structure, testing conditions and most importantly the MW of PEI have a tremendous impact on transfection efficiency and toxicity as well.

PEI MWs between 5 and 25 kDa are generally believed to be suitable for gene delivery [4]. At higher MW cell-surface aggregation of the polymer typically leads to excessively increased cytotoxicity, which is also one of the major limiting factors for *in vivo* usage. Low MW PEI in turn is less toxic but usually also less effective, because at the same time the ability to condense nucleic acids is reduced. One promising strategy to overcome this discrepancy is the linkage of shorter PEI chains [40] or oligo-amines [41] via local environment specific bioreducible disulfide bonds. This approach was reported to reduce the cytotoxicity and simultaneously enhance the gene transfer activity.

5.2 Hydrophilic modification

The most prominent modification of PEI homopolymers is clearly the attachment of hydrophilic moieties, at the very most PEG, to reduce the cytotoxic effects of cationic charges. Covalent attachment of PEG generally involves the formation of PEG-PEI block copolymers, assembling to core-shell type structures upon complexation; core-forming complexes are surrounded by shielding PEG shells [4, 21]. This PEGylation commonly leads to the above described effects on toxicity, circulation time, transfection efficiency and proinflammatory signalling (Section 4.1.4).

5.3 Hydrophobic modification leading to amphiphilic block copolymers

PEG segments in PEG-PEI diblock copolymers facilitate the formation of hydrophilic shells upon complexation with nucleic acids. Beyond that basic diblock structure, the incorporation of hydrophilic and hydrophobic blocks into the PEI structure results in amphiphilic block copolymers (ABCs). ABCs are extensively used in pharmaceutical technology for controlled release of drugs and/or nucleic acids [42]. Several triblock copolymers comprising PEG, PEI plus an additional hydrophobic block have been reported to spontaneously self-assemble to various multifunctional carrier types in aqueous milieu, even in absence of complex-forming negative charges (compare Table I.1). Therefore, delivery vehicles from ABCs can be manufactured in a first step and are subsequently capable of loading with drugs and/or nucleic acids. Consequently, optimising complex properties by applying various loading techniques or stabilising and storing loaded and unloaded carriers for further use is a reasonable and promising approach.

Table I.1: Literature overview of amphiphilic block copolymers used in drug- and gene-delivery

hydrophilic segment	hydrophobic segment	cationic segment	payload	interaction mechanism	reference
PEG	PCL	-	-	-	[43, 44]
PEG	PCL	-	Neurotrophic Agent (FK505/L-685,818)	encapsulation	[45]
PEG	PCL	-	Nimodipine	encapsulation	[46]
PEG	PCL	-	Indomethacin	encapsulation	[47, 48]
PEG	PCL	-	Insulin	encapsulation	[49]
PEG	PCL	-	Hydroxycamphothericin	encapsulation	[18]
PEG	PCL	-	Phthalocyanine 4	encapsulation	[50]
PEG	PCL/PLA	-	Doxorubicin	encapsulation	[51]
PEG	PCL/PLA	-	Sagopilone	encapsulation	[52, 53]
PEG	PCL/PLA/TMC	-	-	-	[54]
PEG	pVaL ^a	-	Camphothericin	encapsulation	[55]
PEG	PLA	-	-	-	[56, 57, 58, 59, 60]
PEG	PLA	-	Doxorubicin	conjugation	[61]
PEG	PLA	-	Procain	encapsulation	[62]
PEG	PLA	-	β -Lapachone	encapsulation	[63]
PEG	PLGA	-	-	-	[20]
PEG	PLA/PLGA	-	Antiestrogen RU58668	encapsulation	[64]
PEG	PPDO-PLA ^b	-	pDNA	electrostatic	[65]

^apoly(valerolactone)^bpoly(p-Dioxanone-co-L-Lactide)

hydrophilic segment	hydrophobic segment	cationic segment	payload	interaction mechanism	reference
PEG	PCL-TMC ^c	-	Amphotericin B	encapsulation	[66]
PEG	-	PMDS ^d	pDNA	electrostatic	[67]
PEG	-	lPEI	-	-	[68]
PEG	-	lPEI	pDNA	electrostatic	[38]
-	PCL	PDMAEMA	siRNA/Paclitaxel	electrostatic, encapsulation	[69]
-	pBMA ^e	PDMAEMA	siRNA/Doxorubicin	electrostatic, encapsulation	[70]
-	p(IPAAm-co-DMAAm) ^f	PLA	-	-	[71]
-	PDMS ^g	PDMAEMA ^h	-	-	[72]
PEG	PCL	PPEEA ⁱ	siRNA	electrostatic	[73, 74]
PEG	PCL	PPEEA ⁱ	siRNA/Paclitaxel	electrostatic, encapsulation	[75]
PEG	PCL	bPEI	-	-	[76]
PEG	PCL	bPEI	pDNA	electrostatic	[77, 78, 79, 80]
PEG	PCL	bPEI	siRNA	electrostatic	[19, 81]
PEG	PCL	bPEI	pDNA/Doxorubicin	electrostatic, encapsulation	[82]

^cPCL-co-poly(Triethylenecarbonate)

^dpoly(N-methyldietheneamine sebacate)

^epoly(butylmethacrylate)

^fpoly(N-isopropylacrylamide-co-N,N-dimethylacrylamide)

^gpoly(dimethylsiloxane)

^hpoly(2-dimethylamino ethyl methacrylate)

ⁱpoly(2-aminoethyl ethylene phosphate)

hydrophilic segment	hydrophobic segment	cationic segment	payload	interaction mechanism	reference
PEG	PCL	lPEI	siRNA/Doxorubicin	electrostatic, encapsulation	[83]
PEG	PCL	P2VP ^j	-	-	[84]
PEG	PLys(Z) ^k	bPEI	-	-	[85]
PEG	PS	P2VP	-	-	[86, 87]
PEG	PBLG ^l	bPEI	pDNA	electrostatic	[88]

^jpoly(2-vinylpyridine)

^kpoly(ϵ -benzyloxy-carbonyl-L-Lysine)

^lpoly(γ -benzyl-L-glutamate)

5.3.1 Employed hydrophobic polymers

In contrast to the omnipresence of PEG as a hydrophilic block, diverse hydrophobic moieties have been employed for block copolymer manufacturing. Methacrylic polymers, poly(amino acids), poly(siloxanes), different types of poly(esters) as well as their copolymers have been reported. Table I.1 gives an overview of various compounds with different hydrophilic and hydrophobic segments in literature. Some of the most frequently used materials consist of polyesters, including poly(glycolic acid), poly(lactic acid) (PLA), copolymers from lactide/glycolide (PLGA) and poly(ϵ -caprolactone) (PCL) [42]. Those polymers have been employed in biomaterials or drug delivery systems for a long time and they have a history of safe application in humans. Moreover, polyesters are well known for their degradability via unspecific hydrolytic cleavage. In case of polyester containing copolymers, cleavage of the ester bonds may lead to small enough (<30 kDa) non-degradable fragments (such as PEG or PEI) that may be excreted via the kidneys [30]. This is paramount important after (repeated) systemic application to prevent accumulation in body tissues, that maybe lead to unknown long-term toxicity effects. Usually the degradation half-live of PCL is greatly enlarged as compared to PLA or PLGA; whereas PCL degrades typically over a period of several years [89], the degradation behaviour of PLGA can easily be controlled from a few months up to several years by altering the copolymer ratio [90]. However, the presence of hydrophilic and/or amine moieties was reported to accelerate hydrolytic degradation [79, 76].

5.3.2 Self organisation

The unique chemical composition of covalently tethered hydrophilic and hydrophobic segments makes ABCs capable of self-organisation, leading to the formation of nanoscopic, typically core-shell-structured assemblies in aqueous milieu. Hydrophobic core regions may increase stability and serve as reservoirs for hydrophobic drugs or dyes, shell moieties protect from aggregation or phagocytosis. Co-loading of hydrophobic substances allows simultaneous delivery of nucleic acids and drugs (e.g. chemotherapeutics) or dyes (e.g. for “theranostic” approaches). Depending on the nature of the core-forming block, drugs may be incorporated by chemical, physical or electrostatic means [91]. As a function of the MW-ratio of hydrophilic and hydrophobic blocks, different types of carriers, such as polymeric micelles, nanoparticles, polymersomes and a couple of more complicated structures have been reported in literature [92]. As each structure has distinct advantages regarding drug solubilisation, circulation time or the drug release profile it may be possible to tailor those properties by controlling the structure of the assemblies. Despite the knowledge

about the general relationships between polymer and carrier structure, details are still unclear [3]. The overall goal must be to deduce a relationship between chemical structure and important biological properties such as toxicity and transfection efficiency *in vitro* and *in vivo*.

Polymeric micelles Predominantly hydrophilic block copolymers are known to preferably form polymeric micelles [42] (Figure I.7). Driven by thermodynamic force in order to achieve a state of minimum free energy (G°), self-assembly appears above the critical micelle concentration (CMC) in a reversible process, as described in equation I.1, with the gas constant R (8.31 J/mol/K) and the CMC in mol/L.

$$\Delta G^\circ = RT \cdot \ln(\text{CMC}) \quad (\text{I.1})$$

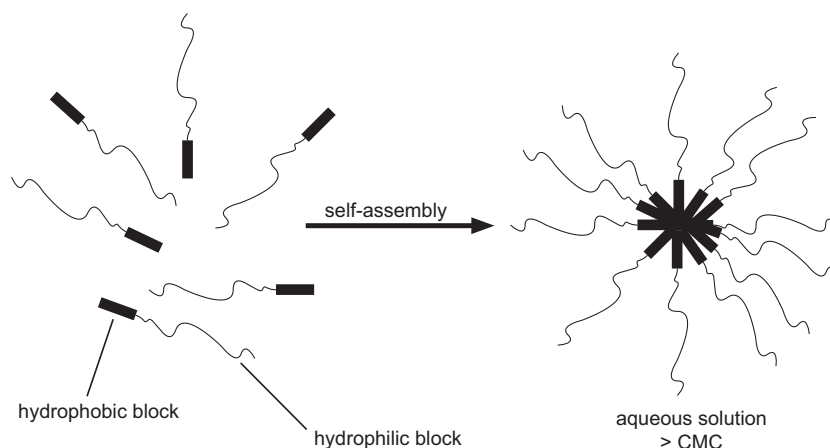


Figure I.7: Micellisation model for an amphiphilic AB-diblock copolymer

Typical CMC values for polymeric micelles are in the range of 10^{-7} - 10^{-6} M, which is generally much lower than in case of low molecular weight surfactants (10^{-4} - 10^{-3} M) [42]. This involves a distinct advantage of polymeric micelles as consequently those are more robust against disassembly upon rapid and extreme dilution, which is a prerequisite for intravenous injection. In addition to thermodynamic stability, polymeric micelles typically also exhibit increased physical stability due to the interaction of hydrophobic chains leading to a more stable kinetically “frozen” core. Typical sizes for polymeric micelles range from 10 to 100 nm [93]. In addition to spherical structures, a variety of more complicated shapes such as nanorods, worm-like micelles or polymersomes with structures similar to lipid bilayers have been reported [13]. Ultimately the shape of the micelle can be controlled by fine-tuning the ratio of hydrophilic and hydrophobic block-length [92].

Particles Nanoparticles are typically generated from block copolymers with predominant hydrophobic segments. The equilibrium dynamics is greatly reduced as compared to polymeric micelles and the manufacturing process can be described by a precipitation rather than a self-assembly process. Hydrophobic cores are largely matrix-like, which was reported to be superior regarding loading capacity and colloidal stability [92]. Typical sizes are larger than those of polymeric micelles, range from 50 to 200 nm and in contrast to polymeric micelle sizes further vary depending on the kinetic control variables during the manufacturing process [92]. Hence, monitoring diameters at different manufacturing conditions provides a technique to distinguish between micelle- and particle-like assemblies. However, the terms “particle” and “micelle” are often used imprecisely in literature. Nevertheless, a clear distinction is not always possible or desirable and in literature hybrid structures are described.

5.4 Multifunctional carriers

Apparently, a successful gene delivery vehicle ought to be multifunctional, and modular designed ABCs represent a versatile platform for these approaches. Recently, first representatives of this new class of smart carriers have emerged: Firstly hydrophobic reservoir moieties have been used for co-loading with additional cytostatic drugs or dyes. Secondly by decoration with receptor ligands, targeting functionality for specific cell types was achieved. Furthermore, *in situ* forming sensing formats were employed for elucidating intracellular trafficking and last but not least stimuli responsive carriers enable target specific unpacking.

5.4.1 “Theranostics”

It is the aim of “theranostics” to combine drug therapy with diagnostic imaging, nucleic acid delivery and/or biosensing applications all in one single engineered nano-carrier [94]. Therefore, polymers have been tagged with imaging labels such as iron oxide or gold nanoparticles for magnetic resonance imaging or photothermal treatment [95]. Furthermore, fluorescence based methods have widely been used to study intracellular trafficking mechanisms [96]. Semiconductor nano-crystals, or quantum dots (QDs), have recently begun to replace conventional fluorophores. QDs consist of a semiconductor metal core (e.g. CdSe) surrounded by a coating of wider bandgap semiconductor metals (e.g. ZnS). As compared to conventional fluorescent molecules, QDs offer unique optical properties such as wideband excitation and narrow emission spectra, increased photostability and high quantum yield [97]. By

varying semiconductor materials and sizes, QDs provide a full range of emission wavelength from the UV to the near IR, which renders them amongst the ideal candidates for visualisation in biological environment of cells and tissues [94].

5.4.2 Fluorescence resonance energy transfer (FRET)

To complement “theranostic” imaging, *in situ* forming nano-sensors based on fluorescence (or Förster) resonance energy transfer (FRET) have recently received great attention. FRET is a physical process and involves the non-radiative transfer of excitation energy from a donor fluorophore to a proximal acceptor molecule by dipole-dipole interaction [98]. Prerequisites for this phenomenon to occur are an overlap in donor emission and acceptor excitation spectra and a short distance (<10 nm) between the two fluorophores (plus a suitable three-dimensional alignment). Therefore, FRET has been utilised as an optical ruler to probe the dissociation process between two fluorescently labelled biomolecules [99]. The above mentioned outstanding optical properties of QDs allow them to function as excellent FRET donors and QD-FRET sensing formats have recently been incorporated into several carrier systems. Energy transfer between fluorescently labelled carrier and siRNA allows these systems to function as on/off-switch (Figure I.8) to monitor the timely dissociation of the complex [96]. Subsequently, dual labelling allows independent tracking of carrier and nucleic acid to study the intracellular fate *in vitro* or the biodistribution *in vivo*. Surely, these smart imaging formats have the potential to provide a deeper understanding of fundamental delivery processes and accelerate a more rational design of prospective gene carriers.

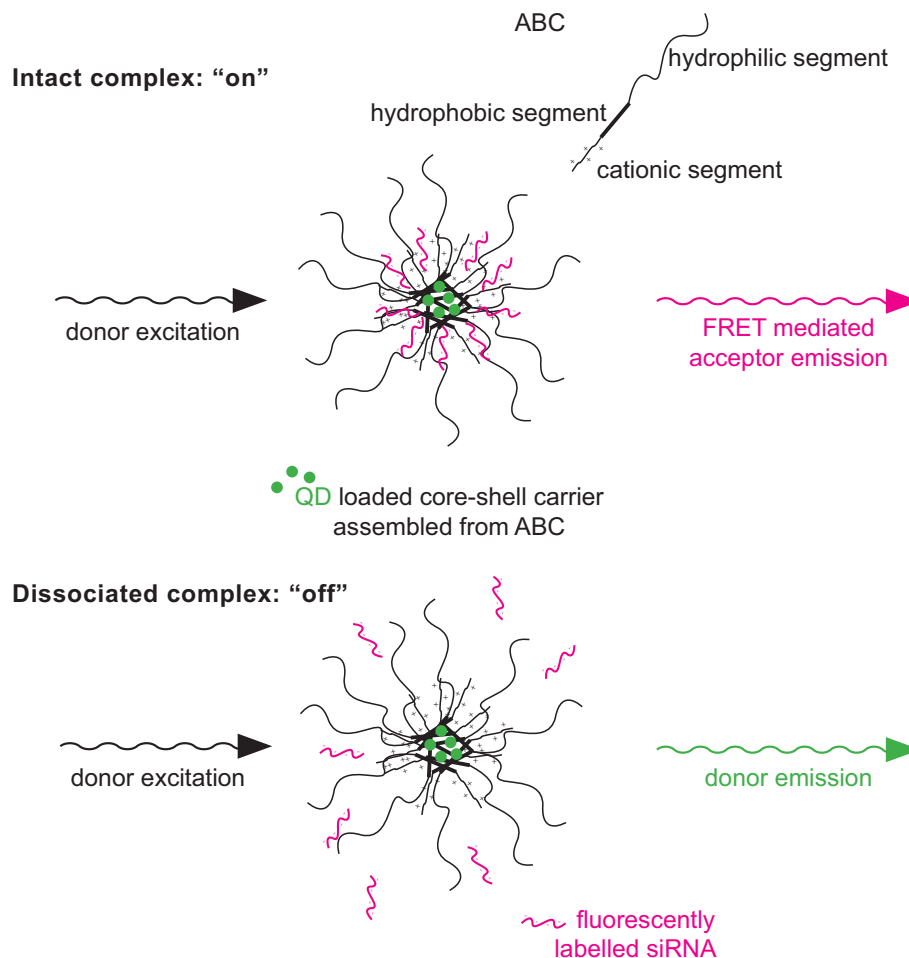


Figure I.8: Exemplary illustration of FRET switching functionality; upon donor excitation, intact QD-FRET complexes emit light via energy transfer at acceptor emission wavelength; In contrast to that, dissociated complexes simply emit light at donor emission frequency.

5.4.3 Stimuli responsive systems

Stimuli responsive systems promise release of the cargo just in time and at the right place. Lee *et al.* for instance have reversibly grafted anionic charges onto the polymer backbone to result in gene carriers with increased colloidal stability in physiological environments; then, upon acidification in the endosome, anionic functionalities are cleaved, leading to charge conversion and release into the cytosol [100]. A similar strategy was reported by Shim *et al.* for acid degradable PEI-based carrier systems, leading to efficient siRNA unpacking upon endosomal release [2]. Similarly, conjugation of siRNA-carrier-complexes with poly(styrene-co-maleic anhydride) polyanions leads to pH-responsive functionality and subsequently enhanced endosomal release [70]. Thermoresponsive polymeric micelles were assembled from block copolymers comprising poly(N-isopropylacrylamide-co-N,N-dimethylacrylamide) and PLA. Mi-

celles were reported to be stable below 40 °C, whereas higher temperatures led to aggregation and release of the loaded material. This approach may be useful for local cancer therapy in combination with cancer heating [71]. Additionally, magnetic iron-oxide particles may be employed as a heat source or as a contrast agent for “theranostic” magnetic resonance imaging. Those are just a few examples for smart stimuli responsive vector systems. After all, recent progress in nucleic acid therapy is largely due to advances in vector technology [1] and the evolution of delivery systems is a currently on-going process.

6 Aims and objectives

The overall goal of this thesis was to contribute to the development of non-viral delivery systems by establishing a versatile, potent, biodegradable and biocompatible PEG-PCL-PEI-based vector platform. However, a trial and error approach via screening various types of cationic polymers or polymer blends was not the aim of this study. In fact, a systematic bottom up study considering all crucial aspects of non-viral gene delivery was pursued. This included:

- (1) systematic chemical manufacturing and characterisation of a library of PEG-PCL-PEI compounds
- (2) testing the feasibility of assembling gene-delivery vehicles from those polymers plus the physicochemical and toxicological characterisation of the assemblies
- (3) optimising the process of carrier formation and nucleic acid loading
- (4) reproducible storage of carriers for later *in vitro* and *in vivo* use
- (5) *in vitro* and *in vivo* testing of selected polymer vectors
- (6) the manufacture of multifunctional delivery vehicles by co-loading the hydrophobic PCL cargo with drugs or dyes

Part I reviews general aspects of gene therapy with focus on the specific requirements for the manufacture of multifunctional non-viral vehicles for delivery of siRNA.

Part II covers the issues (1) and (2). It was the aim to establish a polymer library comprising vectors with systematically altered hydrophilic/hydrophobic ratio. In that way a relationship between chemical composition and carrier properties was to be derived. This necessitated the assembly of polymer molecules to gene carriers via the solvent displacement process and a thorough physicochemical

characterisation of the assemblies. Those investigations included hydrodynamic diameter, morphology, surface charge, PEG shell thickness, colloidal stability and *in vitro* toxicity as well as the correlation of those features to the chemical structure. The balance of hydrophilic and hydrophobic segments is well-known to be a crucial parameter for all of those properties. Results of part II represent the basis for all subsequent work and promising polymers were selected for further investigations.

Part III deals with the assembly and loading process (3) of previously selected polymers with the aim of manufacturing compactly condensed, stable and uniform siRNA complexes. Low N/P ratios (for a decreased toxicity) and highly concentrated carrier suspensions (due to a limited injection volume) were required for subsequent *in vivo* studies. Therefore, assembly process and the siRNA loading were optimised by investigating various techniques of the solvent displacement and the siRNA-loading procedure (including siRNA loading while and after carrier assembly). It was hypothesised that a more uniform condensation process leads to a more homogeneous distribution of charges during the complexation of siRNA. This improved process in turn may result in smaller complex sizes, more uniform size distributions, superior complex stability and protection of nucleic acids as well as increased reproducibility. The combination of these factors may also lead to a boost in transfection performance. Therefore, complexes formed via a consistent microfluidic mixing process are believed to be superior to those prepared by rapid batch mixing.

Part IV concerns the transfer of preassembled carriers to the dry state (4) for an increased shelf-life, which is a prerequisite for effective *in vitro* and *in vivo* usage. This was to be achieved by lyophilisation in presence of a lyoprotectant. By comparing size, morphology and transfection efficiency of dry-stored and freshly-prepared samples, the feasibility of freeze-drying was to be proven. Lyoprotectant concentration and N/P ratio were regarded as critical parameters upon the lyophilisation process.

Part V deals with *in vitro* investigation of transfection efficiency and cell uptake of previously selected carriers and the correlation of the results to those obtained under *in vivo* conditions (5). One goal was to relate vector performance to chemical composition. Furthermore, it was the aim to utilise the hydrophobic cargo for encapsulation of hydrophobic fluorescent QDs (6). The resulting multifunctional carrier system represents a promising hybrid system for “theranostic” purposes or co-delivery of drugs and dyes. Furthermore, a FRET capable system was to be established by complexation of these fluorescent carriers with fluorescently labelled

siRNA. As an *in situ* forming on/off-switch this system may contribute to elucidating the nucleic acid unpacking process and the intracellular fate.

Part II

Self-assembled biodegradable amphiphilic PEG-PCL-lPEI triblock copolymers at the borderline between micelles and nanoparticles designed for drug and gene delivery

Authors

Thomas Endres, Moritz Beck-Broichsitter, Olga Samsonova, Thomas Renette, Thomas Kissel^a

Authors' contributions

Cytotoxicity measurements were carried out *in vitro* by Olga Samsonova. CMC experiments were conducted by Thomas Renette and Thomas Endres. AFM was operated by Roelf-Peter Baumann (Department of Physical Chemistry, Philipps-Universität Marburg), CryoSEM by Michael Hellwig (WZMW, Philipps-Universität Marburg), NMR-spectrometer by Thomas Kämpchen and Stefan Newel (Institute of Pharmaceutical Chemistry, Philipps-Universität Marburg). All other experiments were carried out by Thomas Endres. Manuscript was written by Thomas Endres.

Published in *Biomaterials* 32 (2011), 7721–7731.

^acorresponding author

Abstract

Amphiphilic PEG-PCL-PEI triblock copolymers self-assemble into nano-scaled, positively charged, multifunctional carriers, suitable for drug and gene delivery. A set of block copolymers with varying hydrophilic/hydrophobic ratio (systematically altered at the borderline of micelle and particle forming polymers) was synthesised, characterised and assembled into carriers. A detailed structural characterisation in the liquid state of these assemblies was carried out: carrier size was determined using dynamic light scattering, cryogenic scanning electron microscopy and atomic force microscopy. Nuclear magnetic resonance analyses elucidated carrier's core-shell structure. ζ -potential and thickness of the hydrophilic outer polymer shell were determined by laser Doppler anemometry. Subsequently the impact of carrier's structure on its features (stability and toxicity) was investigated. Polymers hydrophilic in nature formed small (<40 nm) micelle-like carriers, whilst hydrophobic polymers aggregated to larger particle-like assemblies (>100 nm). Monitoring carrier size as a function of initial polymer concentration clarified different assembly mechanisms. Shell thickness, colloidal stability and toxicity were found to depend on the length of the hydrophilic polymer block. Due to controllable size, charge, stability and toxicity, this class of novel carriers is a promising candidate for prospective co-delivery of drugs and nucleic acids.

1 Introduction

Non viral delivery of nucleic acids for treatment of genetic diseases, including cancer [101] possesses tremendous potential, yet successful clinical applications of these new therapeutic agents are still scarce. The lack of efficient and safe delivery systems remains a critical factor for translational efforts. In the field of drug delivery poor aqueous solubility represents a severe drawback for many hydrophobic drugs, such as Sagopilone [53] or Paclitaxel [69]. Essential requirements for delivery vehicles in both fields are quite similar: Stability and protection from degradation or rapid excretion, low toxicity, biocompatibility and biodegradability, targeting of specific cells or tissues.

Recently, amphiphilic block copolymers have attracted increasing attention, owing to their ability to form various types of nano-carriers that can be optimally engineered [73]. In aqueous media self organisation leads to formation of aggregates, particles, micelles, vesicles [92] and even more complex structures [102]. In case of polyethylene glycol(PEG)-polyester diblock copolymers mainly micelle like structures and nanoparticles (NPs) have been reported. Sizes and structures generally depend on the molecular weight (MW) ratio of hydrophilic and hydrophobic segments [20, 103]. Tuning this delicate balance might help to alter physical properties, and optimise delivery performance and cytotoxicity.

Cationic amphiphiles make simultaneous delivery of nucleic acids and drugs possible. Among different vectors multifunctional ABC type block copolymers consisting of PEG, a polyester block like poly- ϵ -caprolactone (PCL) and a polycation segment such as linear poly(ethyleneimine) (IPEI) have emerged as promising carriers [73, 75]. In aqueous media PEG acts as the shell forming, hydrophilic block, counteracting protein absorption while maintaining suspension stability. Due to its hydrophilicity, chain flexibility, electrical neutrality and absence of functional groups, serum proteins cannot be bound to the PEG modified surfaces [58]. Generally, high surface density, complete surface coverage and long PEG chains (typically at least 2k Da) are necessary for effective shielding [15]. PCL segments arranged as a hydrophobic core could be suitable reservoirs for water insoluble drugs. Biocompatibility of both, PEG and PCL, have been demonstrated previously and aliphatic polyesters like PCL have proven to be biodegradable in aqueous media [76]. Cationic segments located at the interface between core and shell forming blocks, are in particular useful for condensation of nucleic acids or negatively charged drugs. Upon delivery, those can be easily unpacked despite being protected by surrounding PEG chains. Furthermore positive charges increase colloidal stability and enable cell interaction. In terms of gene delivery PEI is a well known polymer and has shown

superior transfection efficiency due to high amine density and effective buffering capacity [3]. As to toxicity, PEI's positive charges are known to disrupt lipid bilayer membranes and adhere to outer cell membranes [104]. High MW PEI compounds generally showed increased cytotoxicity [30], but also the three dimensional structure and conformational flexibility were demonstrated to have an effect [33]. Compared to generally utilised branched PEI25k Da, lower MW (2500 Da) linear PEIs (along with PEG shielding [30]), applied in this work, promise reduced toxicity. Presence of hydrophobic and cationic moieties makes the carrier multifunctional for co delivery of nucleic acids and drugs or for theragnostic purposes [69, 83, 75]. To design a biocompatible and stable vector, the ideal block lengths for hydrophilic, hydrophobic and charged segments are to be found.

The finding of a structure activity relationship was the main goal of this study. Therefore a set of PEG-PCL-IPEI triblock copolymers with varying PEG and PCL molecular weights was synthesised and characterised. In contrast to established water soluble copolymers, the hydrophilic/hydrophobic balance was fine tuned at the borderline between nanoparticle and micelle forming polymers. Completely water soluble polymeric vectors are known to assemble with DNA to charged polyelectrolyte complexes, so-called "polyplexes", which are commonly used for gene delivery [3]. Hydrophobic triblock copolymers, presented in this work, self assemble to nano-carriers of different size and structure, even without addition of surfactants or oppositely charged compounds. With decreasing hydrophilic/hydrophobic ratio a transition from partly water soluble micelle like assemblies to mainly water insoluble particle like precipitates is observed, even though a clear distinction between micelle and particle is not always possible or desirable. A detailed structural characterisation of carriers using methods that allow direct analysis of the structure in the liquid state was carried out. Structural features were correlated to physical characteristics and physiochemical properties. Controlling carrier structure is believed to be the key for tailoring subsequent carrier features.

2 Materials and methods

2.1 Reagents and chemicals

Tin(II)-ethylhexanoate ($\text{Sn}(\text{Oct})_2$, approx. 95%), acryloyl chloride (96%, stabilised), ϵ -Caprolactone (ϵCL , purum), monomethyl PEG (mPEG, MW=5k/2k/550 Da), Triethylamine (puriss.), 3-(4,5-dimethylthiazol-2-yl)-2,5-diphenyl tetrazolium bromide (MTT) as well as further chemicals and solvents not mentioned in detail were supplied from Sigma Aldrich GmbH (Steinheim, Germany). Chloroform and

methyl alcohol (extra dry) plus HPLC grade eluents were purchased from Acros Organics (Geel, Belgium). Deuterated solvents for nuclear magnetic resonance (NMR) analyses were obtained from Merck (Darmstadt, Germany). Poly(ethyleneimine) linear (MW=2500 Da) was provided by Polysciences Inc. (Warrington, PA, USA). Albumin (BSA, Fraction V, >99%, pulv. Bovine) was acquired from Roth GmbH (Karlsruhe, Germany).

2.2 Synthesis

Synthesis was carried out by a modified synthesis route that has been described in detail elsewhere [79]. Briefly, mPEG and ϵ CL (amount calculated to result the designated PCL block length) were put into a reaction flask and dried at reduced pressure at a temperature of 45 °C (for PEG500) respectively 65 °C (for PEG2k/5k). Subsequently the flask was purged with dry argon and Sn(Oct)₂ (0.1 mol% corresponding to ϵ CL), dissolved in dry tetrahydrofuran (THF, c=0.25 M), was injected. Then, THF was removed in vacuo over 3 h and bulk polymerisation was carried out at a temperature of 135 °C for 12 h. After cooling to room temperature (RT), the yellow solid was dissolved in chloroform, purified by precipitation in cold methanol and dried in vacuo (yield: 80.0%). In a second reaction step 1.00 eq of PEG-PCL diblock copolymer, dissolved in benzene (c=0.2 g/mL), was put into a reaction flask, equipped with a condenser. Following, 1.00 eq of triethylamine and 2.00 eq acryloyl chloride were injected. During 12 h refluxation time at 80 °C, the transparent solution misted due to crystallisation of NHEt₃Cl. After removing the salt by filtration, the polymer was purified by precipitation in cold hexane and dried in vacuo (yield: 94.7%). For comparison reasons monomethyl PCL (mPCL) with a molecular weight of 10k Da was synthesised by methanol initiated polymerisation of ϵ CL monomer. Reaction was carried out analogous to PEG-PCL compounds (yield: 91.6%). Conclusively, in a third reaction step, IPEI2500 was coupled onto the PEG-PCL linker copolymer by Michael type microaddition reaction. 1.00 eq of IPEI and 1.00 eq PEG-PCL-linker were added into separate reaction flasks and dried in vacuo for 3 h. After purging with dry argon, the copolymer was dissolved in chloroform (c=0.35 g/mL), IPEI in methanol (c=0.15 g/mL). The PEI containing flask was heated to 60 °C and subsequently the block copolymer solution was added drop wise. The reaction mixture was provided with a condenser and stirred at 60 °C for 24 h. After cooling to RT, the crude product was purified by precipitation in cold diethyl ether and dried in vacuo (yield: 70.1%). The yields of all three steps are reported exemplarily by means of PEG500-PCL2400-IPEI2500.

2.3 Basic polymer characterisation

2.3.1 NMR

NMR data was typically collected at 30 °C in ppm relatively to solvent signal using Jeol ECA-400 and ECA-500 spectrometers (Eiching, Germany) operating at 400 respectively 500 MHz.

2.3.2 FT-IR

FT-IR spectra were recorded using a Nicolet FT-IR 510 P spectrometer (Thermo Fischer Scientific Inc., Waltham, MA, USA) in a range between 4000 and 400 cm^{-1} . The powder sample was mixed with KBr and pressed into tablets for measurement.

2.3.3 Gel permeation chromatography (GPC)

GPC was used to determine the number- and weight-average molecular weights (\bar{M}_n , \bar{M}_w) and the polydispersity (D). Equipment consisted of two PSS SDV linear M columns (Mainz, Germany) plus precolumn of the same type, a Merck T6300 column oven (Darmstadt, Germany) operating at 35 °C, a 6200A pump by Merck-Hitachi (Darmstadt, Germany) and a Wyatt Optilap DSP RI-detector (Dernbach, Germany). A 2.5% (m/m) solution of LiBr in N,N-dimethylacetamide (DMAc) (HPLC grade) was used as eluent at a flow rate of 0.5 mL/min. Samples were dissolved in DMAc/LiBr at concentrations of 2 mg/mL. For each measurement 200 μL polymer solution was injected. The molecular weights of samples were calculated based on a calibration curve generated by Poly(methyl methacrylate) standards, which have a known narrow molecular weight distribution.

2.3.4 Differential scanning calorimetry (DSC)

DSC measurements were carried out on a DSC822e (Mettler Toledo, Schwerzenbach, Switzerland) at a heating rate of 20 °C/min using dry nitrogen purge gas. The samples were first heated to 100 °C, subsequently cooled to -100 °C with liquid nitrogen and heated again to 180 °C. Thermograms were normalised to sample weight. The DIN midpoint of the slope change of the heat flow plot of the second heating scan was considered as the glass transition temperature (T_g) and the heat flow capacity change (Δc_p) was determined. The melting temperatures (T_m) were taken as the maximum of endothermic peaks. PEG and PCL homopolymers of identical molecular weights than blocks incorporated in copolymers were measured in comparison to PEG-PCL diblock copolymers.

2.3.5 Cu²⁺-assay

Cu²⁺-assay [105] was utilised to determine the amine fraction per overall polymer mass. Polymers were dissolved in a mixture (1:1) of double distilled and filtrated water and N-Methyl-2-pyrrolidone in concentrations of 0.4 mg/mL. 50 μ L of this solution were mixed vigorously with 50 μ L of an aqueous CuSO₄ solution (c=0.145 mg/mL dissolved in 0.1 N KAc, pH=5.5). Subsequently absorption was measured at 280 nm employing a Pharmacia Biotech Ultrospec 3000 (GE Healthcare, Little Chalfont, Buckinghamshire, UK). Using a bPEI25k Da calibration curve together with the molecular weight determined by ¹H NMR analysis, the amount of PEI per overall polymer mass was calculated. All data reported represent the mean values of at least three replicates \pm standard deviations.

2.3.6 Critical micelle concentration (CMC)

Polymers were dissolved in double distilled and filtrated water (PEG500-PCL2500-IPEI2500: c=0.05 mg/mL, PEG2k-PCL2500-IPEI2500: c=0.20 mg/mL, PEG5k-PCL2500-IPEI2500: c=1.00 mg/mL) and pipetted successively to 80 mL of double distilled and filtrated water at constant temperature of 25 °C. Surface tension was measured after each addition step using a Krüss K11 MK2 tensiometer (Hamburg, Germany) equipped with a PL01 Wilhelmy Plate. Solution was tempered stirring magnetically for 10 min between measurements. The intersection of two linear regressions was considered as the CMC value. Volume increase was regarded mathematically.

2.4 Assembly of nano-carriers from triblock copolymers

Nano-carriers were prepared by a solvent displacement technique, described in detail elsewhere [106]. Carriers were typically prepared by dissolving 5-30 mg block copolymer in 1 mL of acetone. The resulting solution was subsequently injected into a magnetically stirred (500 rpm) phase of 5 mL double distilled and filtrated water using an Heidolph Pumpdrive 5001 (Nürnberg, Germany) at constant flow rate (8 ml/min). The ratio of water and organic phase (w:o=5) was kept constant. After injection of the organic phase, the resulting colloidal suspension was stirred for 3 h under reduced pressure to remove organic solvent. Nanosuspensions (NSs) were characterised and used directly after preparation.

2.5 Characterisation of nano-carriers

2.5.1 Size and ζ -potential

The average particle size and size distribution of the obtained nano-carriers were determined by dynamic light scattering (DLS) using a Zetasizer NanoZS/ZEN3600 (Malvern Instruments, Herrenberg, Germany). ζ -potential was measured by LDA using the same device. Analyses were typically performed at a temperature of 25 °C using samples appropriately diluted with filtrated and double distilled water. The particle mean diameter (z-ave.), the width of the fitted Gaussian distribution, which is displayed as the polydispersity index (PDI), as well as the average ζ -potential values was calculated from data of at least 10 runs. Data are displayed as the mean value of at least three measurements \pm standard deviation.

2.5.2 Fixed aqueous layer thickness (FALT)

FALT was determined examining the influence of ionic strength on particle surface charge as described in detail elsewhere [107]. Carriers were prepared as described above ($c(\text{NS})=10$ mg/mL) and diluted using NaCl stock solution and double distilled and filtrated water to reach the desired electrolyte concentration at a polymer concentration of 0.5 mg/mL. Subsequently size and ζ -potentials of different dilutions were measured as described above. Data displayed as the mean value of at least three measurements \pm standard deviation.

2.5.3 Atomic force microscope (AFM)

10 μL of the respective NSs ($c=1$ mg/mL) were pipetted onto a 1.1 cm substrate piece of freshly cleaved mica and incubated for 5 min. The samples were then rinsed several times with double distilled and filtrated water in order to remove any excess material. Once mounted onto the sample stage of the AFM, the sample was allowed to reach thermal equilibrium (30 min) before analysis. AFM imaging was performed in liquid phase (double distilled and filtrated water) on a Nanoscope IV system (Veeco, Santa Barbara, CA, USA). Pyramidal, oxide sharpened Si_3N_4 tips attached to a V-shaped substrate (Olympus, Tokyo, Japan) were used for imaging. All images were measured using tapping mode AFM with constant amplitude attenuation. The cantilever approach was performed with a drive amplitude of 250 mV. To achieve high-resolution images the drive amplitude was lowered to ~ 75 mV, while the set point was adjusted to minimal forces.

2.5.4 Cryogenic scanning electron microscope (cryoSEM)

CryoSEM images were obtained using a JSM-7500F (Jeol, Tokyo, Japan) equipped with a ALTO-2500 liquid nitrogen (LN2) cryo-transfer system (Gatan Inc., Pleasanton, CA, USA) enabling SEM observation at a specimen temperature of -140 °C. Samples were sputtered with a thin platinum layer directly using the ALTO system. Carriers were observed at an accelerating voltage of 4 kV.

2.5.5 Structure elucidation via ^1H NMR spectroscopy

To elucidate structural features of nano-carriers, a series of ^1H NMR experiments was carried out. Nano-carriers were prepared as described above using deuterated solvents (D_2O , acetone- D_6) ($c(\text{NS})=8$ mg/mL). For temperature-dependent NMR analyses 500 μL NS were filled into the outer chamber of a cylindrical coaxial NMR-tube (Wilmad-LabGlass, NY, USA). The inner compartment was filled with an external standard, a solution of pyridine in D_2O ($c=0.01$ Vol%). ^1H NMR spectra were recorded at different temperatures (30-75 °C, $\Delta T=5$ °C, equilibration time=30 min) at 500 MHz. Position and intensity of pyridine signals were kept constant in all temperature dependent measurements. For measurements in D_2O /acetone- D_6 mixtures NSs were diluted using acetone- D_6 and D_2O to reach the desired acetone concentration at a polymer concentration of 4 mg/mL. ^1H NMR spectra of mixtures were compared to a polymer-solution in acetone- D_6 ($c=4$ mg/mL).

Additionally mPEG5k-PCL10k-IPEI2500 samples, prepared for variable temperature NMR analyses, were further measured in size and charge via DLS and LDA (as described in section 2.5.1). Data was collected at temperatures between 25-90 °C ($\Delta T=5$ °C, equilibration time=15 min). ζ -potential was measured at RT before and after temperature treatment. mPCL10k particles were examined for comparison reasons.

2.5.6 Analysis of colloidal stability

The colloidal stability of nano-carriers was evaluated from their resistance to NaCl- and albumin-induced aggregation. Nano-carriers were prepared as described above ($c(\text{NS})=4$ mg/mL, respectively 2 mg/mL in case of mPCL). NSs were freed from loose aggregates by centrifugation (1 min, 1000·g), mixed with water and subsequently with an albumin/NaCl, stock solution to reach the desired albumin/NaCl concentration at a polymer concentration of 2 mg/mL (respectively 1 mg/mL in case of mPCL10k). After 10 min turbidity was measured employing Pharmacia Biotech Ultrospec 3000 (GE Healthcare, Little Chalfont, Buckinghamshire, UK) at 500 nm.

Measured absorptions were normalised to 100% turbidity. The onset of a dramatic increase in turbidity was considered as concentration of aggregation. Following, size and ζ -potential were measured as described above. Data displayed as the mean value of at least three measurements \pm standard deviation.

2.5.7 Cytotoxicity in HeLa-Luc cells (MTT assay)

MTT assay was performed as described elsewhere [108] to determine the cytotoxicity of PEG-PCL10k-lPEI2500 carriers. HeLa-Luc cells were seeded into 96-well plates (Nunc, Langenselbold, Germany) at a density of 8,000 cells/well 24 h prior to experiment, then the cell culture medium was replaced with increasing polymer concentration (assembled to carriers) in 100 μ L cell culture medium. After 24 h of incubation, medium was replaced by Dulbecco's Modified Eagle's Medium (DMEM) without serum, containing 0.2 mg/mL MTT. After 4 h of incubation at 37 °C, medium was carefully removed and formazane crystals were dissolved in 200 μ L dimethyl sulfoxide per well. Measurement was performed using an ELISA reader (Titertek Plus Ms 212, ICN, Eschwege, Germany) at wavelength of 570 and 690 nm. Relative viability was calculated in % related to cells with untreated cells. Data is presented as means of four measurements \pm standard deviation. The inflexion point of a sigmoidal regression was considered as IC50 concentration.

3 Results

3.1 Synthesis and characterisation

Triblock copolymers were synthesised in three reaction steps according to Figure II.1. In the synthesis of the PEG-PCL diblock copolymers, PCL block length was controlled by the initial amount of ϵ CL and determined by comparing the intensity of relevant ^1H NMR signals of PEG and PCL. Additionally, GPC was employed to analyse the uniformity of molecular weight distributions, which were found to be unimodal with polydispersities between 1.2-1.5 (compare basic polymer characterisation).

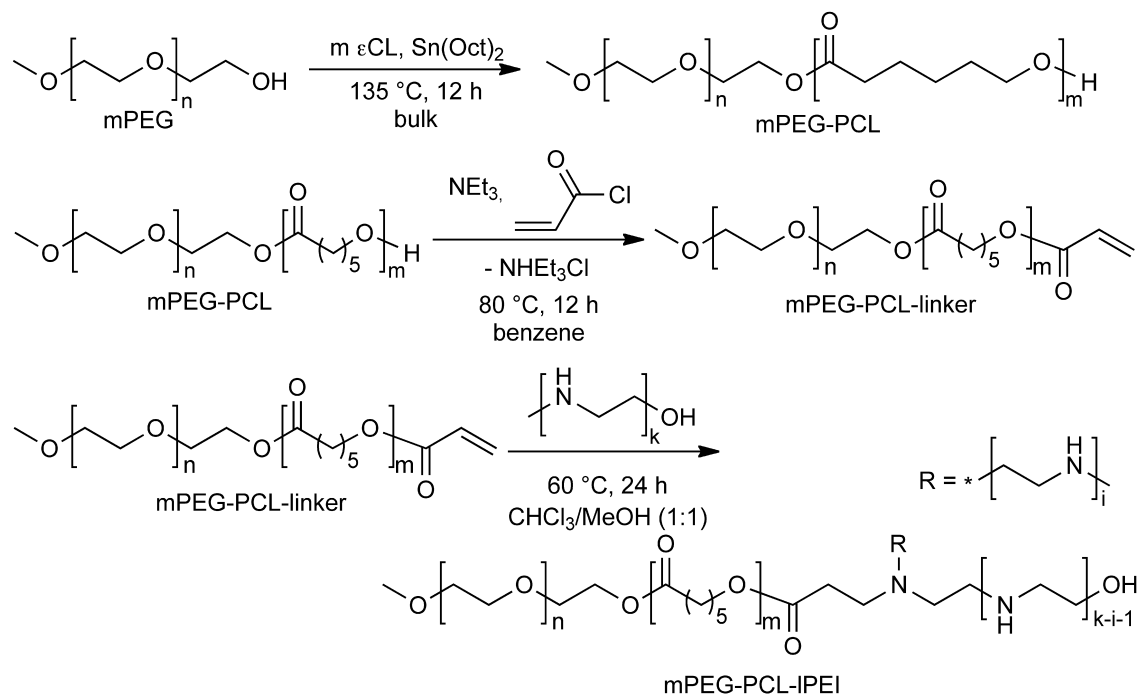


Figure II.1: Synthesis in three steps: (1) PEG-PCL was produced by ring-opening polymerisation initialised by the PEG hydroxyl-endgroup using $\text{Sn}(\text{Oct})_2$ as a catalyst. (2) A double bond was attached onto the PEG-PCL chain-end by esterification of the PEG-PCL hydroxyl group with acryloyl chloride. (3) IPEI2500 was coupled onto the PEG-PCL-linker copolymer by Michael-type microaddition reaction.

Basic polymer characterisation exemplarily for mPEG500-PCL2400-IPEI2500 (all other compounds were characterised in the same manner):

mPEG-PCL diblock copolymer: ^1H NMR (400 MHz, CDCl_3): $\delta=1.34\text{-}1.41$ (m, 65.43 H, $^*\text{-}[\text{CO}-(\text{CH}_2)_2\text{-}\underline{\text{CH}_2}\text{-}(\text{CH}_2)_2\text{-O}]_m\text{-}^*$), 1.62-1.66 (m, 132.25 H, $^*\text{-}[\text{CO-CH}_2\text{-}\underline{\text{CH}_2}\text{-CH}_2\text{-CH}_2\text{-O}]_m\text{-}^*$), 2.29-2.32 (t, $^3\text{J}=7.40$ Hz, 65.24 H, $^*\text{-}[\text{CO-}\underline{\text{CH}_2}\text{-}(\text{CH}_2)_4\text{-O}]_m\text{-}^*$), 3.34 (s, 3.00 H, $\underline{\text{CH}_3}\text{-O-}^*$), 3.55-3.56 (m, 2.07 H, $\text{Me-O-CH}_2\text{-}\underline{\text{CH}_2}\text{-}^*$), 3.60-3.65 (m, 39.29 H, $^*\text{-}[(\underline{\text{CH}_2})_2\text{-O}]_m\text{-}^*$), 3.69-3.70 (t, $^3\text{J}=4.85$ Hz, 3.57 H, $^*\text{-O-}\underline{\text{CH}_2}\text{-CH}_2\text{-O-}[\text{CO}-(\text{CH}_2)_5\text{-O}]_m\text{-H}$), 4.04-4.08 (t, $^3\text{J}=6.75$ Hz, 63.71 H, $^*\text{-}[\text{CO}-(\text{CH}_2)_4\text{-}\underline{\text{CH}_2}\text{-O}]_m\text{-}^*$), 4.21-4.24 (t, $^3\text{J}=4.85$ Hz, 2.43 H, $^*\text{-O-CH}_2\text{-}\underline{\text{CH}_2}\text{-O-}[\text{CO}-(\text{CH}_2)_5\text{-O}]_m\text{-H}$) ppm.

mPEG-PCL-linker: ^1H NMR (400 MHz, CDCl_3): $\delta=1.36\text{-}1.40$ (m, 75.40 H, $^*\text{-}[\text{CO}-(\text{CH}_2)_2\text{-}\underline{\text{CH}_2}\text{-}(\text{CH}_2)_2\text{-O}]_m\text{-}^*$), 1.62-1.65 (m, 158.55 H, $^*\text{-}[\text{CO-CH}_2\text{-}\underline{\text{CH}_2}\text{-CH}_2\text{-CH}_2\text{-O}]_m\text{-}^*$), 2.28-2.32 (t, $^3\text{J}=7.45$ Hz, 74.72 H, $^*\text{-}[\text{CO-CH}_2\text{-}(\text{CH}_2)_4\text{-O}]_m\text{-}^*$), 3.38 (s, 3.00 H, $\underline{\text{CH}_3}\text{-O-}^*$), 3.53-3.56 (m, 2.36 H, $\text{Me-O-CH}_2\text{-}\underline{\text{CH}_2}\text{-}^*$), 3.59-3.68 (m, 38.26 H, $^*\text{-}[(\underline{\text{CH}_2})_2\text{-O}]_n\text{-}^*$), 3.68-3.70 (t, $^3\text{J}=4.80$ Hz, 2.58 H, $^*\text{-O-CH}_2\text{-CH}_2\text{-O-}[\text{CO}-(\text{CH}_2)_5\text{-O}]_m\text{-H}$), 4.04-4.07 (t, $^3\text{J}=6.80$ Hz, 68.02 H, $^*\text{-}[\text{CO}-(\text{CH}_2)_4\text{-}\underline{\text{CH}_2}\text{-O}]_m\text{-}^*$), 4.13-4.16 (t, $^3\text{J}=6.70$ Hz, 2.45 H, $^*\text{-}\underline{\text{CH}_2}\text{-O-CO-C}_2\text{H}_5$), 4.21-4.23 (t, $^3\text{J}=4.80$ Hz, 2.70 H, $^*\text{-O-CH}_2\text{-CH}_2\text{-O-}[\text{CO}-(\text{CH}_2)_5\text{-O}]_m\text{-H}$), 5.81-5.83 (dd, $^2\text{J}=1.30$ Hz, $^3\text{J}_{cis}=10.30$ Hz, 0.78 H, $^*\text{-CO-CH=CHH}$), 6.08-6.15 (dd, $^3\text{J}_{cis}=10.30$ Hz, $^3\text{J}_{trans}=17.40$ Hz, 0.82 H, $^*\text{-CO-CH=CHH}$), 6.37-6.42 (dd, $^2\text{J}=1.30$ Hz, $^3\text{J}_{trans}=17.40$ Hz, 0.80 H, $^*\text{-CO-CH=CHH}$) ppm. ^{13}C NMR (500 MHz, CDCl_3): $\delta=24.93$ ($^*\text{-}[\text{CO-CH}_2\text{-}\underline{\text{CH}_2}\text{-}(\text{CH}_2)_3\text{-O}]_m\text{-}^*$), 25.88 ($^*\text{-}[\text{CO}-(\text{CH}_2)_2\text{-}\underline{\text{CH}_2}\text{-}(\text{CH}_2)_2\text{-O}]_m\text{-}^*$), 28.70 ($^*\text{-CO-}(\text{CH}_2)_3\text{-}\underline{\text{CH}_2}\text{-CH}_2\text{-O}]_m\text{-}^*$), 34.47 ($^*\text{-}[\text{CO-}\underline{\text{CH}_2}\text{-}(\text{CH}_2)_4\text{-O}]_m\text{-}^*$), 59.38 ($\underline{\text{CH}_3}\text{-O-}^*$), 63.80 ($^*\text{-O-CH}_2\text{-}\underline{\text{CH}_2}\text{-O-}[\text{CO}-(\text{CH}_2)_5\text{-O}]_m\text{-}^*$), 64.49 ($^*\text{-}[\text{CO}-(\text{CH}_2)_4\text{-}\underline{\text{CH}_2}\text{-O}]_m\text{-}^*$), 69.53 ($^*\text{-O-}\underline{\text{CH}_2}\text{-CH}_2\text{-O-}[\text{CO}-(\text{CH}_2)_5\text{-O}]_m\text{-}^*$), 70.93 ($^*\text{-}[(\underline{\text{CH}_2})_2\text{-O}]_n\text{-}^*$), 72.30 ($\text{MeO-}\underline{\text{CH}_2}\text{-}^*$), 128.90 ($^*\text{-CO-CH=CH}_2$), 130.90 ($^*\text{-CO-CH=}\underline{\text{CH}_2}$), 173.88 ($^*\text{-}[\text{CO}-(\text{CH}_2)_5\text{-O}]_m\text{-}^*$) ppm.

mPEG-PCL-IPEI: ^1H NMR (400 MHz, CDCl_3): $\delta=1.10\text{-}1.15$ (t, $^3\text{J}=7.06$ Hz, 12.17 H, $\underline{\text{CH}_3}\text{-CH}_2\text{-CO-}^*$), 1.35-1.66 (m, 69.88 H, $^*\text{-}[\text{CO}-(\text{CH}_2)_2\text{-}\underline{\text{CH}_2}\text{-}(\text{CH}_2)_2\text{-O}]_m\text{-}^*$), 1.60-1.66 (m, 137.29 H, $^*\text{-}[\text{CO-CH}_2\text{-}\underline{\text{CH}_2}\text{-CH}_2\text{-CH}_2\text{-O}]_m\text{-}^*$), 2.28-2.33 (t, $^3\text{J}=7.50$ Hz, 69.37 H, $^*\text{-}[\text{CO-}\underline{\text{CH}_2}\text{-}(\text{CH}_2)_4\text{-O}]_m\text{-}^*$), 2.60-2.85 (m, 212.47 H, $^*\text{-}[(\underline{\text{CH}_2})_2\text{-NR}]_k\text{-}^*$), 3.38 (s, 3.41 H, $\underline{\text{CH}_3}\text{-O-}^*$), 3.40-3.45 (m, 14.34 H, $^*\text{-}(\underline{\text{CH}_2})_2\text{-NC}_3\text{H}_5\text{O-}^*$), 3.53-3.56 (m, 2.42 H, $\text{Me-O-CH}_2\text{-CH}_2\text{-}^*$), 3.60-3.70 (m, 30.01 H, $^*\text{-}[(\underline{\text{CH}_2})_2\text{-O}]_m\text{-}^*$), 4.03-4.08 (t, $^3\text{J}=6.67$ Hz, 66.15 H, $^*\text{-}[\text{CO}-(\text{CH}_2)_4\text{-}\underline{\text{CH}_2}\text{-O}]_m\text{-}^*$), 4.21-4.24 (m, 1.60 H, $^*\text{-O-CH}_2\text{-}\underline{\text{CH}_2}\text{-O-}[\text{CO}-(\text{CH}_2)_5\text{-O}]_m\text{-H}$, $^*\text{-}\underline{\text{CH}_2}\text{-O-CO-}(\text{CH}_2)_2\text{-NR}_2$) ppm. GPC: $\bar{M}_n=7240$ Da, $\bar{M}_w=9230$ Da, $D=1.27$. FT IR (KBr, cm^{-1}) ν 3250 (s, νNH), 2947 (s, $\nu_{as}\text{CH}_2$), 2866 (s, $\nu_s\text{CH}_2$), 1725 (s, $\nu_{cr}\text{C=O}$), 1187/1245 (s, $\nu\text{C-O-C}$).

Polyester block lengths, as determined by ^1H NMR, are reported in Table II.1 and values were found to be in the range of desired molecular weights.

Table II.1: Composition of block copolymers with different hydrophilicity along with hydrodynamic diameters and PDIs (determined by DLS) of carriers assembled from these polymers

Polymer	m(PCL) ^a /Da	m(PEG)/ m(PCL) ^b	z-ave./nm	PDI
PEG500-PCL2400-IPEI2500	3780	0.132	115.6±2.8	0.172±0.020
PEG500-PCL5k-IPEI2500	6470	0.077	123.6±3.6	0.116±0.011
PEG500-PCL10k-IPEI2500	11465	0.044	124.0±6.9	0.089±0.020
PEG2k-PCL2400-IPEI2500	2325	0.608	24.1±0.2	0.212±0.001
PEG2k-PCL5k-IPEI2500	5435	0.333	25.8±0.2	0.216±0.008
PEG2k-PCL10k-IPEI2500	10580	0.165	95.7±2.0	0.165±0.004
PEG5k-PCL2400-IPEI2500	2700	1.850	35.1±1.6	0.229±0.032
PEG5k-PCL5k-IPEI2500	6720	0.744	46.7±3.4	0.288±0.047
PEG5k-PCL10k-IPEI2500	13120	0.381	42.0±2.5	0.173±0.031

^aPCL MWs determined by ¹H NMR spectroscopy; ^bPEG/PCL ratio indicating polymer's hydrophilicity; DLS results presented as mean from at least three repetitions ± standard deviation

Additionally T_m and T_g of diblock copolymers in comparison to homopolymers of the same molecular weight were determined via DSC (Figure II.2). All DSC curves display only one T_g close to the T_g of PCL homopolymer (-50---60 °C), suggesting predominant immiscibility of PEG and PCL moieties [44].

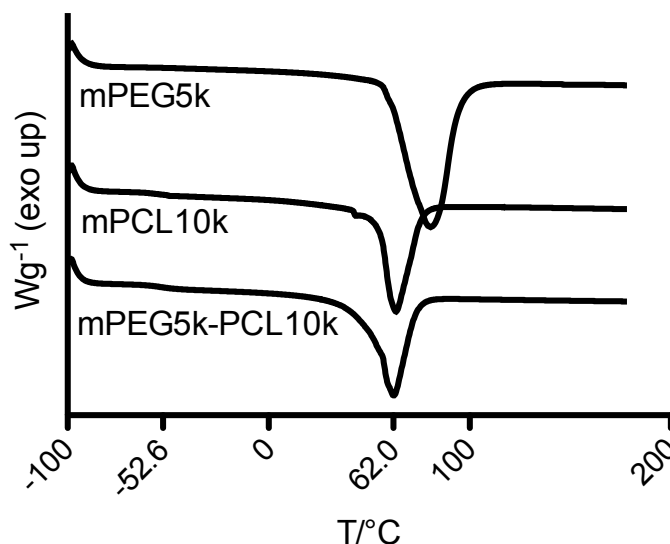


Figure II.2: DSC thermograms of mPEG5k and mPCL10k homopolymers in comparison to mPEG5k-PCL10k diblock copolymer (T_g =-52.6 °C, T_m =62 °C)

In a second reaction step the endgroups of diblock copolymers were modified by esterification; double bond signals in the ^1H NMR spectrum between 5.7 and 6.5 ppm (^{13}C spectrum: 128~131 ppm) proved successful conversion. Finally, vanishing double bond signal upon conjugation with PEI confirmed effective coupling in the third reaction step (Figure II.3).

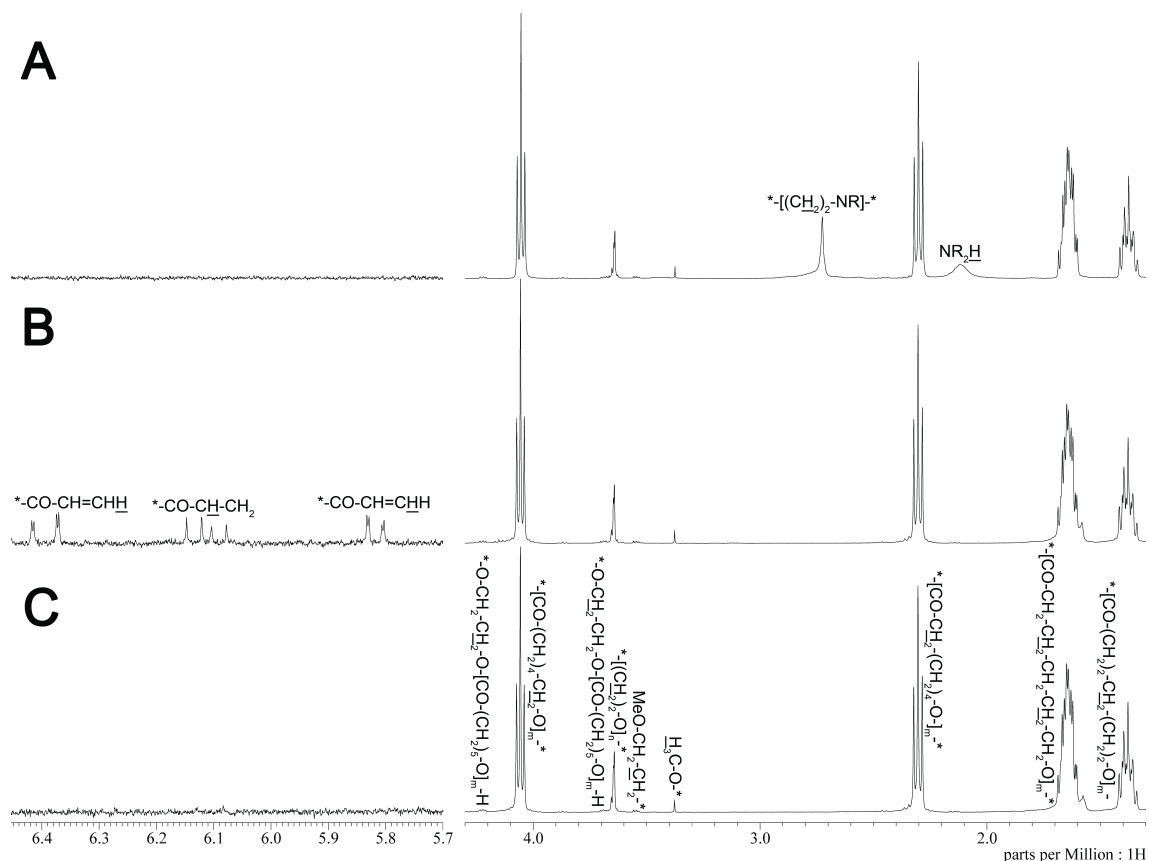


Figure II.3: ^1H NMR spectra of mPEG500-PCL10000 (A), mPEG500-PCL10000-linker (B) and mPEG500-PCL10k-1PEI2500 (C); double bond signals (5.7~6.5 ppm) indicate successful endgroup modification and subsequent PEI conjugation

Furthermore in FT-IR spectra a $\text{C}=\text{O}$ stretch at ~ 1725 , $\text{C}-\text{O}-\text{C}$ stretches at $\sim 1187/1245$ and an amine stretch at $\sim 3250\text{ cm}^{-1}$, prove presence of PCL, PEG and PEI segments (Figure II.4).

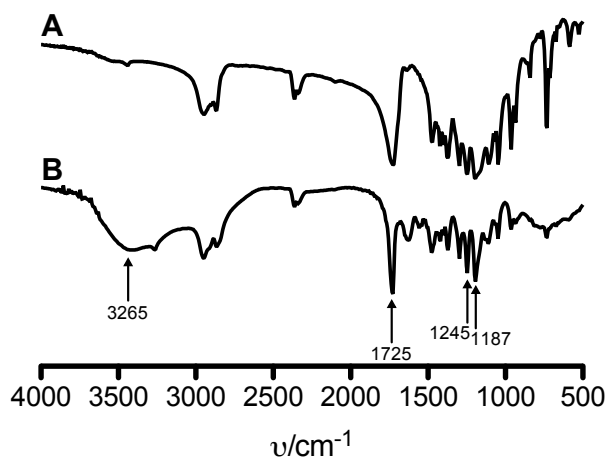


Figure II.4: IR spectra of mPEG500-PCL2400 (A) and mPEG500-PCL2400-lPEI2500 (B); amine stretch at $\sim 3265 \text{ cm}^{-1}$ confirms presence of PEI

By dropwise addition of PEG-PCL-linker to PEI the conjugation ratio is supposed to be close to 1. However, a multi addition of PEG-PCL-linkers on more than one amine of the same PEI molecule is feasible and integration of the PEI signal in ^1H NMR spectra of all synthesised compounds revealed a coupling ratio close to 1 (data not shown). The Cu^{2+} -assay was utilised to quantify amine mass fraction per overall molecular weight. As expected, amine weight fraction decreases with increasing PEG/PCL molecular mass as displayed in Figure II.5A, also illustrating polymers' hydrophilicity. Molecular weight composition, as determined by ^1H NMR spectroscopy and Cu^{2+} -assay, is presented in Figure II.5B. Yields for the three reaction steps were $\sim 75\%$, $\sim 90\%$ and $\sim 70\%$, respectively, depending on PEG-PCL composition.

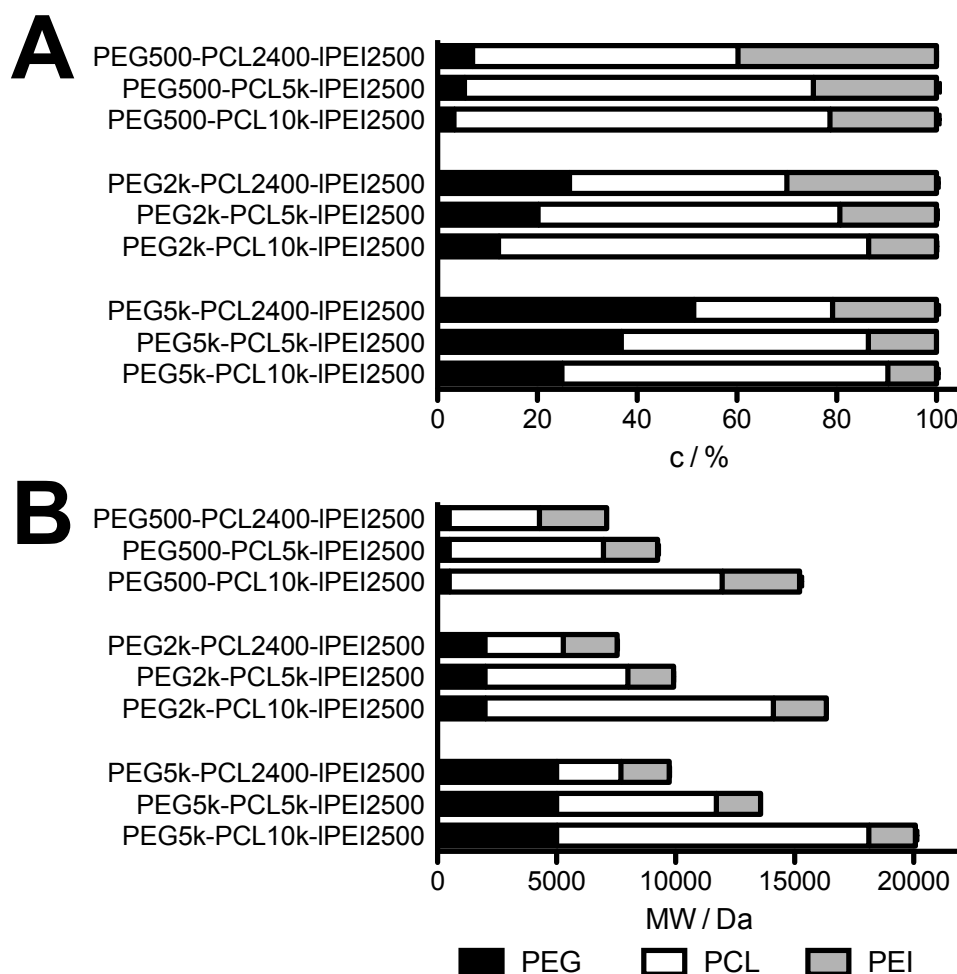


Figure II.5: Block copolymer composition by % (A) and MW (B) (PEG MW as specified by manufacturer, PCL MW as determined by ^1H NMR analysis, PEI weight fraction \pm standard deviation as determined by Cu^{2+} assay from at least three replicates)

3.2 Carrier size and assembly mechanism

The PEG/PCL ratio, as reported in Table II.1, is a characteristic indicator for carrier structure. With increasing ratio the size of carriers (constant initial polymer concentration in acetone: 25 mg/mL) decreases. CryoSEM and AFM images in the liquid state are consistent with DLS measurements and demonstrate spherical shape (Figure II.6). PDI values were found to be unimodal.

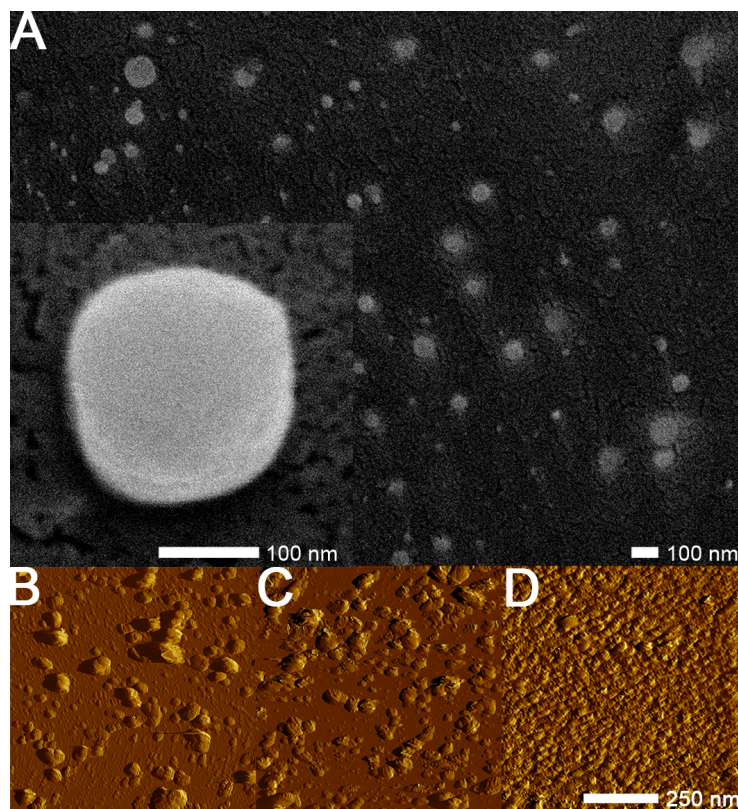


Figure II.6: CryoSEM images of PEG500-PCL10k-IPEI2500 carriers (A); AFM images in the liquid state of PEG500-PCL10k-IPEI2500 (B), PEG2k-PCL10k-IPEI2500 (C) and PEG5k-PCL10k-IPEI2500 (D) carriers

Trends in size and structure as a function of polymer hydrophilicity can be explained by diverse carrier forming mechanisms: hydrophobic polymers precipitate quickly upon injection into the water phase, whereas longer PEG segments control carrier formation leading to smaller micelle-like structures. To monitor the transition from particles to micelles, carriers were formed as a function of initial polymer concentration in the acetone phase during solvent displacement process (Figure II.7). Hydrophobic carriers develop in size (70-140 nm) upon rise of polymer concentration, whereas hydrophilic carriers remain fairly constant (~ 35 nm).

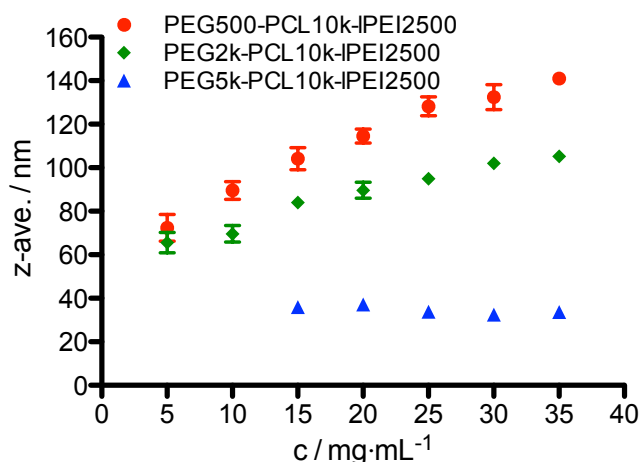


Figure II.7: Carrier size as a function of initial polymer concentration in the organic phase during solvent displacement process; data acquired from at least three repetitions \pm standard deviation

3.3 PEG shell thickness measurements

FALT of the outer PEG shell was determined by measuring the ζ -potential as a function of electrolyte concentration (c). In pure water, decreasing ζ -potential with increasing PEG MW reflects increased shielding of PEI charges on the PCL surface by presence of the outer PEG shell. The hydrophilic PEG moisture shifts the slipping plane away from the surface of the PCL core and this subsequently results in a reduced ζ -potential. With an increase in ionic strength, ζ was found to decrease according to the Gouy-Chapmann theory. A plot of $\ln(\zeta)$ against κ ($\kappa=3.3\cdot\sqrt{c}$, where κ^{-1} is the Debye length) gives the thickness of the PEG polymer layer in nm (d_{shell}) as the slope of a linear regression (Figure II.8A). The determined shell thickness was found to increase with increasing PEG MW. Observed d_{shell} values for PEG500, 2k and 5k are in a good agreement with theoretical calculations for a random coil, where the radius of gyration (R_g) is calculated by Equation II.1 or II.2, depending on solvency power [109] (Table II.2); where a is the segment length (which is 0.36 in case of PEG [109]) and N is the degree of polymerisation (which is calculated from the PEG molecular weight specified by the manufacturer). Together with DLS data the core diameter of the respective carrier can be easily calculated. Figure II.8B shows a dimensional sketch of the three different core-shell carriers bearing different PEG chain length linked to PCL and PEI segments of constant size. Although the FALT is increasing from 1.7 to 3.3 nm with increasing PEG MW, the decreasing core diameter is the size-dominating factor.

$$R_g = a \cdot N^{1/2} \quad (\Theta \text{ solvent}) \quad (\text{II.1})$$

$$R_g = a \cdot N^{3/5} \quad (\text{good solvent}) \quad (\text{II.2})$$

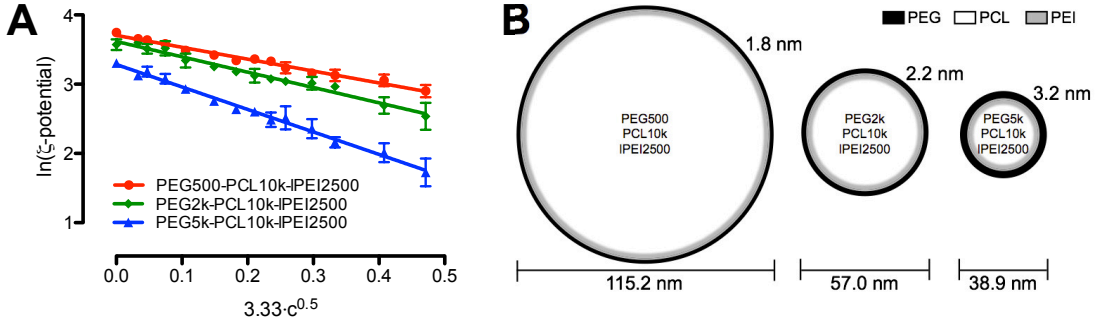


Figure II.8: FALT-measurements: PEG shell thickness (which can be read of the slope) increases with increasing PEG MW; values presented as means from at least three measurements \pm standard deviation (A); dimensional sketch of carriers assembled from polymers bearing different PEG MWs (B)

To estimate the surface potential (Ψ_0) the Eversole and Boardman equation was utilised by plotting $-\ln \left[\tanh \left(\frac{e\zeta}{4kT} \right) \right]$ versus κ as described elsewhere [110]; where e is the electron charge ($1.60 \cdot 10^{-19}$ C), k is the Boltzmann constant ($1.38 \cdot 10^{-23}$ J/K) and T is the absolute temperature (298.15 K). Furthermore the surface charge density σ_0 was derived from Ψ_0 , employing Equation II.3, where n is the ion number per volume unity ($6.02 \cdot 10^{23} \text{ m}^{-3}$), ϵ_0 is the dielectric permittivity ($8.85 \cdot 10^{-12} \text{ C} \cdot \text{V}^{-1} \cdot \text{m}^{-1}$), ϵ_r is the dielectric constant of water at RT (78.28) and z is the valency of the ion [111]. The number of charges was calculated from σ_0 together with the surface area of the PCL core and e . Ψ_0 and σ_0 , together with the number of positive charges on the surface of each PCL sphere, are displayed in Table II.2. The number of positive charges was found to decrease with increasing hydrophilicity. Since IPEI2500 contains approximately 60 aminogroups (being only partly protonated plus some amines are possibly trapped inside the PCL core due to phase mixing), calculated charges are in the expected range.

$$\sigma_0 = \sqrt{8kTn\epsilon_0\epsilon_r} \cdot \text{sh} \left(\frac{ze\Psi_0}{2kT} \right) \quad (\text{II.3})$$

Table II.2: Shell thickness values of carriers with different PEG block length determined by FALT measurement (d_{shell}) in comparison to calculated values (R_g) and electrochemical characteristics

compound	d_{shell}^a /nm	R_g^b /nm	Ψ_0 /mV	σ_0 /mC·cm ⁻¹	# of charges ^c
PEG500-PCL10k-IPEI2500	1.7±0.1	1.2~1.6	39.6±0.6	0.322±0.006	789±14
PEG2k-PCL10k-IPEI2500	2.2±0.1	2.4~3.5	36.3±0.9	0.290±0.009	158±5
PEG5k-PCL10k-IPEI2500	3.3±0.1	3.8~6.2	26.1±0.7	0.200±0.006	41±1

^avalues determined by FALT measurements; ^bradii of gyration, calculated from Equation II.1 and II.2; ^cnumber of charges located on the surface of the PCL core surface; values are presented as means from at least three measurements ± standard deviation

3.4 Structure elucidation using ¹H NMR techniques

The change in NMR line width can be utilised to examine the hypothetical core shell structure. ¹H NMR spectra of PEG5k-PCL10k-IPEI2500 dissolved in acetone-D6 were compared to carriers of the same polymer suspended in D2O/acetone-D6 mixtures (Figure II.9). As acetone-D6 is a good solvent for PEG and PCL, the copolymer is dissolved as a homogenous solution: Both, PEG ethylene protons at ~3.6 ppm and PCL signals (e. g. triplet at ~4.1 ppm), are sharp and completely resolved (Figure II.9A). However, spectra in D₂O (Figure II.9B-F) change: With increasing D₂O concentration PCL signals get weaker in intensity and poorer in resolution, while the PEG signal keeps fairly constant in size and shape (apart from minor changes).

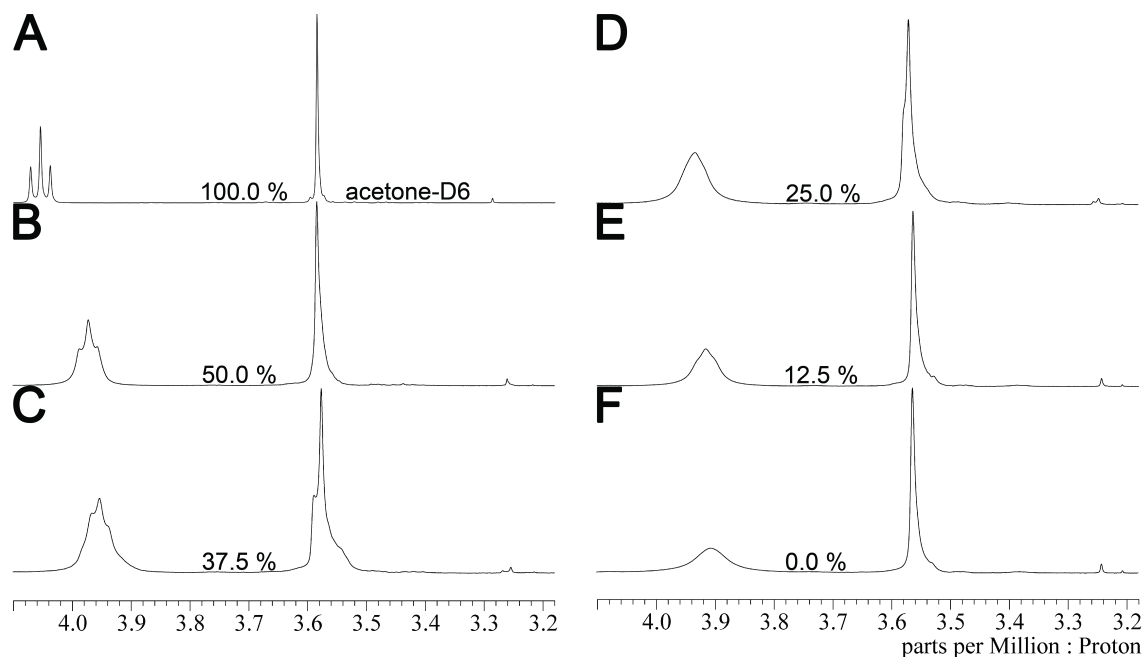


Figure II.9: ^1H NMR spectra of PEG5k-PCL10k-IPEI2500 dissolved in acetone-D6 (A) in comparison to carriers of the same polymer suspended in D₂O/acetone-D6 mixtures (B-F)

A set of variable temperature ^1H NMR analyses in D₂O with pyridine (signals between 7.2~8.5 ppm not shown) as an external standard was carried out (Figure II.10). Evidently at higher temperatures there is an increase in signal intensity and resolution of PCL signals, while the PEG signal intensity decreases (along with an upfield-shift).

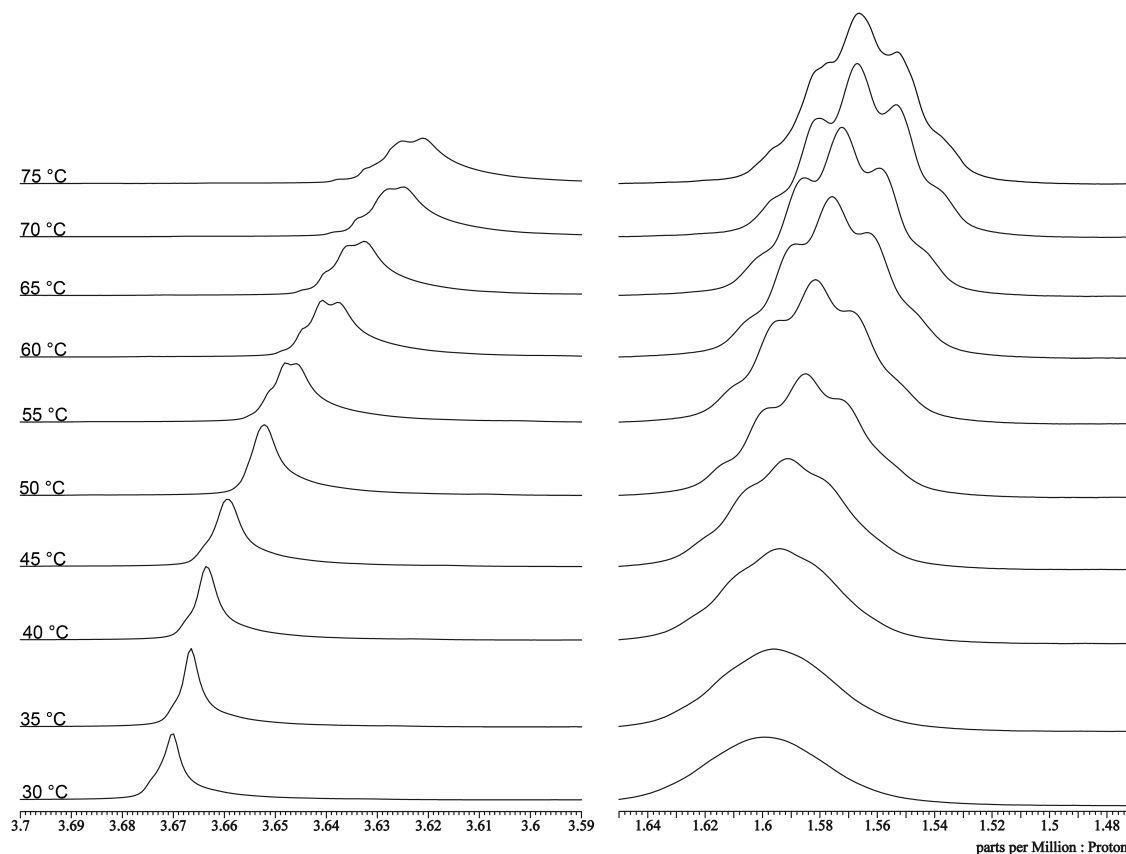


Figure II.10: Temperature dependent ^1H NMR spectra of PEG5k-PCL10k-lPEI2500 carriers suspended in D_2O

Samples prepared for temperature dependent NMR analyses were further characterised in size and ζ -potential via DLS and LDA (Figure II.11). PCL particles increase in size starting at ~ 60 °C, probably indicating swelling and beginning disassembly due to melting. mPEG5k-PCL10k-lPEI2500 carriers, however, first gradually decrease in size between $40\sim 80$ °C, followed by rapid enlargement starting at ~ 80 °C. ζ -potentials measured at RT before and after temperature treatment revealed a decreased charge (-14.3 ± 3.4 mV), indicating an irreversible structure change.

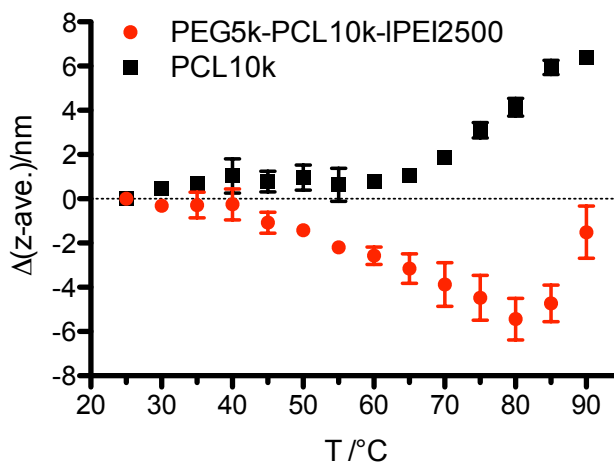


Figure II.11: Size difference of mPEG5k-PCL10k-IPEI2500 carriers in comparison to mPCL10k particles as a function of T

3.5 Analysis of stability

Colloidal stability was first analysed by determining the resistance to aggregation in presence of NaCl. PCL10k particles were compared to PEG-PCL10k-IPEI2500 carriers. An increase in turbidity (Figure II.12A), hydrodynamic diameter and PDI (Figure II.13) signed beginning PCL precipitation above concentrations of ~ 12 mM solutions of NaCl. By contrast all three tested triblock copolymers showed greatly improved stability up to the highest tested concentration of 500 mM. Next, albumin was used as a less polarising polyanion to probe the shielding effect of the PEG corona. Under these conditions stability of the three tested triblock copolymers was found to increase in a PEG MW dependent manner (Figure II.12B). PEG5k-PCL10k-IPEI2500 carriers completely resisted to aggregation up to the highest tested concentration (10 mg/mL).

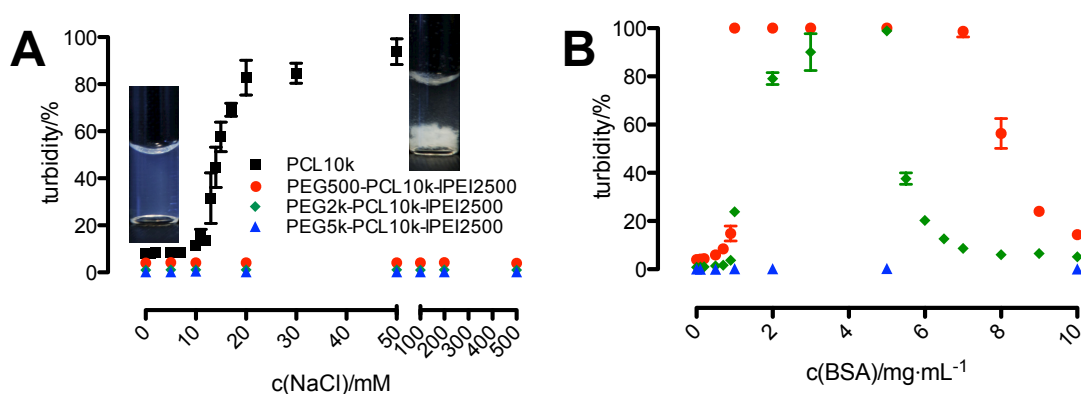


Figure II.12: Stability against NaCl (A) and albumin (B); values presented as means from at least three measurements \pm standard deviation

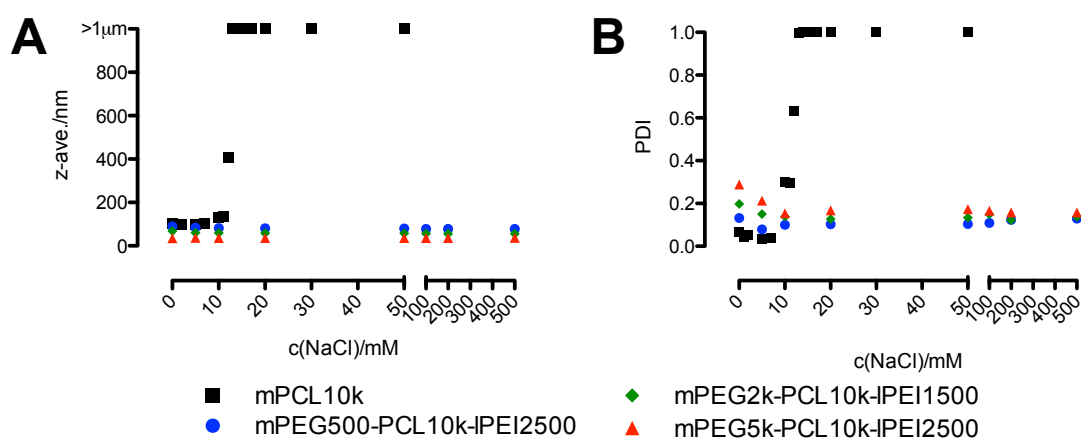


Figure II.13: Hydrodynamic diameter (A) and PDI (B) of nano-carriers with different PEG shell thickness as a function of NaCl concentration monitored by DLS; increase in size and PDI sign PCL aggregation

At concentrations above ~ 5 mg/mL aggregated PEG500 and 2k containing carriers were found to resuspend, most likely due to an albumin coating layer leading to peptisation. This is in agreement with ζ -potential measurements at different electrolyte concentrations, showing a reversal of the charge sign between 2~4 mg/mL for all the three compounds (Figure II.14). Thus improved stability of the PEG5k compound is truly due to PEG repulsion, as it has proven to be stable despite charge neutrality.

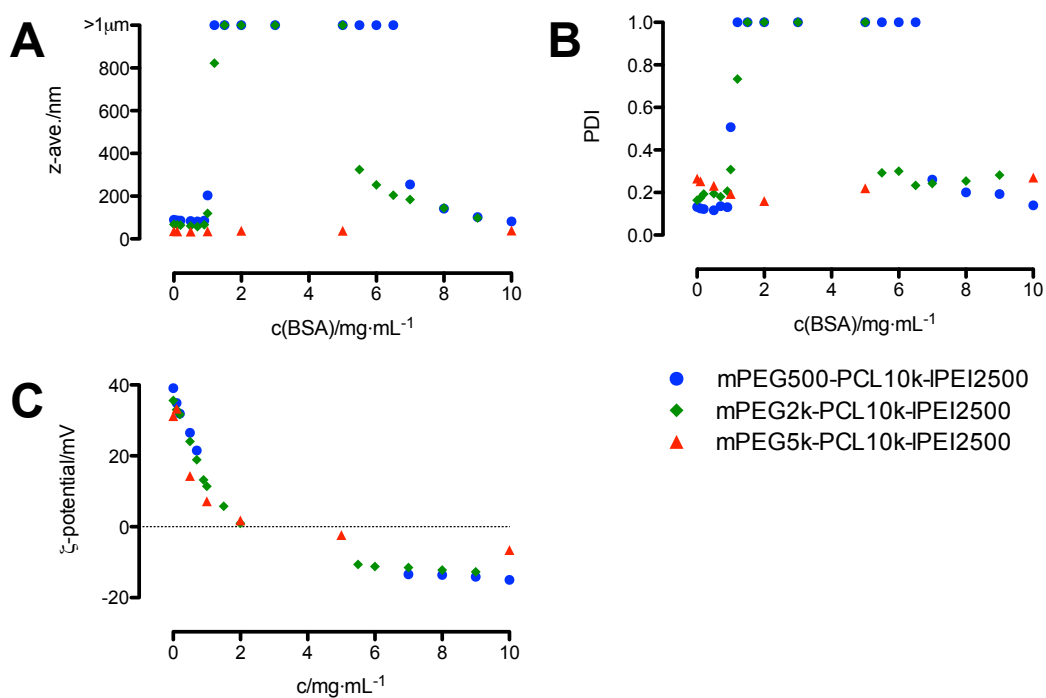


Figure II.14: Hydrodynamic diameter (A), PDI (B) and ζ -potential of nano-carriers with different PEG shell thickness as a function of albumin concentration monitored by DLS; increase in size and PDI sign aggregation mPEG500 and mPEG2k bearing carriers in a PEG length dependent manner; reversal of the ζ -potential charge sign 2~4 mg/mL

Further, thermodynamic stability of more hydrophilic, micelle-like carriers (PEG-PCL2400-IPEI2500) was probed utilising CMC measurements. For the three different PEG500, 2k and 5k compounds CMC values were found to be 0.408, 0.374 and 0.268 $\mu\text{g}/\text{mL}$. Together with the molecular weight, determined by NMR measurements, molar concentrations ($6.0 \cdot 10^{-7}$, $5.5 \cdot 10^{-7}$, $2.6 \cdot 10^{-7}$ M) as well as the free energies (ΔG° , -41.2, -41.4, -43.3 kJ/mol) were calculated according to Equation II.4, with the gas constant R ($8.31 \text{ J} \cdot \text{mol}^{-1} \cdot \text{K}^{-1}$) and the CMC in mol/L (Figure II.15, Table II.3).

$$\Delta G^\circ = RT \cdot \ln(\text{CMC}) \quad (\text{II.4})$$

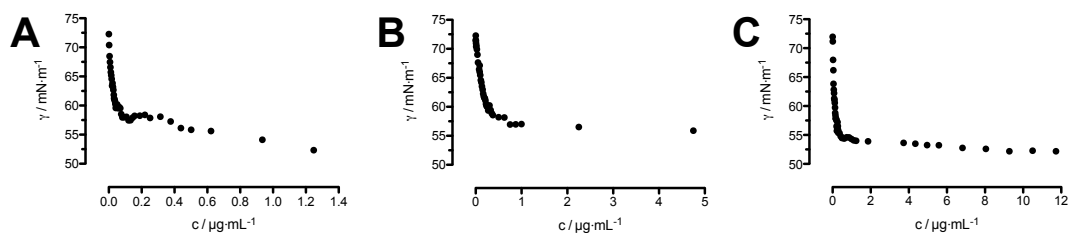


Figure II.15: CMC determination of hydrophilic copolymers mPEG500-PCL2400-IPEI2500 (A), mPEG2k-PCL2400-IPEI2500 (B) and mPEG5k-PCL10k-IPEI2500 (C) via tensiometer (Willhelmy Plate) measurement; CMC determined as the intercept of two linear regressions

Table II.3: CMC and ΔG° values calculated using MWs derived from ^1H NMR analyses

compound	CMC/mg·mL ⁻¹	CMC/10 ⁻⁸ mol·L ⁻¹	ΔG° /kJ·mol ⁻¹
PEG500-PCL2400-IPEI2500	0.408	6.0	-41.2
PEG2k-PCL2400-IPEI2500	0.374	5.5	-41.4
PEG5k-PCL2400-IPEI2500	0.268	2.6	-43.3

3.6 Cytotoxicity assay

MTT assay was utilised to determine *in vitro* cytotoxicity of carriers assembled from more hydrophobic PEG-PCL10k-IPEI2500 polymers, IPEI2500 was included for comparison reasons. By contrast to water-soluble compounds, MTT assay was utilised to determine carrier's cytotoxicity considering its three-dimensional structure. Cytotoxicity was found to decrease with increasing PEG molecular weight. Furthermore, all block copolymer compounds were less toxic compared to IPEI2500 (Figure II.16). bPEI25k Da, tested under the same conditions, was found to be more toxic (IC₅₀: 7.5±0.5 μg/mL).

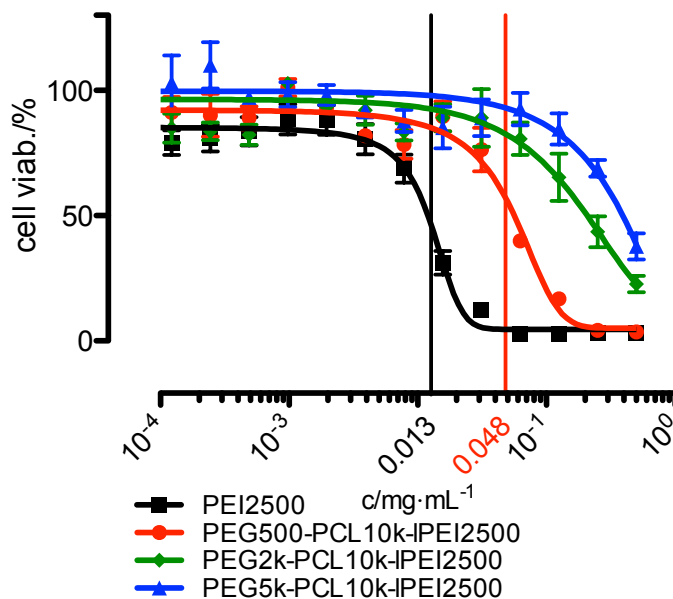


Figure II.16: Cytotoxicity of polymers bearing different PEG MWs in comparison to IPEI2500 determined by MTT assay; values presented as means from four measurements \pm standard deviation

4 Discussion

A flexible carrier system, forming structures well positioned between particles and micelles, was successfully synthesised and characterised to elucidate the structure activity relationship of carriers intended for drug and gene delivery. Compared to coupling methods using Dicyclohexylcarbodiimide/*N*-Hydroxysuccinimide chemistry [77], the synthesis route offers fewer steps, milder reaction conditions and a more effective purification [79]. Apart from ammonium salt in the second reaction step, the absence of by-products allows straightforward purification by simple precipitation. By contrast to physically adsorbed PEG or surfactants coated on the particle surface, covalently bound PEGs were proven to be more effective in shielding [20].

Sizes of carriers, assembled from those polymers, were demonstrated to decrease with increasing polymer hydrophilicity. Similar trends in size have previously been reported on the basis of PEG-poly(lactide) (PEG-PLA) [103], PEG-poly(lactide-co-glycolide) (PEG-PLGA) [20] and PEG-PCL [53] diblock as well as PCL-PEG-PCL [46] triblock copolymers. Even microparticles from PEG-PCL diblock copolymers prepared via double emulsion technique follow the same rules [44]. Amphiphilic triblock copolymers consisting of PEG (~ 2 kDa), PCL (~ 10 kDa) and cationic poly(2-

aminoethyl ethylene phosphate) (PPEEA), synthesised by Wang *et al.*, formed carriers of 100~120 nm in diameter [75]; more hydrophilic carriers with similar structure bearing a shorter PCL segment (~3.5 kDa) lead to considerable smaller assemblies (~60 nm) [73]. Unimodal PDI values indicate the absence of subpopulations with different degrees of association [56]. Gradually increasing PDI values with increasing hydrophilicity are somehow unexpected, as PDI is supposed to decrease with the formation of higher ordered structures [93]. As observed in this experiment an increasing PDI for micelle-like carriers, however, might reflect the dynamic nature of these associates. Systematic studies focusing on size and structure of carriers made from amphiphilic cationic triblock copolymers have, to our knowledge, not yet been reported.

Trends in size can be explained by different assembly mechanisms, leading to distinct carrier structures. In case of hydrophobic polymers, formation is mainly governed by polymer agglomeration, leading to larger (> 100 nm) particle like precipitates. In FALT measurements, those aggregates were demonstrated to bear less charge density, surrounded by a smaller, less dense PEG shell. Assembly mechanism was clarified by formation at varying initial polymer concentration: As size is controlled by the local polymer concentration at the particle formation site, higher polymer concentrations subsequently lead to larger particles. As to more hydrophilic polymers, rather small (<40 nm) core corona polymeric micelles are formed. The PEG block exerts a strong effect on micelle formation, by moderating association of polymer molecules and preventing agglomeration of PCL segments. Those micelle-like structures were shown to have a higher charge density plus a thicker PEG shell (FALT measurements). Formation mechanism of micelle-like carriers is unaffected by initial polymer concentration, as geometry of polymer unimers rather than their concentration controls the size of a micellar system. These structural differences between hydrophobic and more hydrophilic carriers have a considerable impact on carrier properties and are supposed to affect vector efficiency as well.

FALT was employed for measuring the thickness of the covalently bound PEG shell. FALT is a reliable technique, e. g. for measuring the amount of hydrophilic polymer coated onto negatively charged liposomes [112], polystyrene (PS) [113] or PLGA [109] nanoparticles. Thicker hydrophilic layers have proven to enhance protein-repelling properties and affect biodistribution profiles [18]. By giving the distance from the outer PEG sphere to the positively charged core surface, measurements in particular contribute to structure elucidation, indirectly constituting the PCL-PEG core shell structure with PEI accessible located at the interface. Resulting sizes depend on PEG chain length and are in the same order of magnitude than

those determined on PEG2k modified liposomes [112] and micelles [18]. Further, values are in good agreement with theoretical calculations assuming a randomly coiled chain. Slightly lower experimental values, especially in case of increasing PEG MW, may be explained by the formation of loops and tails that are anchored to the PCL surface.

Electrochemical characteristics (Ψ_0 , σ_0 and the number of positive charges on the particle surface) were derived from FALT measurements. Ψ_0 values obtained were close to ζ values as generally observed for moderately charged colloidal systems. As shown in case of liposomes [111], σ_0 is a characteristic indicator for colloidal stability. The number of positive charges on the PCL core surface was found to decrease with increasing polymer hydrophilicity. This in particular points to an effect on the aggregation number of each polymer sphere; assumed that PEI charges are exclusively located on the PCL surface, a carrier bearing less charge subsequently contains fewer polymer molecules. Hence decreasing carrier sizes with increasing hydrophilicity seem to result in decreasing aggregation numbers, which has been clarified above in carrier formation experiments as a function of initial polymer concentration. This phenomenon could be explained by the occupied area per corona chain, which is decreasing with decreasing PEG chain length. To minimise interfacial energy attributed to the corona chain, the aggregation number and the core size increase. From a more visual point of view one could argue with molecular geometry [51]: with increasing PEG chain length the hydrophilic head becomes more bulky, which leads to a more cone shaped molecule; forming a micelle from these molecules leads automatically to a smaller sphere than in case of more cylindrical shaped molecules [103].

^1H NMR measurements in solvent mixtures and as a function of temperature were utilised to further elucidate carrier's core-shell structure. When internal intermolecular motion is restricted, nuclear spin-spin relaxation (T_2 relaxation) is decreased, which leads consequently to a broadening of line widths [81]. In D_2O /acetone- D_6 solvent mixtures, PCL signals successively broaden with increasing D_2O concentration, whereas PEG signal keeps fairly constant. These findings correspond to carrier-structure in aqueous media: Due to H-bonding between ether oxygens and water molecules, PEG segments create an exterior hydrophilic corona, preserving most of their mobility characteristics. PCL groups are in a different environment, forming a central hydrophobic core by minimising solvent interaction. Line broadening of PCL signals occurs due to restricted motion inside the hydrophobic core, while PEG is an extended solvated state in all different solvent mixtures. The slight broadening at the base of PEG signals is expected for a flexible PEG chain at the

end of a rigid PCL core and originates from PEG protons in more than one chemical environment. Those are preferably located at the core facial region, suggesting partial miscibility of PEG and PCL domains. Notably, in comparison PLA-PEG or PLGA-PEG NPs [60], signals of hydrophobic protons in D₂O are suppressed, but could still be observed. This is also the case for surfactant micelles with a liquid-like core [114], which conforms to the hypothesis of micellar dynamics and demonstrates that prepared polymeric carriers are truly in an intermediate state between micelles and particles. Increased core mobility of PCL in comparison to PLA or PLGA might occur due to glass transition temperatures: Whilst for mPCL10k T_g was observed at ~ 60 °C via DSC, glass transition temperatures of PLA or PLGA typically exceed RT (depending on tacticity, crystallinity and in case of PLGA composition) leading to “frozen” micelles in the latter case [115]. In ¹H NMR spectra at higher temperatures, line broadening for PEG signals increases whilst there is a decrease of PCL signals. Similar trends have previously been reported on PEG-PLA structures [60] and suggest that changes in structure and conformation have taken place: With a temperature increase above the lower critical solution temperature (LCST) of PEG (~ 70 °C [60]) the polymer chains turn from hydrophilic to hydrophobic due to a breakage of hydrogen bonding and subsequently collapse onto the hydrophobic carrier core, losing most of their mobility. This leads to a gradual decrease in PEG signal intensity at higher temperatures. Additionally the shift upfield of the PEG signal suggests movement to a less polar environment [114]. However, the higher temperature had an impact on core mobility as well, which leads to a higher amount of PCL protons detectable and increased resolution. Especially above the T_g of PCL (~ 60 °C by DSC), it should be even easier to observe PCL protons, since chain mobility would be greater.

Measuring z-ave and ζ -potential of samples prepared for temperature dependent NMR analyses as a function of T revealed differences between mPEG500-PCL10k-IPEI2500 carriers and mPCL10k particles: The latter increase in size starting at ~ 60 °C, probably indicating swelling and beginning disassembly due to melting. mPEG5k-PCL10k-IPEI2500 carriers, however, first gradually decrease in size between 40~80 °C, followed by rapid enlargement starting at ~ 80 °C. This is in agreement with temperature dependent NMR experiments, suggesting PEG dehydration overlaid by an increase in size due to melting of the PCL core. Maximum detected decrease in size (~ 5 nm), determined at 80 °C, is consistent with FALT measurements. A decreased charge of nano-carriers after temperature treatment indicates an irreversible structure change, suggestive for irreversible phase mixing of PCL and PEI moieties in the molten state.

For finding a structure activity relationship, the impact of different structures on subsequent carrier features like colloidal stability was demonstrated. While increasing ionic strength, PEG steric shielding is supposed to decrease due to a breakdown of hydrogen bonding between PEG ether oxygens and water molecules and a subsequent dehydration of the outer shell. Additionally the electrolyte neutralises core surface charge and Van der Waals interaction between PCL cores will lead to aggregation. Against NaCl, all triblock carriers showed increased stability compared to naked PCL particles. On the one hand this could be due to the sterically shielding PEG layer, but on the other hand positive PEI charges could also further stabilise colloidal suspensions due to repulsive Coulomb forces. In the latter case, according to the principle of hard and soft acids and bases, a rather “soft” polyanion would be more suitable for PEI charge neutralisation than chloride. In experiments with albumin, enhanced colloidal stability for carriers bearing longer PEG chains was clearly demonstrated. Hence, smaller core corona micelle-like carriers were more stable against albumin-induced aggregation than bigger particles surrounded by a thinner less dense PEG shell. This is probably owed to incomplete PEG coating leading to naked PCL patches on the particle surface [62]. Increasing colloidal stability against electrolytes with increasing PEG MW has previously been reported based on PEG-PLA carriers [56]. In case of triblock copolymers presented in this work steric PEG shielding is of prime importance, as stabilising positive charge is reduced upon complexation with negatively charged drugs or nucleic acids.

CMC values, reflecting thermodynamic stability, were found to be in the range of concentrations determined for PEG-PCL [52], PEG-PCL-PEG [46] or PEG-PCL-PPEEA [74] amphiphiles. As carriers are rapidly diluted upon intravenous injection, low CMC values are important prerequisites for *in vivo* experiments. But even at concentrations below CMC values, carriers are not necessarily supposed to fall apart. Micelles formed from block copolymers are commonly also more kinetically stable than those formed from low molecular weight surfactants [42]. Physical interaction of core chains and semi-crystalline moieties [47] decrease the dynamic nature of formed micelles, making carriers less prone to disassembly. Negative ΔG° values prove advantageous thermodynamic stability compared to low MW amphiphiles, as generally observed for polymeric micelles; values in the same order of magnitude, hardly depending on PEG molecular weight, are suggestive for a self-assembly process, hypothesised for all of the hydrophilic carriers bearing short PCL2400 blocks.

Finally the impact of carrier structure on cytotoxicity was investigated utilising a MTT assay. As expected longer PEG chains resulted in reduced toxicity. Generally, charge neutralisation (e.g. by loading with negatively charged compounds [17]) and

sterical shielding (commonly by PEG) are strategies to reduce cytotoxicity. Hence, experiments with placebo carriers in this work reflect the worst-case scenario. Toxicity analysis comparing PEG-PEI block copolymers with different PEG MW and grafting degree revealed, that the number of PEG chains, rather than their MW affects cytotoxicity [116]. However, in those experiments water-soluble PEG-PEI compounds were investigated and charge shielding was mainly dependent on the grafting degree. This work focused on self-assembled carriers of different size and structure. Consequently effective charge shielding depends on the density and thickness of the outer PEG shell, which was found via FALT measurements to increase in size with larger PEG MW. In summary, toxicity tests complete structure activity investigations carried out in this work: Polymers with increased hydrophilicity were found to assemble to smaller, micelle-like carriers with a thicker PEG shells. Those compounds showed decreased ζ -potential and charge density. Fewer charges, surrounded by a larger PEG shell therefore resulted in increased colloidal stability and reduced cytotoxicity.

5 Conclusions

A set of PEG-PCL-PEI triblock copolymers was successfully synthesised and characterised. Block lengths were systematically altered to elucidate the structure activity relationship. As a function of hydrophilicity different assembly mechanisms lead to diverse structures: whereas more hydrophilic carriers assembled to micelle-like structures with core-corona architecture and diameters of several tens of nanometers, more hydrophobic polymers precipitated to larger (>100 nm) particulate carriers. Changes in size were found to result from varying aggregation numbers. Carrier architecture was elucidated (cryoSEM, AFM, ^1H NMR, FALT) and correlated to stability and cytotoxicity: Increasing hydrophilicity results in stability increase, combined with a decrease of cytotoxicity due to effective PEG charge shielding. Those trends in size, structure and properties are fundamental and may be applicable for numerous amphiphile based vector systems in the field of drug and gene delivery. Rather than identifying suitable vectors by trial and error, a more systematic approach was investigated in this work. This strategy could be the key to tailoring the properties of multifunctional carriers.

Acknowledgments

We thank Thomas Kämpchen and Stefan Newel (Institute of Pharmaceutical Chemistry, Philipps-Universität Marburg) for their excellent support with NMR spectroscopy. Andreas Schaper and Michael Hellwig (WZMW, Philipps-Universität Marburg) are gratefully acknowledged for supporting us with cryoSEM. We are grateful to Roelf-Peter Baumann (Department of Physical Chemistry, Philipps-Universität Marburg) for his kind assistance with AFM.

Part III

Optimising the self-assembly of siRNA loaded PEG-PCL-IPEI nano-carriers employing different preparation techniques

Authors

Thomas Endres, Mengyao Zheng, Moritz Beck-Broichsitter, Olga Samsonova, Heiko Debus, Thomas Kissel^a

Authors' contributions

RNase assay and RT-PCR were carried out by Mengyao Zheng. SYBRTM Gold assay was conducted by Mengyao Zheng and Olga Samsonova. CryoTEM images were obtained by Frank Steiniger (Elektronenmikroskopisches Zentrum, Universität Jena). All other experiments were carried out by Thomas Endres. Manuscript was written by Thomas Endres.

Published in J. Controlled Release 160 (3) (2012), 583–591.

^acorresponding author

Abstract

Amphiphilic cationic block copolymers consisting of poly(ethylene glycol), poly(ϵ -caprolactone) and poly(ethyleneimine) spontaneously assemble to nano-sized particulate carriers, which can be utilised for complexation of nucleic acids (small-interfering RNA), representing a multifunctional vector system, designed for drug and gene delivery. Apart from polymer design and charge ratio, a more homogeneous complexation could lead to a more uniform charge distribution, subsequently increasing colloidal stability, RNA protection and consequently transfection efficiency. Microfluidic mixing techniques, bringing cationic polymer and nucleic acid together at a constant ratio during the entire mixing process, have the potential for a gentler complexation. In the present study carriers were prepared by a solvent displacement technique. In a first step complex size for addition of RNA during (addition to the aqueous or the organic phase) or after (classical pipetting or microfluidic mixing) carrier assembly was determined by dynamic light scattering. Suitable N/P ratios have previously been selected by measuring size and ζ -potential as a function of N/P. Subsequently, for the most promising techniques (loading after assembly), colloidal stability, the ability to protect RNA as well as transfection efficiency *in vitro* were compared. Finally, parameters for the superior microfluidic mixing process were optimised with the help of a central composite design. Generally, gentler loading leads to more homogeneous complexes. Hence, possibly due to a more consistent surface coating, loading after carrier assembly resulted in less aggregation. In comparison to bulk mixing, microfluidic assembly exhibited smaller diameters (179 ± 11 vs. 230 ± 97 nm), less heterogeneity (PDI= 0.205 ± 0.028 vs. 0.353 ± 0.161), enhanced RNA protection (RNA recovery= 30.6 ± 1.0 vs. $15.4\pm 1.4\%$) as well as increased transfection performance (34.8 ± 1.5 vs. $24.5\pm 2.2\%$ knockdown). Therefore, microfluidic complexation represents a reproducible alternative for formulating gene delivery carriers with superior colloidal stability, RNA protection and transfection efficiency.

1 Introduction

Administration of small-interfering RNA (siRNA) represents a promising strategy to address various diseases currently considered untreatable. However, transition to clinical trials has been slow due to a lack of suitable carrier systems [101]. Basic requirements for those vectors are: stability, biocompatibility and biodegradability, low toxicity, targeting of specific cells or tissues, the ability to protect nucleic acids from rapid degradation or excretion. The latter is critical in case of siRNA, as it is even more susceptible to degradation than DNA [6]. A class of carriers, having the potential to comply with most carrier requirements, is based on cationic amphiphiles [73, 117]. In aqueous media block copolymers, consisting of poly(ethylene glycol) (PEG), poly(ϵ -caprolactone) (PCL) and linear poly(ethyleneimine) (lPEI), self-assemble spontaneously to core-shell structured nano-carriers [77, 118]. The hydrophilic PEG shell is thought to reduce protein adsorption while maintaining suspension stability, possibly leading to increased blood circulation times *in vivo* [119]. Biodegradable PCL segments, aggregated to a hydrophobic core, could serve as reservoirs for water-insoluble drugs or dyes rendering this carrier system multi-functional for co-delivery of drugs and nucleic acids or for “theranostic” purposes [69]. Cationic PEI segments can be utilised for complexation with nucleic acids (e.g. siRNA). Structure and self-assembly properties of these polymers were previously investigated [118]. While most studies focused on designing adequate carrier molecules, scant attention has been paid to the complexation process itself, even though it has a crucial effect on essential complex characteristics [120, 121], the ability to protect nucleic acids from degradation and subsequently on gene delivery efficiency. One of the most important parameters for complexation is the ratio of positively charged carrier and negatively charged nucleic acid molecules, which is generally calculated on the basis of PEI nitrogen per nucleic acid phosphate (N/P). With decreasing N/P, overall surface charge decreases progressively to the point of aggregation at nearly neutral conditions. Net charge has a direct influence on cell internalisation [122] and toxicity [104, 33]. High positive surface charge might, up to a certain degree, lead to enhanced cell internalisation *in vitro* [6], but it will definitely be detrimental under *in vivo* conditions, where cationic carriers are in contact with negatively charged blood components and tissue membranes. Furthermore, due to toxicity concerns, in most scenarios N/P is rather fixed and it would be advantageous to control complex characteristics without altering the ratio of polymer and nucleic acid. Different complexation conditions and techniques offer the opportunity for optimising carrier loading at fixed N/P. Typical complexation procedure for water-soluble cationic polymers comprises mixing of aqueous polymer and nucleic

acid solutions by pipetting [120], whereas the order of addition is unclear: Some experimenters prefer addition of cationic polymer solution to a solution of nucleic acid [74, 123, 124], while others favour vice versa [82]. Moreover, a dependency on the N/P has been claimed [125]. In addition, predominantly hydrophobic assemblies with a rather rigid structure are capable of loading after carrier formation, which is believed to be advantageous for controlling complex size and charge [74, 123]. More recently, fluidic mixing techniques have emerged [126]; these automated devices, bringing cationic polymer and nucleic acid together at a constant ratio during the entire mixing process, have the potential to increase complex homogeneity and avoid order of addition problems. Fluidic setups have been employed for creation of micro droplets by mixing two immiscible solvents [127] or (as used in the present study) for mixing aqueous phases. In the latter case fabrication of poly- or lipoplexes using mm- [120, 128] or μm -scaled [129, 130] channels has been reported, whereas smaller volumes (as utilised in the present study) promise even greater control, due to a more confined diffusion [127]. In case of all preparation conditions and techniques, a more homogeneous complexation process is supposed to give rise to a tighter complexation. This is believed to increase colloidal stability and siRNA protection. More uniform complexes with enhanced stability and a size suitable for endocytosis (150-200 nm [131, 6]) are easier to characterise and are thought to boost transfection efficiency. To prove this hypothesis, it was the aim of the present study to correlate different complex preparation techniques to subsequent carrier properties. Therefore, two complexation techniques after carrier assembly (classical pipetting and microfluidic mixing) were compared to two methods during assembly (addition of siRNA to the aqueous or the organic phase) and the effect on complex size was monitored by dynamic light scattering (DLS). Furthermore, for the two most promising techniques, complex stability as a function of incubation time (10-240 min), resistance of condensed siRNA against degradation (RNase digestion) as well as transfection efficiency *in vitro* were evaluated. Among all employed techniques, microfluidic mixing facilitates gentler preparation conditions and therefore represents a promising alternative for complexation of nucleic acids.

2 Materials and methods

2.1 Reagents and chemicals

Non-coding control DsiRNA and hGAPDH-DsiRNA for RT-PCR experiments as well as 2'-O-methylated 25/27mer DsiRNA targeting Firefly Luciferase for all other complexation experiments were purchased from Integrated DNA Technologies (IDT,

Leuven, Belgium). Fetal Calf Serum used in stability and transfection experiments was obtained from Cytogen (Sinn, Germany). Heparin sodium (150000 IE/g) for displacement of siRNA was applied from SERVA Electrophoresis (Heidelberg, Germany). First Strand cDNA Synthesis Kit and RNase I (#EN0531) were obtained from FERMENTAS (St. Leon-Rot, Germany). QuantiFastTM SYBRTM Green PCR Kit, Hs_GAPDH_primer, Hs_β-actin-primer and DNase I (18U) were provided by Qiagen (Hilden, Germany). SYBRTM Gold reagent, LipofectamineTM 2000 (LF) and PureLinkTM RNA Mini Kit were applied from Invitrogen (Karlsruhe, Germany). Other chemicals and solvents were supplied by Sigma Aldrich GmbH (Steinheim, Germany) at the highest grade commercially available.

2.2 Polymer synthesis and characterisation

PEG-PCL-IPEI triblock copolymer was synthesised and characterised as described in detail elsewhere [118]. Block length for PEG, PCL and PEI are 500, 10000 and 2500 Da, respectively.

2.3 Cu²⁺-assay

Cu²⁺ assay was utilised to determine the amine fraction per overall polymer mass [105]. Polymers were dissolved in a mixture (1:1) of double-distilled and filtrated water and N-Methyl-2-pyrrolidone in concentrations of 0.4 mg/mL. 50 μL of this solution were mixed vigorously with 50 μL of an aqueous CuSO₄ solution (c=0.145 mg/mL dissolved in 0.1 N potassium acetate buffer, pH=5.5). Subsequently absorption was measured at 280 nm employing a Pharmacia Biotech Ultrospec 3000 (GE Healthcare, Little Chalfont, Buckinghamshire, UK). Using a IPEI2500 Da calibration curve, the amount of PEI per overall polymer mass was calculated.

2.4 Assembly of unloaded nano-carriers

Nano-carriers were prepared by a solvent displacement technique described in detail elsewhere [132]. Briefly, 1 mg of block copolymer was dissolved in 200 μL of acetone. This solution was subsequently injected into a magnetically stirred (500 rpm) phase of 1 mL double-distilled and filtrated water. The resulting colloidal suspension was stirred for 3 h under reduced pressure to remove organic solvent. Nano-suspensions (NSs) were characterised and used directly after preparation.

2.5 Carrier loading by different techniques

Two different post-assembly loading techniques were applied: conventional mixing by pipetting aqueous siRNA solution to previously prepared unloaded NSs (**T1**) and microfluidic-assisted mixing (**T2**). In case of conventional carrier loading for each measurement a fresh sample was prepared. The appropriate amount of siRNA was added to an aliquot of NS in one single step followed by vigorous mixing. Size and ζ -potential were measured after 10 min of incubation at room temperature (RT). For microfluidic-assisted loading, the Fluence Microfluidic Tool Kit (Epigem Ltd., Redcar, UK) was used. Setup consisted of a three-way mixing chip (50-100R3), plugged onto the baseboard (Fig. 2). Chip inlets were independently fed with NS and aqueous siRNA solution employing syringe-pump drives (Aladdin-1000, World Precision Instruments, Sarasota, USA) equipped with 500 μ L syringes (Hamilton, Bonaduz, Switzerland). Flow rate (FR) ratio and/or concentration of fluids were modified to adjust final carrier loading ratio. Up to reaching dynamic equilibrium the first 200 μ L of each run were discarded. Subsequently loaded carriers were collected and characterised directly after preparation. For loading during solvent displacement process, carriers were assembled with additional siRNA in the water (**T3**) or acetone phase (**T4**) and mixed vigorously before organic phase injection. Size and ζ -potential were measured directly after carrier assembly.

2.6 Cryogenic transmission electron microscopy (cryoTEM)

CryoTEM was carried out as described in detail elsewhere [133]. Briefly, 6 μ L NS were placed on a perforated copper grid (R 3.5/1, Quantifoil Micro Tools GmbH, Jena, Germany) and the sample was frozen in liquid ethane (\sim -180°C) in a cryo box (Carl Zeiss NTS GmbH, Germany). The sample was then transferred with a liquid nitrogen cooled holder (626, Gatan Inc., USA) into the pre-cooled cryo-electron microscope (CM 120, Philips, Netherlands) operated at 120 kV and viewed under low dose conditions. The images were recorded with a 1k CCD Camera (FastScan F114, TVIPS, Gauting, Germany).

2.7 Size and ζ -potential

The average size and size distribution as well as the ζ -potential of nano-carriers were determined by DLS and laser Doppler anemometry (LDA) using a Zetasizer NanoZS/ZEN3600 (Malvern Instruments, Herrenberg, Germany) equipped with low volume sizing- (ZEN2112) or ζ -cell (ZEN1010). Analyses were performed at a temperature of 25 °C using samples appropriately diluted with filtrated and double-

distilled water. The particle mean diameter (z-ave.), the width of the fitted Gaussian distribution, which is displayed as the polydispersity index (PDI), as well as the average ζ -potential values were calculated from data of at least 10 runs.

2.8 Stability

Stability of complexes, assembled ($c(\text{RNA})=100 \mu\text{M}$, $c(\text{NS})=0.5 \text{ mg/mL}$) by classical pipetting (**T1**) and microfluidic mixing (**T2**), was investigated via DLS at respective N/P ratios (9, 13, 20) in filtrated and double-distilled water as well as in serum (10% of bovine serum was added 10 min after carrier assembly). Values were determined after $t=30, 60, 120, 240$ min in comparison to $t_0=10$ min. Changes in z-ave. and PDI are displayed as variations in the ratio of final and initial values (t/t_0).

2.9 RNase assay in presence of heparin

Firstly, stability of carriers was tested by measuring siRNA displacement from complexes in presence of the competing polyanion heparin. $30 \mu\text{L}$ aliquots of complexes, freshly-prepared by classical pipetting or microfluidic mixing at N/P=9 ($c(\text{RNA})=100 \mu\text{M}$, $c(\text{NS})=0.5 \text{ mg/mL}$), were incubated with heparin at various concentrations (6.25, 12.50, 31.25, 43.75, 62.50, 312.50, 625.00 mg/L) in PBS buffer (pH=7.4) for 20 min at RT. Subsequently, SYBRTM Gold intercalation assay was carried out as previously reported [134]. Fluorescence intensity ($\lambda_{ex}=495 \text{ nm}$, $\lambda_{em}=537 \text{ nm}$) was analysed in opaque FluoroNunc 96 well plates (Nunc, Thermo Fisher Scientific, Langenselbold, Germany) using a Safire II (Tecan Group Ltd., Männedorf, Switzerland). Uncomplexed siRNA served as a positive control and relative amounts of displaced siRNA at respective heparin concentrations were calculated. Subsequently, to prove stability and integrity of siRNA complexes, RNase digestion in presence of heparin was investigated. Above-mentioned complex-heparin mixtures were repeatedly prepared with additional RNase ($9 \mu\text{g}/\text{aliquot}$). The samples were then incubated for 1 h at $37 \text{ }^\circ\text{C}$ and additional 30 min at $70 \text{ }^\circ\text{C}$ to inactivate RNase. Intact siRNA was then displaced from the polymer by adding excess heparin ($50 \mu\text{g}/\text{aliquot}$) and detected via SYBRTM Gold intercalation assay. Relative values of recovered siRNA were calculated and the total amount of displaced siRNA in presence of heparin plus recovered siRNA in presence of heparin and RNase was normalised to 100%.

2.10 RT-PCR

SKOV3 cells were seeded in 6-well-plates (Nunc, Thermo Fisher Scientific, Langensfeld, Germany) at a density of 5000 cells/well, 24 h before transfection. Subsequently, fresh medium (containing 10% bovine serum) and 100 μL of NS, loaded via **T1** and **T2** at N/P=9 (c(RNA)=100 μM , c(NS)=0.5 mg/mL), were added to each well at a final siRNA concentration of 100 pmol/well. LF (0.5 μL /10 pmol of siRNA) served as a positive control. After 4 h of incubation at 37 °C, medium was exchanged and cells were incubated for another 24 h before they were washed with cold PBS and lysed with lysis buffer. Afterwards, mRNA was isolated from culture cells using the PureLinkTM RNA Mini Kit (with additional DNase I digestion) and reverse transcribed to cDNA employing the First Strand cDNA Synthesis Kit on a TGradient thermocycler (Biometra GmbH, Goettingen, Germany). RT-PCR was performed employing the SYBRTM Green PCR Kit and a Rotor-Gene 3000 RT-PCR thermal cycler (Corbett Research, Sydney, Australia). Hs_GAPDH-primers were used to quantify hGAPDH_gene expression and Hs_ β -actin-primers were utilised as internal standard to determine relative expression levels for each gene. Calibration curves for GAPDH and β -actin mRNA were prepared by serial dilutions of cDNA of the blank sample (untreated cells).

2.11 Response surface design

Parameters for microfluidic carrier loading were optimised employing a response surface design. An orthogonal circumscribed central composite design, which includes additional centre and star points, (24 + 2·4 star points + 4 centre points, $\alpha=1.607$) was chosen to study the effect of four factors on z-ave. (Table III.1) in 28 runs. The order of experiments has been fully randomised to avoid bias. Factors of interest and their limits were determined in preliminary experiments. Intervals were chosen to maintain the orthogonalised values of the design. NS was prepared under constant conditions as described above to minimise variability. For statistical analysis the Statgraphics Plus software (V2.1, Statpoint Technologies, Warrenton, Virginia, USA) was utilised.

2.12 Statistics

Unless otherwise noted, all measurements were carried out in quadruplicates and values are presented as mean values \pm standard deviation. To identify statistically significant differences, ANOVA with t-test analysis was performed. Probability

values of $p < 0.05$ were considered as statistically significant (* $p < 0.05$, ** $p < 0.01$, *** $p < 0.001$).

3 Results and discussion

3.1 Aggregation behaviour as a function of N/P

Z-ave. and ζ -potential of unloaded carriers were determined via DLS and LDA (85 ± 5 nm, 39 ± 2 mV). Diameters measured by cryoTEM are in a good agreement and demonstrate spherical shape (Figure III.1A). Analogous to typical “polyplex” preparation, carriers were firstly loaded by pipetting nucleic acid solution to a small batch of NS (T1). To determine an N/P range suitable for further investigations, the evolution of z-ave. and ζ -potential of complexes as a function of carrier/siRNA ratio was measured (Figure III.1B). With decreasing N/P carrier size increases from unloaded ($N/P = \infty$) up to a maximum at $N/P \approx 7$, which is attained close to the neutralisation point, as evidenced by the inversion of the ζ -potential. At lower N/P, particle diameter as well as ζ -potential decrease down to the size of ~ 130 nm and ~ -17 mV.

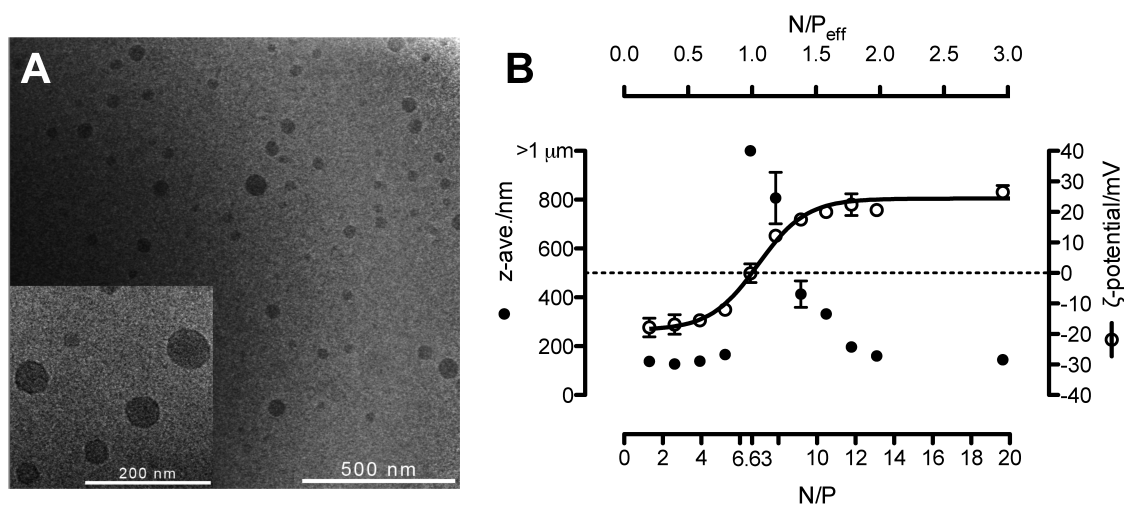


Figure III.1: CryoTEM images of blank carriers (A). Z-ave. and ζ -potential (including a sigmoidal regression) of loaded carriers (T1, $c(\text{RNA}) = 100 \mu\text{M}$, $c(\text{NS}) = 0.5 \text{ mg/mL}$) as a function of N/P obtained by DLS and LDA. N/P_{eff} was calculated by recalibrating N/P in reference to the isoelectric point. Measurements were carried out in quadruplicates and values are presented as mean values \pm standard deviation (B).

The observed aggregation behaviour, often referred to as reentrant condensation, was previously reported in a variety of polyelectrolyte-colloid systems such as micelles [135], liposomes [136] or solid particles [137]. It is defined by a balance

of short-range attractive and long-range repulsive forces [138]. The former originate from inhomogeneous surface covering, caused by electrostatic interaction. Upon surface coating, polyelectrolyte chains avoid each other, maximising their distance on the carrier surface which leads to a patchwork-like coating, comprising domains with excess positive or negative charge. The resulting dipolar structure gives rise to a short-range attractive potential. Repulsive forces stem from the net charge of like-charged carriers. With decreasing N/P, this charge decays progressively from the positive value of bare carriers, inverting its sign at the isoelectric point, down to negatively charged carriers with anionic surface coating. The addition of more counterions than necessary for neutralisation is commonly referred to as overcharging effect [138]. Close to isoelectric conditions, due to prevailing attractive forces, large clusters are observed; whilst at low N/P the size of carriers equals again their original unloaded size plus a layer of adsorbed siRNA. From here on further decreasing the N/P in equilibrium leads to an excess of siRNA, which does not adsorb to the carrier but remains freely dissolved. Due to charge sign and insufficient protection of nucleic acid, those negatively charged complexes (N/P < 7) are not suitable for cell internalisation despite their relatively small diameter. Regarding charge, size and cytotoxicity the N/P range between 9~20 appears to be attractive for further investigation. Furthermore one might argue that the N/P ratio at the isoelectric point where charges counterbalance is supposed to be 1 rather than ~7. In case of a block copolymer, calculation of the N/P requires knowledge of the protonable PEI fraction, which can be either calculated from the molecular weight (MW) of distinct blocks or by Cu²⁺-assay. The latter method, which was applied for these experiments, quantitatively determines the amount of PEI per molecular mass. However, both methods consider every single nitrogen, lacking information on the 3D structure of the complex. Hence, the observed discrepancy between calculated and expected N/P supposedly occurs due to amine groups, inaccessible for complexation with nucleic acid phosphates. This could either be due to encapsulation into the hydrophobic PCL core, or due to steric shielding of PEG moieties. Both, shielding by hydrophilic PEG [118] as well as hydrophobic PCL [139, 82] or poly(methyl methacrylate) [123] was previously demonstrated to affect toxicity and cell internalisation. Additionally, (especially at neutral or basic pH) incomplete amine protonation could further increase the gap between stoichiometric composition and experimental ζ -potential. Wang *et al.* assembled particle-like carriers from cationic PEG-PCL-poly(2-aminoethyl ethylene phosphate) amphiphiles for siRNA loading after assembly [74]. Similarly, those systems exhibited a mismatch between stoichiometric N/P (calculated from MW) and charge. Isoelectric conditions were

reached between N/P 1~5. Consequently, the effective N/P ratio (N/P_{eff}), representing the ratio of accessible nitrogen charges and siRNA phosphates for complexation, is believed to be the decisive parameter. As shown in Figure III.1B, the isoelectric point could be utilised for N/P-scale recalibration: conventional values are converted to effective ones.

3.2 Different loading techniques

Due to toxicity concerns, in most scenarios the applicable N/P range is rather limited. To reach the goal of small and uniform complexes with a slightly positive net charge, different loading techniques were compared at three different N/P ratios (9, 13, 20). Loading after assembly was carried out by classical pipetting (**T1**) or by employing a microfluidic device (**T2**) (Figure III.2).

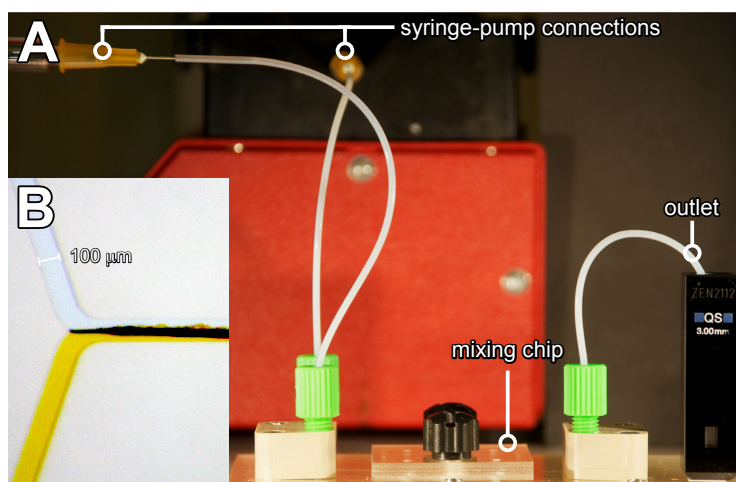


Figure III.2: Setup of the microfluidic mixing device (A). Microscope image of the mixing chip operated with aqueous Nile Blue and Fluorescein solutions (B).

For loading during assembly siRNA was added to the aqueous (**T3**) or the organic (**T4**) phase. The trend of larger diameters in the proximity of the isoelectric point was found for all tested techniques. However, especially at low N/P ratios, post-assembly loading appears to be superior for formulating compactly condensed complexes. Loading during assembly generally produced larger diameters together with greater aggregation (Figure III.3). In addition, for all tested N/P ratios microfluidic loading further reduced the carrier diameter.

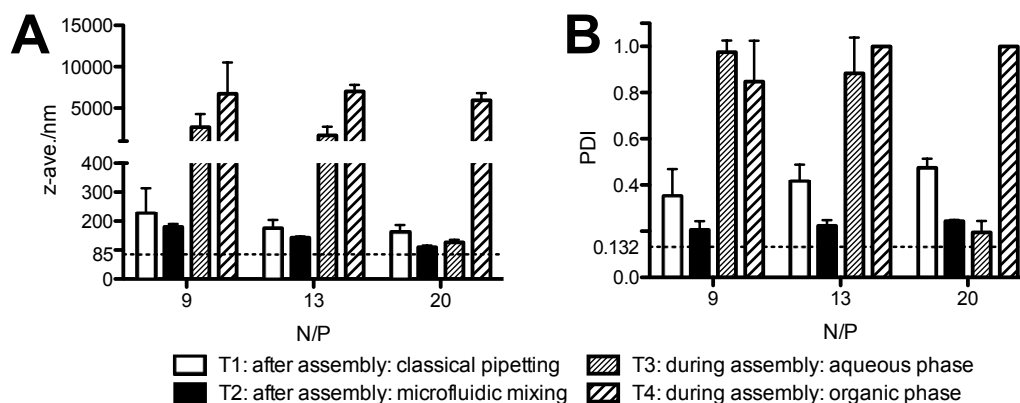


Figure III.3: Z-ave. (A) and PDI (B) of unloaded carriers ($z\text{-ave.}=85\pm 5$ nm, $\text{PDI}=0.132\pm 0.023$) in comparison to those loaded with siRNA by different techniques at defined N/P ratios (N/P ratio was determined by Cu^{2+} assay). Measurements were carried out in quadruplicates and values are presented as mean values \pm standard deviation.

Homogeneous charge distribution upon complexation is important for minimising short-range attractive forces, which will consequently lead to less pronounced aggregation peaks in the proximity of the isoelectric point. This is believed to be the reason for increased complex size in case of loading during assembly: rapid aggregation processes upon injection into the water phase could lead to inhomogeneous distribution of charges, while loading after assembly enables successive surface coating. Microfluidic loading, enabling consistent fusion, exhibited the smallest complexes with very low standard deviation for all investigated N/P ratios. Optimising process parameters might help to further reduce aggregation.

3.3 Comparison of classical pipetting and microfluidic mixing

Due to a significantly reduced complex diameter, we focused on loading after carrier assembly. Thus, classical pipetting was directly compared to microfluidic mixing. Z-ave. of carriers loaded after assembly by both techniques, using different siRNA concentrations (1.5, 15, 100 μM) at previously selected N/P ratios (9, 13, 20) was detected via DLS (Figure III.4). In case of high N/P and diluted concentrations results are comparable. Vice versa microfluidic mixing leads to smaller complexes: Forming carriers via classical pipetting at N/P=9 with a 100 μM siRNA solution results in complexes 230 ± 97 nm ($\text{PDI}=0.353\pm 0.161$) in diameter, whereas merging the same volumes and concentrations by a microfluidic device results in 179 ± 11 nm ($\text{PDI}=0.205\pm 0.028$) sized complexes. Size distribution of the latter complexes is

unimodal, whilst classical pipetting leads to a mixture of at least two different size distributions (Figure III.4).

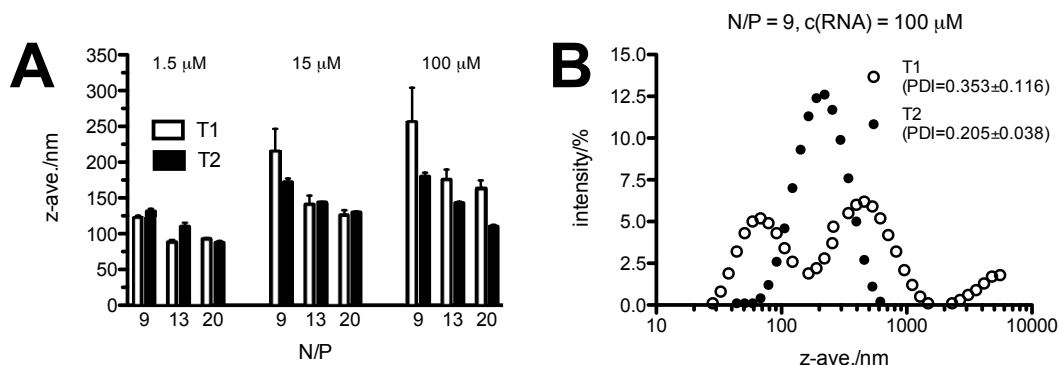


Figure III.4: Z-ave. determined by DLS of carriers loaded via **T1** (classical pipetting) and **T2** (microfluidic mixing) at previously evaluated N/P ratios using three different siRNA concentrations (1.5, 15, 100 μM) ($c(\text{NS})=0.5 \text{ mg/mL}$). Measurements were carried out in quadruplicates and values are presented as mean values \pm standard deviation (A). Detailed size distribution at N/P=9 using $c(\text{RNA})=100 \mu\text{M}$ (B).

Stability as a function of incubation time of complexes, assembled ($c(\text{RNA})=100 \mu\text{M}$, $c(\text{NS})=0.5 \text{ mg/mL}$) via **T1** and **T2** at respective N/P ratios, was investigated by DLS in water as well as in serum (10%). As to samples in pure water, negligible changes in size and PDI were detected for both assembly techniques up to the longest tested time span of 240 min (Figure III.5). By contrast, in presence of serum, an increase in z-ave. and PDI was observed, especially for carriers assembled by classic pipetting (**T1**) at high N/P ratios (Figure III.6). The latter finding appears to be unexpected, as in pure water aggregation was previously found to decrease at higher N/P (Figure III.1B). However, this can be explained by charge interaction: Carriers bearing high positive surface charge are known to be unstable in presence of polyanionic (blood) components such as serum albumin [118], whereas nearly isoelectronic assemblies are more likely to resist ion induced aggregation. Hence, carriers assembled in the vicinity of the neutralisation point (e.g N/P=7, Figure III.1B) show an increased stability in presence of polyanions and the importance of assembling slightly positive carriers is pointed out once again. Complexes prepared via microfluidic device (**T2**) generally showed increased stability in presence of serum (Figure III.6C/D), supposedly due to a more homogeneous distribution of surface charges and avoidance of naked cationic patches [62].

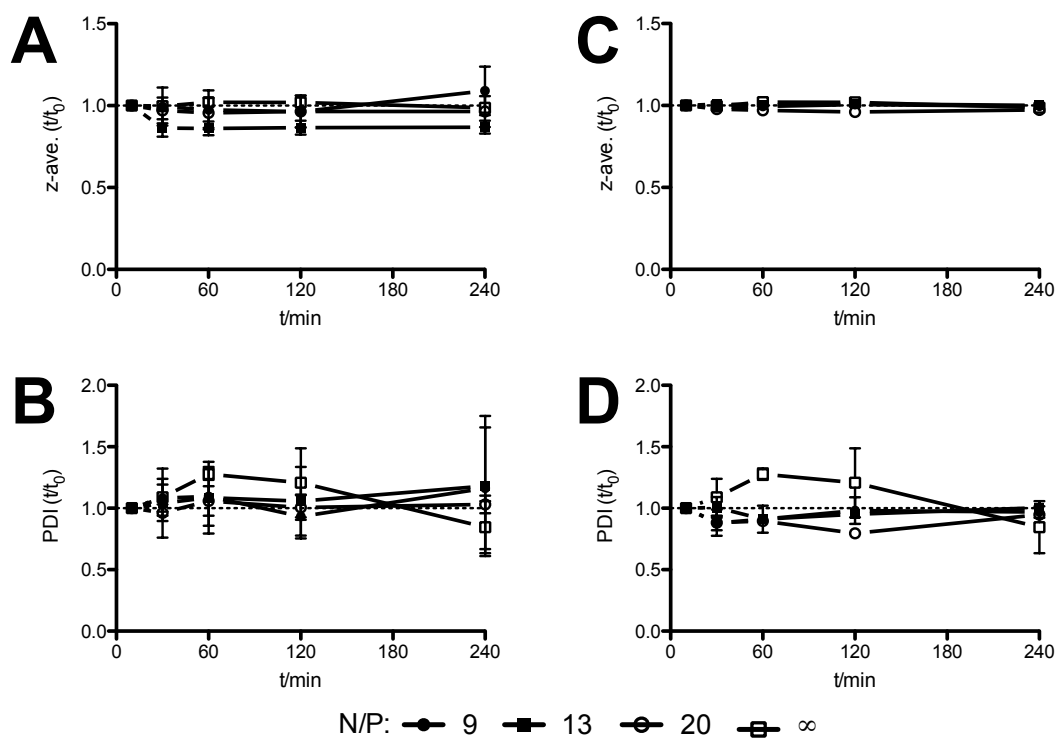


Figure III.5: z -ave and PDI after incubation in water for $t=30, 60, 120, 240$ min determined by DLS. Ratio of values determined at t and $t=10$ min (t_0) of complexes loaded via **T1** (classical pipetting, A/B) and **T2** (microfluidic mixing, C/D). Unloaded carriers ($N/P=\infty$) were measured for comparison reasons. Measurements were carried out in quadruplicates and values are presented as mean values \pm standard deviation. The experimental points are connected by lines to guide the eye only.

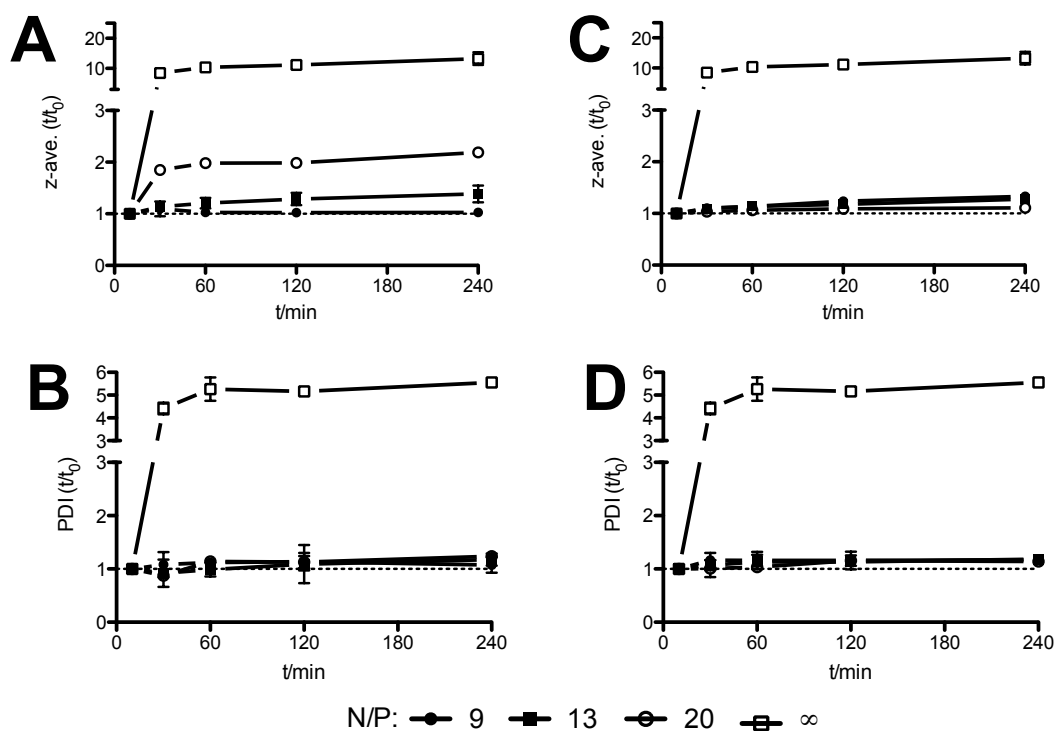


Figure III.6: z -ave and PDI after incubation in bovine serum (10%) for $t=30, 60, 120, 240$ min determined by DLS. Ratio of values determined at t and $t=10$ min (t_0) of complexes loaded via **T1** (classical pipetting, A/B) and **T2** (microfluidic mixing, C/D). Unloaded carriers ($N/P=\infty$) were measured for comparison reasons. Measurements were carried out in quadruplicates and values are presented as mean values \pm standard deviation. The experimental points are connected by lines to guide the eye only.

The amount of free siRNA was detected by SYBRTM Gold assay and due to more stable complexes decreased values were detected for microfluidic-assisted fusion in comparison to classical pipetting (Figure III.7). The carrier's ability to resist enzymatic degradation by RNase was demonstrated in digestion studies. In a preliminary experiment complexes prepared by both techniques ($N/P=9$, $c(\text{RNA})=100 \mu\text{M}$) were incubated with different amounts of RNase. Free siRNA served as a control. Whilst uncomplexed siRNA was degraded rapidly, it was protected almost completely by both complex types even at high RNase concentrations (Figure III.8).

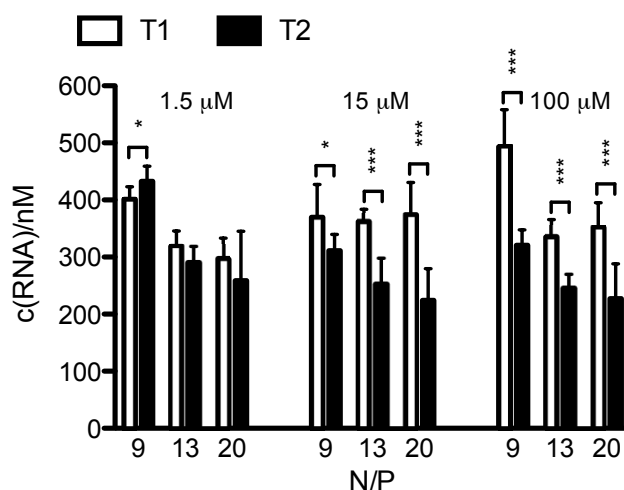


Figure III.7: Accessible siRNA concentration of carriers loaded via **T1** (classical pipetting) and **T2** (microfluidic mixing) at previously evaluated N/P ratios using three different siRNA concentrations (1.5, 15, 100 μM) determined by SYBRTM Gold assay. Measurements were carried out in quadruplicates and values are presented as mean values ± standard deviation.

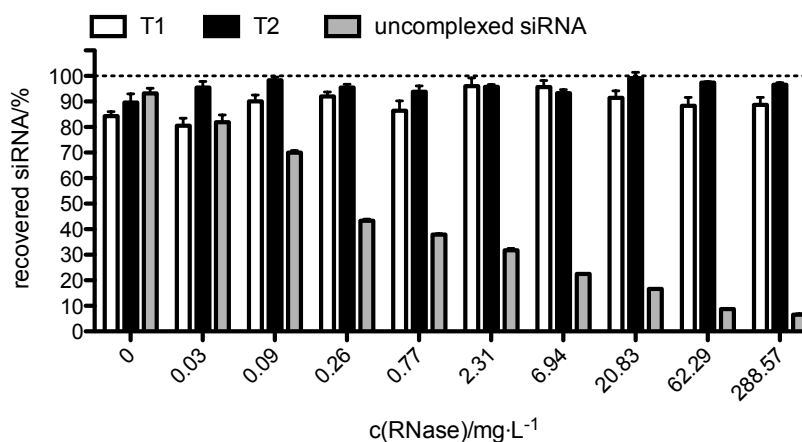


Figure III.8: Recovery of siRNA after RNase digestion. Carriers were assembled by classical pipetting (**T1**) and microfluidic mixing (**T2**). Uncomplexed siRNA was used as a control. Measurements were carried out in quadruplicates and values are presented as mean values ± standard deviation.

To prove the ability of complexes to protect siRNA from digestion in presence of competing anions (heparin), different concentrations of free heparin plus a constant amount of RNase were incubated together with complexes prepared by both techniques. Displaced siRNA before digestion as well as recovered siRNA after digestion were quantified. The amount of recovered siRNA decreases rapidly as a function of

heparin concentration (Figure III.9A). Moreover, in case of microfluidic formed complexes, a higher amount of siRNA was recovered, especially for intermediate heparin concentrations ($c(\text{heparin})=31.25 \text{ mg/L}$: RNA recovery= 30.6 ± 1.0 vs. $15.4\pm 1.4\%$). High heparin concentrations led to almost complete siRNA digestion in case of both complexation techniques. In addition, the two different complex types were tested for transfection efficiency in cell culture experiments (SKOV3 cells). Folate receptor-positive cells may be useful in further active targeting studies [7]. Microfluidic loaded carriers were shown to significantly down-regulate siRNA expression more effectively (34.8 ± 1.5 vs. $24.5\pm 2.2\%$ knockdown, Figure III.9B).

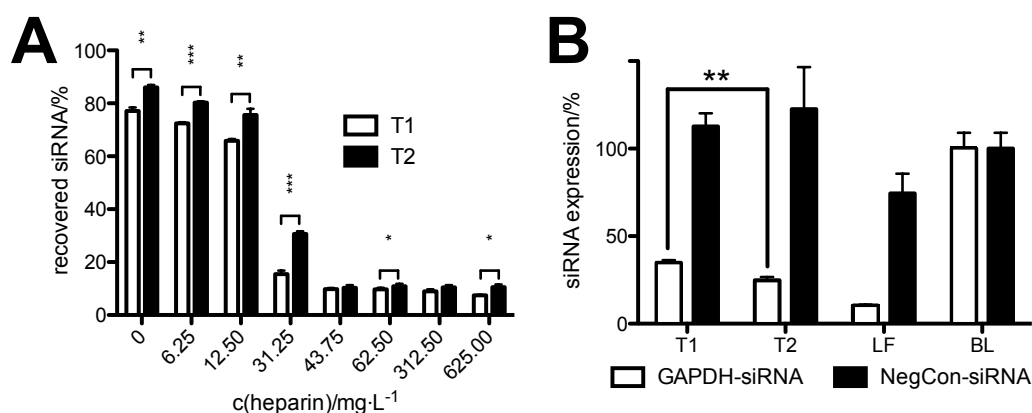


Figure III.9: Carriers were assembled via **T1** (classical pipetting) and **T2** (microfluidic mixing) ($N/P=9$, $c(\text{RNA})=100 \mu\text{M}$, $c(\text{NS})=0.5 \text{ mg/mL}$). Amount of recovered siRNA after incubation with RNase and different concentrations of heparin (A). Transfection efficiency *in vitro* (SKOV3 cells) was determined by RT-PCR. Hs_GAPDH-primers were used to quantify hGAPDH_gene expression, Hs_β-actin-primers were utilised as internal standard to determine relative expression levels for each gene (B). Measurements were carried out in quadruplicates and values are presented as mean values \pm standard deviation.

Decreasing complex size could be achieved by different means: (1) increasing the N/P ratio, (2) working with diluted RNA solutions, (3) employing different loading techniques. Increasing N/P is typically accompanied by higher cytotoxicity. Increasing size of PEI-DNA-polyplexes at up-scaled concentrations was previously reported [131]; by contrast, working in a highly diluted regime of concentrations to reach small carriers gives rise to further problems such as decreasing transfection efficiency *in vitro* [6] or limited injection volume *in vivo*. Consequently an assembly mechanism as homogeneous as possible is believed to be the key for formulating adequately sized and stable carriers bearing slightly positive net charge. This hypothesis is in

agreement with the observation of smaller, more uniform and increasingly stable (as proved for elaborated N/P under serum conditions) complexes for microfluidic-assisted fusion and has previously been reported for microfluidic-assembled poly- [120, 129] or lipoplexes [130, 125]. In addition, for those complexes a smaller amount of free siRNA, increased stability against heparin displacement and RNase digestion in presence of heparin were detected. This is in agreement with the assumption of a tighter compaction of nucleic acids due to a more homogeneous distribution of charges on the carrier's surface, caused by an increasingly uniform loading process. Stability against enzymatic degradation is a precondition for successful *in vivo* application. Complexes prepared by both techniques have proven to be extraordinary effective in siRNA protection. Under harsh conditions in presence of additional polyanions (heparin), microfluidic-assembled complexes were shown to be even more effective. Higher knockdown efficiency of microfluidic-assembled carriers may be explained by size differences: in case of conventional-assembled carriers only the fraction with smaller diameter should be suitable for endocytosis, whilst aggregates may be excluded. Further, enhanced siRNA protection could have been a factor. Since the results are shown as values normalised to β -actin, a slight difference in β -actin expression towards lower expression levels may cause a normalised value of more than 100%. The lower "NegCon-siRNA" bar for Lipofectamine indicated indirectly that Lipofectamine is more toxic than the other samples [134, 140]. For PEI/DNA-polyplexes [129] as well as for lipoplexes [130] fabricated in a microfluidic device, superior transfection efficiencies *in vitro* have previously been reported. However, possibly due to a less defined fusion process, preparing poly- [120] or lipoplexes [128] in a device with mm-scaled tubes did not significantly enhance transfection efficiency. Under *in vivo* conditions greater differences in knockdown performance are expected, as sedimentation of large particles cannot contribute to transfection efficiency [141] and siRNA protection is even more crucial.

3.4 Statistical analysis of the microfluidic mixing technique

As microfluidic mixing emerged as the most promising technique, parameters were studied in detail. Four factors were evaluated as potential for influencing complex size (Table III.1): (A) concentration of the RNA solution ($c(\text{RNA})$), (B) the FR ratio of RNA solution and NS ($\text{FR}_{\text{RNA}}/\text{FR}_{\text{NS}}$), (C) the concentration of the NS ($c(\text{NS})$), (D) the summation of both FRs (FR_{tot}).

Table III.1: Investigated factors and levels of the central composite design

	Factor	Level					Unit
		$-\alpha$	-1	0	1	α	
(A)	c(RNA)	3.48	5.00	7.50	10.00	11.52	mM
(B)	FR _{RNA} /FR _{NS}	0.35	0.50	0.75	1.00	1.15	-
(C)	c(NS)	0.35	0.50	0.75	1.00	1.15	mg/mL
(D)	FR _{tot}	19.64	50.00	100.00	150.00	180.36	mL/min

(A) concentration of the RNA solution; (B) FR ratio of RNA solution and NS; (C) concentration of the NS; (D) summation of both FRs.

Concentrations of the respective fluids (A, C) control the N/P as well as the final concentration. Changing the ratio of FRs (B) represents a straightforward way to precisely control the N/P. The total FR (D) has an effect on shear stress and diffusion behaviour [142], thus influencing complex diameter without altering N/P or concentrations. On the one hand low N/P ratios at high carrier concentrations are prerequisites for prospect *in vivo* experiments, on the other hand, as demonstrated above, those conditions favour aggregation, especially if inappropriate parameters and techniques are chosen for complex formation. A central composite design was chosen to estimate the effects of all variables and their interactions. The experimental plan was carried out on three factor levels, circumscribing the orthogonal design space. Additional star points allow estimation beyond experimental limits. Centre points were measured repeatedly to include scattering data. Analysis of the experimental variation, by calculating average and standard deviation from all experiments carried out with centre point settings (108.5 ± 2.0 nm), proves the robustness of the method. The standardised Pareto chart summarises the result of the statistical analyses (Figure III.10A). The length of each bar is proportional to the standardised effect (estimated effect divided by its standard error). Effects passing the vertical line ($\alpha=0.05$) are considered as statistically significant at the confidence level of 95%. Open bars represent increasing, black bars decreasing complex diameters. Measured sizes range from 77 to 184 nm and were mainly influenced by factors, affecting the ratio of charges (A, B, C). However, an increase of the ratio independent total FR (D) caused a further decrease in carrier size. Response surface analysis of the data resulted in the following second order polynomial regression equation (Equation III.1, $R^2 = 0.970$), quantifying the relationship between significant factors and z-ave.:

$$z - ave. = 104.898 - 0.468 \cdot A + 44.096 \cdot C + 0.269 \cdot D - 167.546 \cdot B \quad (\text{III.1})$$

$$+ 17.142 \cdot AB - 0.002 \cdot D^2 + 96.054 \cdot B^2$$

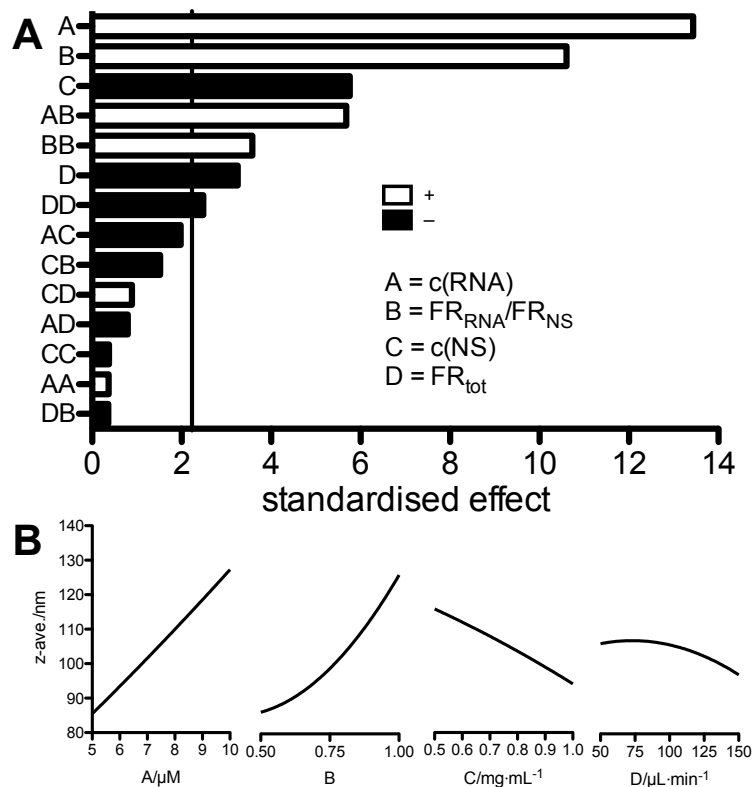


Figure III.10: Standardised Pareto chart (A). Main effect plots (calculated by Eq. III.1 showing z -ave. as a function of each factor (B).

Main effect plots (Figure III.10B) were calculated from this regression equation by modifying the respective factor while residual factors are kept constant at the 0-level. Surface plots (Figure III.11, III.12, III.13) containing two variables, illustrate the interacting influences. As above-mentioned, combinations increasing the N/P lead to a decrease in complex diameter, down to the size of almost unloaded carriers. Raising the total FR to values higher than $\sim 100 \mu\text{L}/\text{min}$ leads to a further decrease in complex size (Figure III.11B). Utilising the data from this design, diameters from any factor combination can easily be predicted. For instance, factorial analysis gives optimised parameters ($A=0.73 \mu\text{M}$, $B=1.15$, $C=0.74 \text{ mg}/\text{mL}$, $D=99.21 \mu\text{L}/\text{min}$) for a desired particle diameter of 150 nm, which in turn corresponds to an N/P of 10.54. DLS measurements of carriers loaded with this parameters yield complexes $154 \pm 6 \text{ nm}$ ($\text{PDI}=0.188 \pm 0.007$) in diameter.

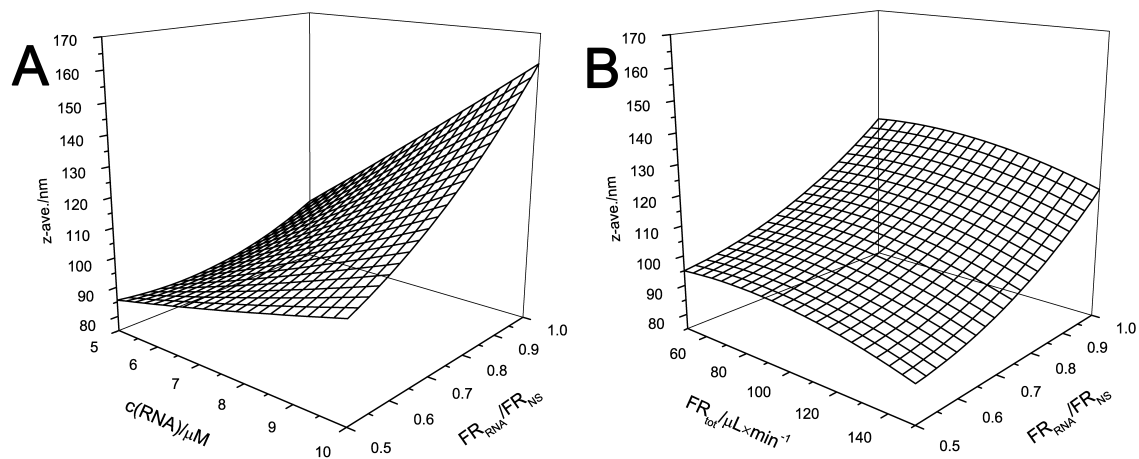


Figure III.11: Surface plots (calculated by Eq. III.1) showing the interacting influences between two factors.

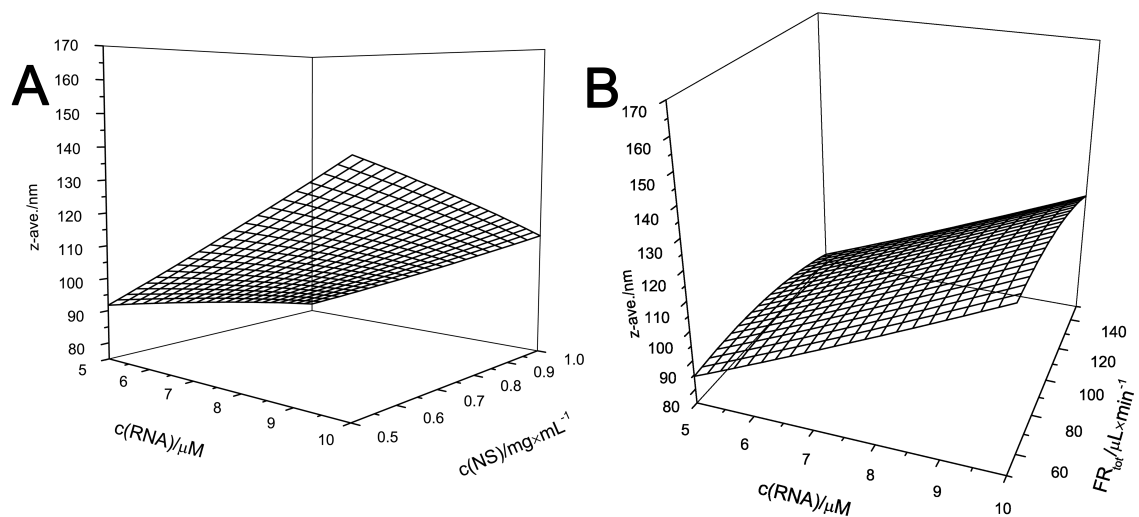


Figure III.12: Surface plots (calculated by Eq. III.1) showing the interacting influences between two factors.

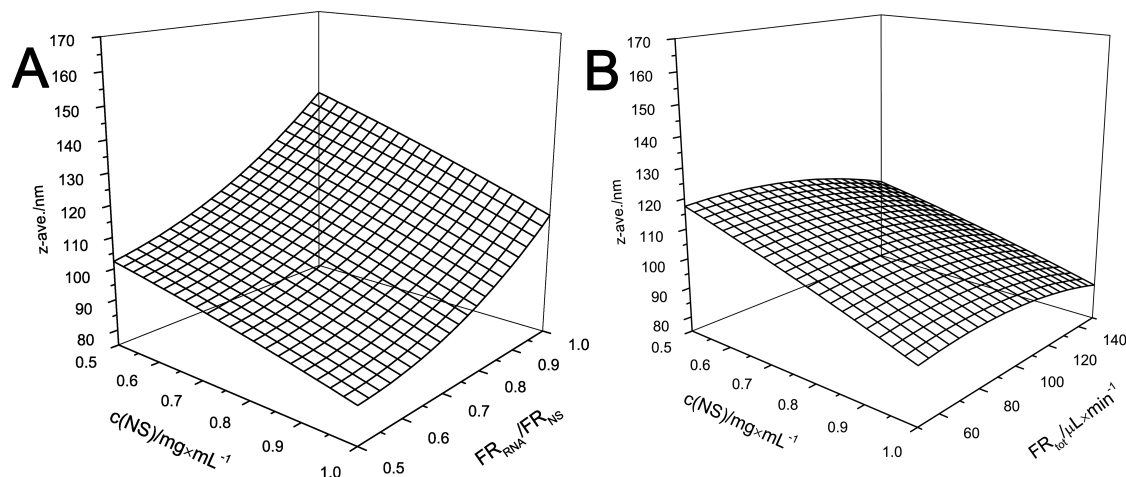


Figure III.13: Surface plots (calculated by Eq. III.1) showing the interacting influences between two factors.

In this approach statistical tools were utilised for optimising process parameters. Decreasing sizes with increasing mixing speeds due to increasing shear stress and a shorter time for the particle to grow have previously been reported [143, 120]. Model predictions are in accordance with what one would expect and prove the reproducibility of microfluidic loading as well as the usability of factorial analysis for evaluating formulation variables in an efficient and comprehensive manner.

4 Conclusions

Apart from polymer design and N/P there are several formulation parameters (concentration of used solutions, addition of nucleic acids while or after carrier assembly, style and speed of mixing carrier with nucleic acid), which need to be considered when assembling complexes for gene delivery purposes. This was demonstrated on the basis of complexes, assembled from predominantly hydrophobic PEG-PCL-IPEI amphiphiles and siRNA. To evaluate suitable N/P ratios for further investigations, size and charge of carrier-siRNA complexes as a function of N/P were monitored. A discrepancy between the observed N/P at isoelectric conditions and the expected N/P for a stoichiometric mixture of charges was found. This mismatch can be explained by the 3D structure, partly blocking cationic charges from complexation. The straightforward approach of recalibrating the N/P scale with the help of the isoelectric point may be applicable for other particulate cationic carrier systems. Subsequently, the diameters of complexes, prepared by four different techniques were compared. Loading after carrier assembly generally led to less pronounced aggregation in the vicinity of the isoelectric point, possibly due to

a more gentle complexation procedure. Therefore, complexes prepared after carrier assembly by bulk pipetting and microfluidic mixing were thoroughly investigated: At low N/P ratios and high siRNA concentrations the latter were smaller in size (179 ± 11 vs. 230 ± 97 nm) and PDI (0.205 ± 0.028 vs. 0.353 ± 0.161). Whereas complexes prepared by bulk mixing comprised a mixture of different sizes, microfluidic assembly led to unimodal size distributions. Further, for those assemblies, a smaller amount of free siRNA, increased stability against heparin displacement and increased resistance against RNase digestion in presence of heparin were detected (c(heparin)=31.25 mg/L: RNA recovery= 30.6 ± 1.0 vs. $15.4\pm 1.4\%$). Furthermore at elevated N/P under serum conditions, microfluidic assembled complexes exhibited superior colloidal stability. *In vitro* microfluidic-assembled carriers exhibited significantly increased transfection efficiency (34.8 ± 1.5 vs. $24.5\pm 2.2\%$ knockdown). Hence, microfluidic complexation offers an easy to use, scalable and reproducible alternative to classical pipetting. Those findings on assembly mechanism and techniques are fundamental and may be applied to further particulate cationic carrier systems in the field of drug and gene delivery, giving rise to more uniform, stable and less toxic formulations.

Acknowledgments

We would like to thank Martin Westermann, Ming Chen and Frank Steiniger (Elektronenmikroskopisches Zentrum, Universität Jena) for their kind assistance with cryo-TEM.

Part IV

Lyophilised ready-to-use formulations of PEG-PCL-PEI nano-carriers for siRNA delivery

Authors

Thomas Endres, Mengyao Zheng, Moritz Beck-Broichsitter, Thomas Kissel^a

Authors' contributions

RT-PCR was carried out by Mengyao Zheng. CryoSEM was operated by Michael Hellwig. All other experiments were carried out by Thomas Endres. Manuscript was written by Thomas Endres.

Published in Int. J. Pharm 428 (1-2) (2012), 121–124.

^acorresponding author

Abstract

The purpose of the present study was to transfer aqueous PEG-PCL-PEI nano-suspensions into dry ready-to-use formulations, suitable for delivery of siRNA. Therefore, freshly-prepared nano-suspensions were lyophilised with glucose as lyoprotectant. Firstly, the required glucose concentration for sufficient stabilisation of unloaded carriers was determined via dynamic light scattering. Morphology of fresh and rehydrated carriers was visualised by cryoSEM. Subsequently, the feasibility of siRNA loading before and after lyophilisation was investigated. For both strategies complex diameter and *in vitro* transfection efficiency were determined and correlated to freshly-prepared samples. Hydrodynamic diameter (95.2 ± 1.4 nm) and size distribution (0.132 ± 0.019) of unloaded nano-suspension were restored after rehydration by addition of $\geq 1.5\%$ of glucose before lyophilisation. Moreover, after loading of rehydrated carriers with siRNA, no significant difference in complex size was observed as compared to freshly-prepared ones. Stabilisation of pre-formed carrier/siRNA complexes during lyophilisation is feasible at elevated N/P (e.g. 20) and glucose concentrations above 5%. As determined via real-time-PCR, lyophilised samples were as active as freshly-prepared ones regarding transfection efficiency. In conclusion, lyophilisation is an effective technique to produce physically stable PEG-PCL-PEI formulations. These general findings may be applicable to further particulate gene delivery systems to shelf ready-to-use formulations.

1 Introduction

In recent years many nonviral gene delivery vehicles, such as liposomes, micelles, “polyplexes”, solid particles or intermediate structures were widely investigated [119]. Most of these formulations basically consist of aqueous colloidal systems, suffering from inherent thermodynamic instability, subsequently leading to aggregation over time [144]. This unstable nature of colloidal systems necessitates preparation immediately before administration and hampers reproducibility as well as their clinical application. Lyophilisation, offering the opportunity of dry storage and in situ sample rehydration, has been employed for particles [145], liposomes [146] or “polyplexes” [144] with encouraging results: In a vast majority of colloidal systems, carrier diameters could be completely restored, if proper lyoprotectants in adequate lyoprotectant/nano-carrier ratios were used. Applicable additives were typically sugars (e.g. glucose, sucrose and trehalose) [147], whereas the sugar type seems to be of lesser importance [148]. Protectants in general limit mechanical damage upon freezing and carriers are incorporated in a glassy matrix, which inhibits nano-carrier aggregation [149]. However, full maintenance of physicochemical properties does not ensure complete recovery of transfection efficiency [150]. It is well known, that structural changes during lyophilisation of DNA [151] and PEI/DNA complexes [150] may possibly decrease transfection efficiency and siRNA is even more susceptible to degradation than DNA [6]. By contrast, there are examples of successfully regaining transfection efficiency after freeze-drying [152, 144].

A promising class of multifunctional gene delivery carriers is based on cationic amphiphiles [73]. In aqueous media block copolymers, consisting of poly(ethylene glycol) (PEG), poly(ϵ -caprolactone) (PCL) and poly(ethyleneimine) (PEI), self-assemble spontaneously to core-shell structured nano-carriers. Core-forming biodegradable PCL segments, which could serve as reservoirs for water-insoluble drugs or dyes, are surrounded by hydrophilic PEG moieties, maintaining suspension stability. Cationic PEI segments are amenable for complexation with nucleic acids (e.g. siRNA) [118].

It was the aim of the present study to transfer aqueous PEG-PCL-PEI nano-suspensions into dry ready-to-use formulations, suitable for delivery of siRNA. Therefore, freshly-prepared suspensions were lyophilised together with glucose (glc) as lyoprotectant. Firstly, freeze-drying of unloaded carriers was investigated as a function of glc concentration (c_{glc}) before and after lyophilisation and rehydration by means

of dynamic light scattering (DLS). Morphology was visualised by cryogenic scanning electron microscopy (cryoSEM). In addition to lyophilisation of unloaded carriers, the feasibility of siRNA loading before and after lyophilisation and rehydration was investigated at different polymer/siRNA ratios (the ratio is generally referred to as PEI nitrogen per nucleic acid phosphate: N/P). Diameters and *in vitro* transfection efficiency of complexes assembled with siRNA before or after lyophilisation and rehydration were determined and compared to freshly-prepared samples.

2 Materials and methods

PEG-PCL-IPEI triblock copolymer was synthesised and characterised as described in detail elsewhere [118]. Block length for PEG, PCL and PEI are 500, 10000 and 2500 Da, respectively. 2'-O-methylated 25/27mer DsiRNA targeting Firefly Luciferase was purchased from Integrated DNA Technologies (IDT, Leuven, Belgium). QuantiFastTM SYBRTM Green PCR Kit, Hs_GAPDH_primer and Hs_β-actin-primer were provided by Qiagen (Hilden, Germany). LipofectamineTM 2000 (LF) was obtained from Invitrogen (Karlsruhe, Germany).

Nano-carriers were prepared by solvent displacement [132]. For complexation, the appropriate amount of siRNA was added to an aliquot of nano-suspension (NS) in one single step followed by vigorous mixing. Lyophilisation was conducted on an Alpha 1-4 LSC freeze-dryer (Martin Christ, Osterode, Germany).

The mean particle diameter (z-ave) and polydispersity index (PDI) were determined by DLS (Zetasizer NanoZS/ZEN3600, Malvern Instruments, Herrenberg, Germany). CryoSEM images were obtained on a JSM-7500F (Jeol, Tokyo, Japan) equipped with an ALTO-2500 liquid nitrogen (LN2) cryo-transfer system (Gatan Inc., Pleasanton, CA, USA). Samples were sputtered with platinum using the ALTO system. Optical microscope images were captured on a light microscope (Stemi 2000-C, Carl Zeiss, Jena, Germany) on samples prepared in transparent 96 well plates (Nunc, Thermo Fisher Scientific, Langenselbold, Germany).

Transfection efficiency *in vitro* was investigated via real-time-PCR (RT-PCR). SKOV3 cells were lysed 24 h after transfection. mRNA was isolated from culture cells and reverse transcribed to cDNA. Subsequently, RT-PCR was performed using a SYBRTM Green PCR Kit and a Rotor-Gene 3000 RT-PCR thermal cycler (Corbett Research, Sydney, Australia). Calibration curves for GAPDH and β-actin mRNA were prepared by serial dilutions of cDNA of the blank sample (untreated cells).

All measurements were carried out in triplicates and values are presented as mean values ± standard deviation.

3 Results and discussion

Z-ave and PDI of freshly-prepared unloaded carriers were determined via DLS (95.2 ± 1.4 nm, $\text{PDI} = 0.132 \pm 0.019$). Freeze-drying without lyoprotectant resulted in a fibrous polymer residue, forming large, visible aggregates upon rehydration. However, employing a c_{glc} of $\geq 1.5\%$ led to incorporation of carriers into an amorphous, honey-like matrix and ensured virtually unchanged carrier size and size distribution after rehydration (Fig. 1A). CryoSEM images of freshly-prepared nano-suspensions were in agreement with the results from light scattering experiments and revealed a uniform distribution with marginal aggregation. Images after rehydration proved that spherical carriers were still intact. However, despite unchanged carrier sizes as determined by DLS, onset aggregation to worm like assemblies was observed (Fig. IV.1C). Stabilisation of unloaded carriers has previously been reported for other core-shell type particulate carrier systems [145], required concentrations of sugar protectant are consistent with literature [149].

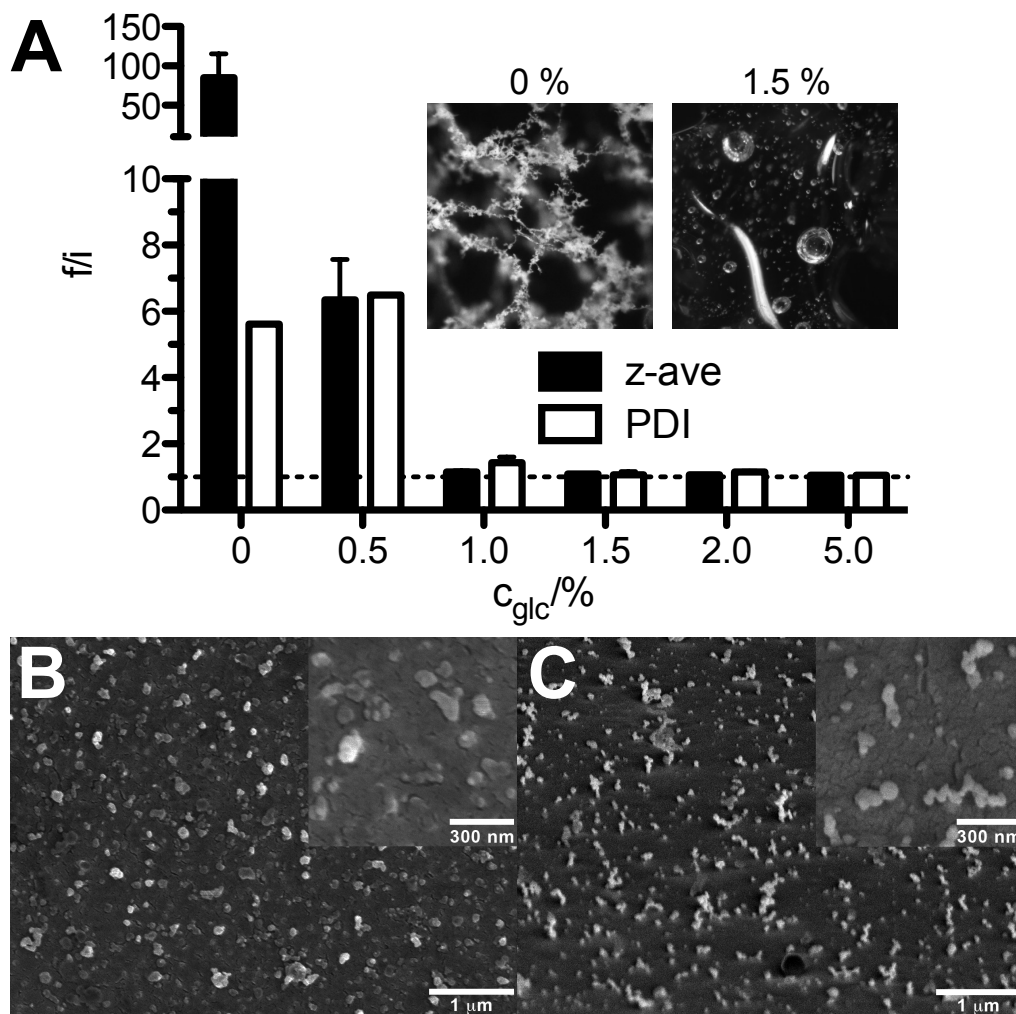


Figure IV.1: Ratio of final and initial (f/i) z -ave and PDI of nano-carriers, lyophilised as a function of c_{glc} . Insets: Optical microscope images of dry nano-carriers, lyophilised with 0 and 1.5% of glc (A). Cryo-SEM images of freshly-prepared (B) and rehydrated (C) nano-carriers ($c_{glc}=1.5\%$).

In addition to lyophilisation of unloaded carriers, the feasibility of complexation with siRNA was investigated. Generally, complexation could be carried out after (L1) or before (L2) lyophilisation (Fig. IV.2A). On the one hand, lyophilisation of pre-formed complexes, for formulation of easy-to-use transfection agents sounds appealing. On the other hand, there is the risk of nucleic acid degradation [146] or alteration in complex structure [150] during lyophilisation and long-term storage. For both strategies, direct lyophilisation in well plates (Fig. IV.2A) enables straightforward rehydration by addition of cell culture medium [153]. Stability of unloaded suspensions is mainly owed to electrostatic repulsion of PEI charges. Successive neutralisation upon addition of siRNA leads to poor stability at low N/P

ratios. Therefore, at these conditions, there is also an increased risk of aggregation during freeze-drying and the applicable route of lyophilisation and formulation is ultimately a question of N/P and the amount of lyoprotectant. Z-ave and PDI of complexes, formed via strategy **L1** or **L2** at two different N/P ratios (10 and 20) were compared to their freshly-prepared counterparts (Fig. IV.2B). No significant changes between freshly-prepared complexes and those assembled after lyophilisation (**L1**) were observed. By contrast, formulation route **L2** resulted in pronounced aggregation, especially at low N/P. An increased need of lyoprotectant with larger amounts of nucleic acid was expected [154] and therefore lyophilisation of complexes (**L2**) was further investigated at elevated glc concentrations (1.5-15%, Tab. IV.1). In case of N/P=20 recovery of complex diameter was virtually attained above $\sim 5\%$ of glc. At N/P=10 complete recovery of complex characteristics could not be achieved even at c_{glc} as high as 15%. Albeit there was a decrease in aggregation as a function of c_{glc} and carriers are likely to be regained by a further increase in protectant concentration, this would not be reasonable in order to attain highly concentrated, nearly isotonic nano-suspensions after rehydration.

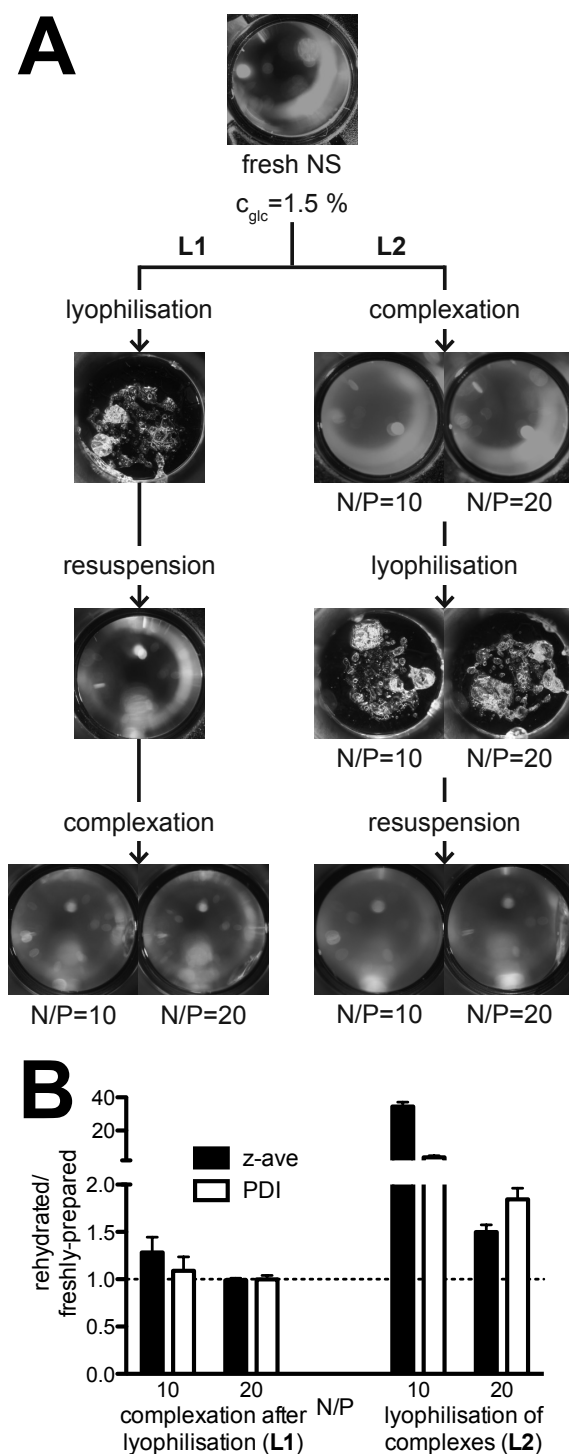
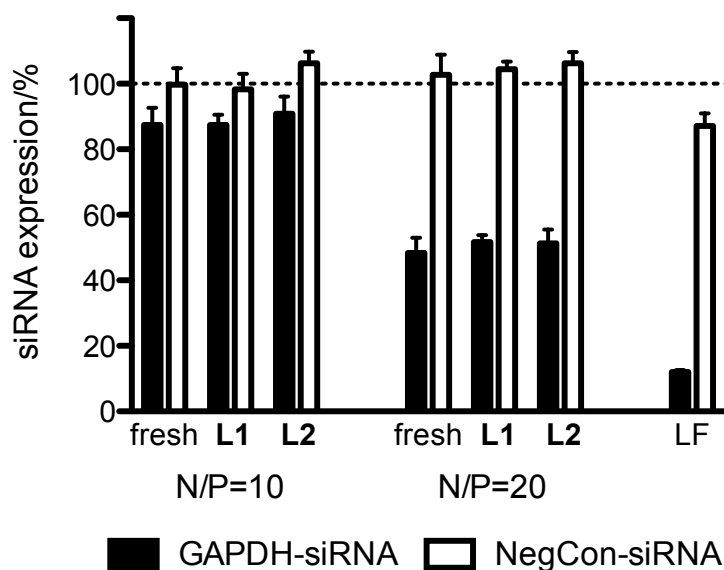


Figure IV.2: Organisation chart of different formulation strategies (**L1**: complexation after lyophilisation, **L2**: lyophilisation of complexes). Nano-suspensions and residues after lyophilisation were captured with a light microscope in 96 well plates (A). Ratio of final and initial (f/i) z-ave and PDI of carriers loaded at various N/P ratios (10 and 20) and lyophilised by different strategies (L1, L2, $c_{glc}=1.5\%$) (B).

Table IV.1: Ratio of final and initial (f/i) z-ave and PDI of complexes lyophilised (**L2**) at two different N/P ratios (10 and 20) as a function of c_{glc} .

$c_{glc}/\%$	N/P=10		N/P=20	
	z-ave (f/i)	PDI (f/i)	z-ave (f/i)	PDI (f/i)
1.5	34.49±5.29	3.93±1.89	1.54±0.13	2.06±0.30
3.0	33.49±4.74	1.80±0.34	1.21±0.04	1.24±0.12
5.0	30.44±3.47	1.82±0.91	1.22±0.13	1.13±0.14
10.0	16.92±8.75	3.59±1.55	1.06±0.01	1.26±0.11
15.0	4.47±1.01	2.61±0.38	1.00±0.01	1.21±0.14

Transfection activity of formulations, lyophilised via both strategies, was determined via RT-PCR and compared to freshly-prepared complex suspensions (Fig. IV.3). Effective knock-down was detected at N/P=20 and all stored formulations were as efficient as freshly-prepared. This is in agreement with reports on lyophilised non-viral delivery systems [146, 155], even though there is some controversy in literature [37]. Therefore, minor changes in aggregation tendency of resuspended unloaded carriers (as previously observed in cryoSEM) are not regarded to be critical.

**Figure IV.3:** Transfection efficiency (SKOV3-cells) was determined *in vitro* by RT-PCR. Hs_GAPDH-primers were used to quantify hGAPDH_gene expression, Hs_β-actin-primers were utilised as internal standard to determine relative expression levels for each gene. Lipofectamine (LF) was used as a positive control. Freshly-prepared complexes were compared to ones assembled after (**L1**) and before (**L2**) lyophilisation ($c_{glc}=5\%$, N/P=10 and 20).

4 Conclusions

In conclusion, the results of this study demonstrate that lyophilisation is a very effective technique to produce physically stable PEG-PCL-PEI formulations. Size and PDI of unloaded nano-suspensions (95.2 ± 1.4 nm, $\text{PDI} = 0.132 \pm 0.019$) were preserved during lyophilisation upon addition of lyoprotectant ($\sim 1.5\%$ of glc). No significant difference between freshly-prepared complexes and those assembled from lyophilised carriers was observed. Furthermore, higher glc concentration ($\sim 5\%$) facilitates the stabilisation of pre-formed carrier/siRNA complexes at elevated N/P ratio of 20. In case of lower N/P (10), stabilisation could not be achieved in the range of applicable c_{glc} . RT-PCR experiments *in vitro* proved, that all lyophilised formulations were as active as freshly-prepared ones. These findings are fundamental and may be applicable to further charged particulate gene delivery systems to reproducibly shelf ready-to-use formulations for prospect *in vitro* and *in vivo* studies.

Acknowledgments

We thank Andreas K. Schaper and Michael Hellwig (WZMW, Universität Marburg) for supporting us with cryoSEM.

Part V

Amphiphilic and biodegradable PEG-PCL-PEI triblockcopolymers for dual delivery of siRNA and quantum dots: *in vitro* and *in vivo* investigation of a FRET capable carrier system

Authors

Thomas Endres^a, Mengyao Zheng^a, Ayşe Kılıç, Agnieszka Turowska, Moritz Beck-Broichsitter, Harald Renz, Olivia Merkel, Thomas Kissel^b

Authors' contributions

In vitro experiments as well as the SYBRTM Gold assay were carried out by Mengyao Zheng. *In vivo* measurements were conducted by Mengyao Zheng, Ayşe Kılıç and Agnieszka Turowska. CLSM images were obtained by Xiang Yu and Raimo Hartmann (Institute of Physics and WZMW, Philipps-Universität Marburg) as well as Mengyao Zheng and Thomas Endres. All other experiments were carried out by Thomas Endres. Manuscript was written by Thomas Endres.

Intended for publication in Nanomedicine: Nanotechnology, Medicine and Biology.

^athese authors contributed equally to this work

^bcorresponding author

Abstract

Amphiphilic cationic triblock-copolymers based on polyethylene glycol, poly- ϵ -caprolacton and polyethylene imine represent a versatile gene delivery platform, capable of co-delivery of nucleic acids, drugs and/or dyes. It was the aim of the current study to provide basic knowledge for a more rational vector design by deriving a structure-activity relationship *in vitro* and *in vivo* together with the establishment of an imaging technique which is sensitive for nucleic acid unpacking. The latter is based on quantum dot mediated fluorescence resonance energy transfer method (QD-FRET). Cell uptake *in vitro* was measured by flow cytometry. Transfection efficiencies of nano-carriers with different PEG shell thicknesses were determined *in vitro* and *in vivo* by quantitative real time PCR. For *in vivo* experiments a nanosuspension was intracheally instilled to balb/c mice. Furthermore, a prototype FRET pair was established by co-loading with QDs and fluorescently labelled siRNA and switching functionality was demonstrated by fluorescence spectroscopy as well as fluorescence microscopy *in vitro*. While nano-carriers prepared from the rather hydrophobic PEG500-block-copolymer showed good transfection efficiency ($61\pm 5\%$ knockdown *in vitro*, $55\pm 18\%$ knockdown *in vivo*), poor performance was found in case of the predominantly hydrophilic PEG5000-counterpart ($13\pm 6\%$ knockdown *in vitro*, $30\pm 17\%$ knockdown *in vivo*). This is in agreement with flow cytometry studies, revealing 5-fold higher cellular uptake of carriers with thinner PEG shell after 240 min of incubation. QD-FRET complexes emitted light at the acceptor's emission wavelength upon donor excitation, proving successful FRET-effect and hence, complex integrity. Upon complex dissociation, which was simulated by addition heparin, a dose-dependent decrease in FRET-efficiency was observed. In summary, we successfully established a FRET-capable multifunctional gene delivery system, applicable for pulmonary delivery of siRNA. We believe that *in vitro/in vivo* correlation of structure and function as well as sensitive imaging functionality for mechanistic investigations are prerequisites for a more rational design of amphiphilic gene carriers.

1 Introduction

Development of safe and effective non-viral gene or siRNA delivery systems represents a strong scientific barrier [119]. The rational development of new delivery platforms, however, requires knowledge of the delivery process on a systemic and cellular level. To gain those mechanistic insights, efficient tracking and sensing formats are required and experiments not only need to be carried out *in vitro*, but also *in vivo*.

Since the early attempts of using cationic homopolymers such as polyethylene imine (PEI) for complexation of nucleic acids a constant evolution of vector technology led us to increasingly smarter multifunctional delivery vehicles [1]. Notably, tailored multifunctional polymeric vectors for simultaneous transport of different therapeutic agents gained increasing interest [69, 117, 156], especially for pulmonary co-delivery of drugs and nucleic acids [157]. Due to their modular design and their possibility to be optimally engineered amphiphilic block-copolymers, which are capable to self-assemble to various types of colloids (e.g. micelles, nanoparticles) [69, 74, 73], are especially suitable for multifunctional delivery of hydrophobic drugs (e.g. paclitaxel [69]), nucleic acids [117] and/or dyes [13]. Recently, amphiphilic block-copolymers comprising polyethylene glycol (PEG), poly- ϵ -caprolacton (PCL) and PEI segments were shown to be effective, stable, biodegradable and biocompatible delivery vectors, particularly for small interfering RNA (siRNA) [118, 76, 158]. Self-assembly in aqueous milieu leads to nano-carriers with a “core-corona-structure”, whereas the stabilising and protecting hydrophilic PEG shell surrounds the hydrophobic PCL core. The PCL domain serves as a reservoir for hydrophobic drugs or dyes. The ratio of hydrophilic and hydrophobic segments was shown to have a strong impact on the physicochemical and biological characteristics [118]. Whereas increasing PEG shell-thickness is known to reduce toxicity and increase colloidal stability [118], this generally leads to a diminished transfection activity [80]. However, pronounced stealth properties may prove advantageous for prospective receptor mediated targeting approaches [159]. PEI, located at the interface between hydrophilic and hydrophobic moieties, is capable of electrostatic interaction with nucleic acids [158]. Polyplexes which are assembled from PEI or PEG-PEI and nucleic acids exclusively by electrostatic interaction are oftentimes prone to disassembly especially in a medium of high ionic strength (e.g. under serum conditions) [80]. As compared to those systems, amphiphilic PEG-PCL-PEI carriers are formed by a

self-assembly process even in absence of opposite charges and in addition to its cargo functionality the hydrophobic core region is furthermore capable to increase carrier stability [80, 139]. Moreover, to increase flexibility and reproducibility, carriers may be shelved in absence of nucleic acids under dry conditions. Afterwards, rehydration and nucleic acid loading can take place directly before usage [160, 158].

As dyes for “theranostic” approaches luminescent semiconductor quantum dots (QDs) have begun to replace conventional fluorophores due to their unique properties such as wideband excitation and narrow emission spectra, high quantum yields and photo/chemical stability [94]. Furthermore, the emission wavelength can be tuned in the full range from UV to near infrared (NIR), allowing excitation and visualisation in biological environments of cells and tissues as *in vitro* and *in vivo* imaging probes [99, 161]. The presence of a core-shell structure (e.g. CdSe/ZnS) can reduce heavy metal cytotoxicity and prevent leaching [94]. Moreover, QDs were shown to replace conventional fluorophores as more powerful donors for fluorescence resonance energy transfer (FRET) [94]. FRET involves the non-radiative transfer of excitation energy from a fluorescent donor to a proximal acceptor owing a suitable excitation spectrum. With two fluorophores, independently attached onto a pair of distinct biomolecules, FRET has proven to be a versatile tool for probing a variety of biological processes [98, 96]. The incorporation of QD-FRET based sensing formats into gene delivery carriers may be useful to provide a deeper understanding in fundamental aspects of gene therapy by functioning as a highly sensitive on/off-switch to probe the dissociation in the course of the unpacking procedure [94, 162], which is a crucial step in the gene delivery process; ultimately, in order to be effective, the complex has to be designed in a way to protect nucleic acids from degradation in the bloodstream or the endosomal compartment plus to enable the release of genetic material on target [3]. FRET based monitoring capabilities may facilitate the design of a carrier exhibiting a in this vein tailored complextion strength. Subsequent to carrier-nucleic acid dissociation, both fluorophores may be individually tracked e.g. via fluorescence microscopy.

In the literature QDs most often serve as a central nanoscaffold, around which diverse functionalities are chemically tethered [94, 163, 95, 99, 164] or for labelling via covalent linkage [165, 99]. Herein, we report a straightforward and versatile approach of tagging gene carriers via physical entrapment. The encapsulation of hydrophobic QDs into the PCL core of amphiphilic siRNA delivery vehicles combines nucleic acid delivery and imaging capabilities in one single carrier platform. In order to fabricate a FRET-capable delivery vehicle, which is designed for the elucidation of the gene-delivery process, QD-loaded carriers were subsequently com-

plexed with Alexa Fluor(AF)-labelled siRNA. However, depending on the intended purpose, the QDs employed in this prototype “theranostic” delivery system, may easily be exchanged by arbitrary nanoscaled hydrophobic substances.

The aim of the current study was the evaluation of a multifunctional and QD-FRET-capable delivery platform *in vitro* and *in vivo*. We believe that those theranostic imaging and delivery formats have the potential to provide deeper insights into the siRNA-delivery process, leading to the design of more rational, tailored colloidal gene carriers.

2 Material and methods

2.1 Reagents and chemicals

Non-coding control Dicer substrate interfering RNA (DsiRNA), hGAPDH-DsiRNA, mGAPDH-DsiRNA and AlexaFluor647-labelled DsiRNA (AF-siRNA) were purchased from Integrated DNA Technologies (IDT, Leuven, Belgium). Fetal Calf Serum (FCS) was obtained from Cytogen (Sinn, Germany). Heparin sodium (150,000 IE/g) was procured from SERVA Electrophoresis (Heidelberg, Germany). First Strand cDNA Synthesis Kit and RNase I (#EN0531) were obtained from FERMENTAS (St. Leon-Rot, Germany). QuantiFastTM SYBRTM Green PCR Kit, Hs_GAPDH_primer, Mm_GAPDH-primer, Hs_β-actin-primer, Mm_β-actin-primer, and DNase I were provided by Qiagen (Hilden, Germany). Hydrophobic cadmium selenide, zinc sulphide core-shell QDs with an emission wavelength of 605 nm (organic QDot 605 ITK), SYBRTM Gold reagent, LipofectamineTM 2000 (LF) and PureLinkTM RNA Mini Kit were purchased from Invitrogen (Karlsruhe, Germany). Balb/c mice were purchased from Harlan Laboratories (Horst, The Netherlands). SKOV3 cells were obtained from ATCC, LG Promochem (Wesel, Germany). Further chemicals and solvents, which are not mentioned in detail, were supplied by Sigma Aldrich (Steinheim, Germany) at the highest grade commercially available.

2.2 Polymer synthesis and characterisation

PEG-PCL-PEI triblock-copolymers were manufactured by a three-step synthesis-route and characterised as described in detail elsewhere [118]. Briefly, in a first reaction step, hydroxy-terminated monomethyl-PEG (in different molecular weights) was employed as a macroinitiator for the Sn(Oct)₂-catalysed ring opening polymerisation of ε-caprolacton (amount calculated to result the designated PCL block length). Subsequently, the endgroup of the resulting PEG-PCL diblock copolymer

was modified by reaction with acryloyl chloride in a second reaction step. Conclusively, in a third reaction step, IPEI2500 was coupled onto the modified PEG-PCL copolymer by Michael-type microaddition reaction. Block length for PCL and PEI are 10,000 and 2500 Da, respectively. To monitor the impact of PEG chain length on transfection efficiency, carriers with two different PEG segment length (500 and 5000 Da) were chosen. Accordingly, the blockcopolymers PEG500-PCL10,000-PEI2500 and PEG5000-PCL10,000-PEI2500 were used in the course of the following investigations.

2.3 Assembly of nano-carriers

Nano-carriers were prepared by a solvent displacement technique, as described in detail elsewhere [118]. Briefly, carriers were prepared by dissolving 1 mg of polymer in 200 μL of acetone. The resulting solution was subsequently injected into 1 mL of magnetically stirred (300 rpm) double distilled and filtrated water. After injection of the organic phase, the resulting colloidal suspension was stirred for 3 h under reduced pressure to remove organic solvent. Nanosuspensions (NSs) were characterised and used directly after preparation.

2.4 QD loading of nano-carriers

Hydrophobic QDs were stored as a 1 μM stock dispersion in decane. Prior to usage, QDs were transferred from decane to acetone by injection of 125 μL of QD dispersion into a magnetically stirred (300 rpm) 2.5 mL phase of acetone. Subsequently, the liquid was evaporated for 3 h while stirring under reduced pressure, whereas acetone was refilled in 10 min intervals. The resulting reddish dispersion was used directly after preparation. Transferred QDs were then added to a solution of the respective polymer in acetone to reach the final polymer/QD ratio and a polymer concentration of 5 mg/mL. The solvent displacement procedure was carried out as described above.

2.5 Complexation of nano-carriers with siRNA

Freshly-prepared nano-carriers (blank or QD-loaded) were complexed with siRNA (or AF-siRNA) at respective N/P-ratios by addition of the appropriate amount of aqueous siRNA solution ($c=100 \mu\text{M}$) to an aliquot of NS ($c=1 \text{ mg/mL}$) followed by vigorous mixing. siRNA-loaded nano-carriers were characterised and used directly after preparation.

2.6 Size measurements

The average particle size and size distribution were determined by dynamic light scattering (DLS) using a Zetasizer NanoZS/ZEN3600 (Malvern Instruments, Herrenberg, Germany). Analyses were performed at a temperature of 25 °C using samples appropriately diluted with filtrated and double distilled water. The particle mean diameter (z-ave.) and the width of the fitted Gaussian distribution, which is displayed as the polydispersity index (PDI), were calculated from data of at least 10 runs and are displayed as the mean value of three independent measurements \pm standard deviation.

2.7 *In vitro* experiments

2.7.1 Cellular uptake

Cellular uptake of nano-carriers was determined by flow cytometry measurements [19]. Nano-carriers were assembled in triplicates and complexed with AF-siRNA at N/P=5 as described above. SKOV3 cells were seeded at a density of $8 \cdot 10^4$ cells per well in 24-well plates 24 h prior to the experiment. Subsequently, freshly-prepared carrier complexes were added to reach a siRNA concentration of 50 pmol per well. After different incubation times (15-240 min), cells were washed with PBS buffer and incubated for 5 min with 0.4% trypan blue to quench extracellular fluorescence. Afterwards, cells were detached using 100 μ L of trypsin and treated with 900 μ L of PBS solution containing 10% FCS. Cells were then collected by centrifugation and resuspended in 300 μ L of FACS Cellfix solution (BD Biosciences, San Jose, CA). Cell suspensions were measured on a FACS CantoTM II (BD Biosciences, San Jose, CA) with excitation at 633 nm and emission filter set to 660 nm bandpass. 10,000 viable cells were evaluated in each experiment and the geometric mean fluorescence intensity (MFI) was calculated as the mean value of three independent measurements. Data acquisition and analysis was performed using FACSDiva software (BD Biosciences, San Jose, CA). Results are presented as mean values \pm standard deviation of three independent experiments.

2.7.2 Transfection efficiency

In vitro transfection efficiency was determined by quantitative real time (qRT-PCR). SKOV3 cells were seeded in 6-well-plates at a density of $1.5 \cdot 10^6$ cells/well 24 h before transfection. Subsequently, fresh medium (containing 10% FCS) and NS complexed with hGAPDH_DsiRNA or negative control DsiRNA at N/P=5, were added to each well to reach a final siRNA concentration of 100 pmol/well. LF (0.5 μ L/10 pmol of

siRNA) served as a positive control. After 4 h of incubation at 37 °C, the medium was exchanged and cells were incubated for another 20 h before they were washed with cold PBS and lysed with lysis buffer (PureLinkTM RNA Mini Kit). Afterwards, mRNA was isolated from culture cells using the PureLinkTM RNA Mini Kit (with additional DNase I digestion, 18 U per isolation) and reverse transcribed to cDNA employing the First Strand cDNA Synthesis Kit on a TGradient thermocycler (Biometra GmbH, Goettingen, Germany). qRT-PCR was performed employing the SYBRTM Green PCR Kit and a RotorGene3000RT-PCR thermal cycler (Corbett Research, Sydney, Australia). Hs_GAPDH-primers were used to quantify hGAPDH gene expression and Hs_β-actin-primers were utilised as internal standard to determine relative expression levels for each gene. Calibration curves for GAPDH and β-actin mRNA were prepared by serial dilutions of cDNA of the blank sample (untreated cells). Measurements were carried out in triplicates. Values are presented as mean values ± standard deviation.

2.7.3 Confocal laser scanning microscopy

CLSM was performed on a Zeiss (Jena, Germany) Axiovert 200M to visualise interactions of FRET-complexes with SKOV3 cells. A diode laser (405 nm) was chosen for excitation; emission was detected in the blue (420-480 nm, DAPI), green (545-635 nm, QD) and red (> 650 nm, AF) channel. QD fluorescence was pseudo coloured as green in order to distinguish it from red AF fluorescence. QD-loaded carriers were prepared and complexed with AF-siRNA at N/P=5 as described above. Cells were seeded at a density of $1.5 \cdot 10^4$ cells per well in 8 well chamber slides. 24 h after seeding, cells were treated with freshly-prepared carrier complexes to reach a concentration of 50 pmol siRNA per well and incubated in medium containing 10% FCS for 4 h at 37 °C. Subsequently, cells were washed with PBS (pH 7.4), quenched with 0.4% trypan blue solution, washed again with PBS and fixed using 4% paraformaldehyde in PBS. Fixed cells were then nucleus-stained with DAPI (Molecular Probes, Eugene, OR, USA), washed with PBS for two more times and finally embedded utilising FluorSave reagent (Calbiochem, Merck Biosciences, Darmstadt, Germany).

2.8 *In vivo* experiments

Six-week-old balb/c mice (~20 g) were used for *in vivo* experiments. All animal experiments were carried out according to the German law of protection of animal life and were approved by an external review committee for laboratory animal care (reference number 2011/43, Regierungspraesidium Giessen). On the day of the experi-

ments, mice were anaesthetised with xylazine (13 mg/kg) and ketamine (65 mg/kg). Mice (n=5 for each group) were intubated through mouth and trachea with the flexible tube of a 24-gauge catheter (BD Insite, Becton Dickinson GmbH, Heidelberg, Germany). Freshly-prepared nano-carriers were complexed with mGAPDH_siRNA or negative control siRNA at N/P=5. After 5 min of incubation, NS containing 35 μ g siRNA per mouse was intratracheally instilled into the lungs. Control mice were treated with the same volume of 5% glucose. After 5 days, mice were sacrificed, and lungs were inflated and fixed in situ with 4% paraformaldehyde. For bronchoalveolar lavage (BAL) tracheae were cannulated and lungs were rinsed 10 \times with 1 mL of fresh ice-cold PBS. Samples for microscopic analysis were embedded in paraffin. The deparaffinised slices (3 μ m) were embedded with FluorSave to protect the fluorophores.

For measuring *in vivo* transfection efficiency tissue samples were placed into a mortar together with a small amount of liquid nitrogen and grinded into a powder using the pestle. After addition of 1 mL peqGOLD TriFastTM (PEQLAB Biotechnologie GmbH, Erlangen, Germany) into the frozen tissue powder, the tissue suspension was incubated at room temperature for 5 min. Subsequently, the suspensions were added to 200 μ L of chloroform each and mixed by shaking for 15 sec. After incubation of 2-15 min at room temperature, the suspensions were centrifuged for 5 min at 12,000 \times g to form a pellet and the supernatant was transferred into a tube for mRNA isolation. After addition of 500 μ L of isopropanol followed by vigorous mixing, the mRNA containing solution was stored at -80 $^{\circ}$ C for 30 min. Then, the sample was allowed to thaw and centrifuged at 4 $^{\circ}$ C and 12,000 \times g for 10 min. The supernatant was discarded and the pellet was vigorously mixed with 1 mL of aqueous ethanol solution (75%). Then, the sample was centrifuged (4 $^{\circ}$ C, 12,000 \times g, 5 min) one more time and the resulting pellet was stored in ethanol at -80 $^{\circ}$ C. The specimen was allowed to thaw, the supernatant was discarded and the pellet was dried under reduced pressure for 30 min. Finally, the pellet was dissolved in 60 μ L of RNase free water and incubated for 10-15 min at 55 $^{\circ}$ C. Samples were stored at -80 $^{\circ}$ C and isolated mRNA was further quantified by qRT-PCR as described above.

2.9 Fluorescence spectra

Fluorescence spectra were utilised to prove FRET induced AF emission upon QD excitation at 430 nm. QD loaded carriers (7.5 pmol QD per mg polymer) were complexed with siRNA at N/P=10. To evaluate the appropriate amount of AF for optimal FRET efficiency, AF-siRNA was mixed with unlabelled siRNA prior to complexation to reach various AF/QD ratios (0, 0.25, 0.5, 1, 2, 4 mmol AF-

siRNA per mg polymer) at constant N/P. Uncomplexed AF-siRNA was measured for comparison reasons. Fluorescence was analysed 30 min after complexation in opaque FluoroNunc 96 well plates (Nunc, Thermo Fisher Scientific, Langenselbold, Germany) with a TECAN Safire 2 plate reader (Männedorf, Switzerland). Emission wavelength step size was set to 1 nm. Relative fluorescence values as a function of emission wavelength were calculated from data of at least 10 reads.

2.10 SYBRTM Gold assay

To mimic FRET switching functionality, fluorescent siRNA was displaced from the carrier by addition of heparin, whereas in parallel SYBRTM Gold intercalation assays were applied to quantify the degree of displacement. The QD-bearing nanoparticle batches, complexed at N/P=10 with AF-siRNA, were standardised to the same polymer concentration, to equalise the absorption of intercalate-signal by the presence of water insoluble polymer, and added to opaque FluoroNunc 96 well plates (Nunc, Thermo Fisher Scientific, Langenselbold, Germany) for analysis. Nano-carriers without siRNA served as blank control. Samples were incubated 10 min in the dark after adding SYBRTM Gold reagent and analysed with the TECAN Safire 2 applying 485 nm excitation and 520 nm emission wavelength. Each data point was recorded as the mean value of 10 runs. Samples were prepared in quadruplicates and values are presented as mean values \pm standard deviation. Subsequent to SYBRTM Gold measurements, fluorescence spectra of FRET-complexes with and without heparin were recorded as described above.

3 Results and discussion

To delineate a relationship between polymer structure and nano-carrier performance, the influence of the PEG shell thickness was evaluated. Two different PEG chain lengths (PEG500, PEG2000) with different abilities to shield the cationic PEI charges were employed in the subsequent experiments to prove the impact on cell interaction and ultimately transfection efficiency. Intracellular uptake was quantified via flow cytometry (Figure V.1). Whereas PEG500-PCL10,000-PEI2500 vectors showed a rapid cell uptake within 2 h, fluorescence of cells incubated with PEG5000-carriers remained at baseline level.

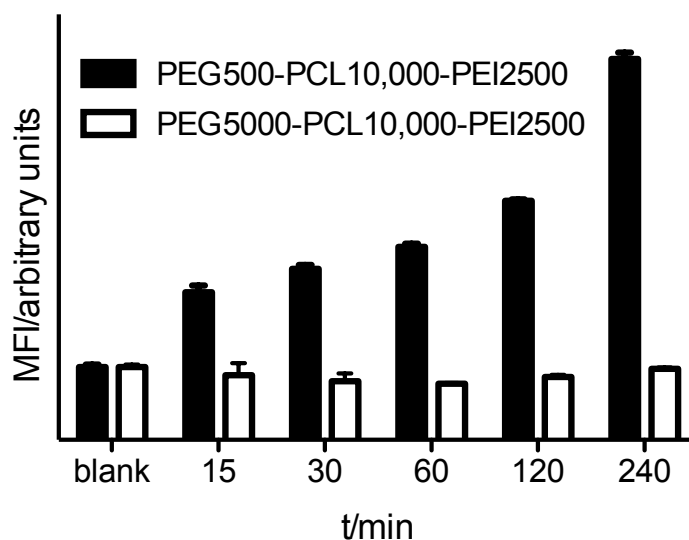


Figure V.1: *In vitro* cell uptake of nano-complexes with different PEG shell-thicknesses determined by flow cytometry (λ_{ex} : 633 nm, λ_{em} : 660 nm); measurements were carried out in triplicates and values are presented as mean values \pm standard deviation.

Flow cytometry results are in a good agreement with transfection efficiencies, that were not only determined *in vitro*, but also *in vivo* (Figure V.2 A). Nano-carriers constructed from polymers with shorter PEG segments (i.e. PEG500) showed superior transfection efficiency ($61 \pm 5\%$ knockdown *in vitro*, $55 \pm 18\%$ knockdown *in vivo*). By contrast, poor transfection performance was observed for the nano-carriers composed of PEG5000-PCL10,000-PEI2500 ($13 \pm 6\%$ knockdown *in vitro*, $30 \pm 17\%$ knockdown *in vivo*). Decreased normalised GAPDH expression for negative control samples of the PEG500 polymer (Figure V.2 A) indirectly suggest elevated toxicity of this vector system. To determine the spatial distribution of AF-siRNA containing carriers in the lung after intratracheal administration, histology specimens of fixed lung samples were investigated by fluorescence microscopy (Figure V.2 B) and emission was predominantly observed in the alveolar region of the lung tissue.

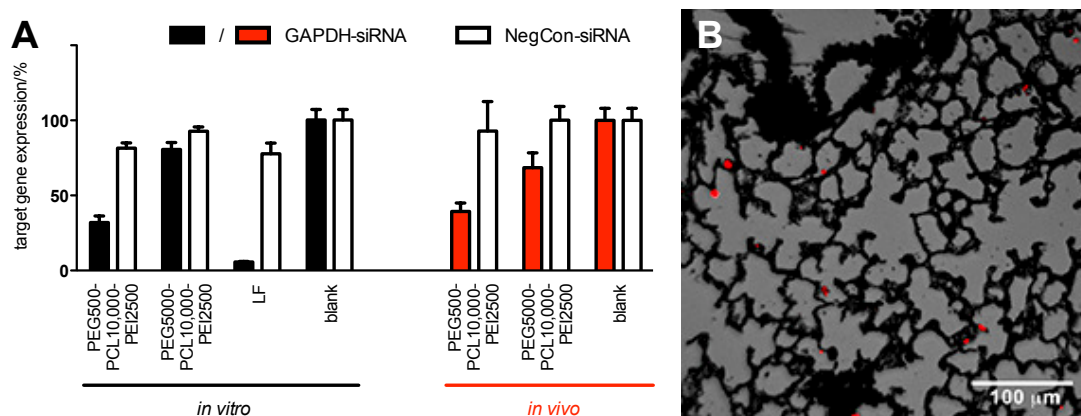


Figure V.2: A: *In vitro* and *in vivo* knockdown efficiency of nano-complexes with different PEG moiety. *In vitro* transfection efficiency (SKOV3 cells) was determined by qRT-PCR. Hs_GAPDH-primers were used to quantify hGAPDH gene expression, Hs_ β -actin-primers were utilised as internal standard to determine relative expression levels for each gene. Lipofectamine (LF) was used as a positive control. Values are presented as mean values \pm standard deviation (n=3). For *in vivo* measurements nano-complexes were instilled into the lungs of balb/c mice 5 d prior to sacrifice. Subsequently, mRNA was isolated from the murine lung tissue and knockdown was determined by qRT-PCR analogous to *in vitro* samples with Mm_GAPDH and Mm_ β -actin primers. Values are presented as mean values \pm standard deviation (n=5 for each group). B: Fluorescence microscopy image of lung tissue instilled with carrier complexes from PEG500-PCL10,000-PEI2500 carriers and AF-siRNA after lavage. Uptake of siRNA into the alveolar epithelium is represented by the fluorescently labelled siRNA shown in red.

The results obtained from cell uptake and transfection efficiency studies are in line with differences in the shielding of positive PEI charges by PEG segments of different length. Surface charge and cytotoxicity of this type of carrier system were previously shown to decrease as a function of PEG segment length [118]. As high surface charge enhances the adhesion of the cationic complexes to the negatively charged cell membranes, an increased cellular uptake of nano-carriers via passive endocytosis is obtained, however, at a higher cytotoxic potential. Similar results were previously reported for branched PEI bearing block-copolymers as a function of PEG graft density [80, 139, 77] as well as for cationic amphiphiles with increasing PEG segment length [67]. While an increased positively-charged carrier surface may result in high transfection efficiency *in vitro*, it can be detrimental under *in vivo* conditions, where interaction with negatively-charged tissues may irreversibly lead to cell death/necrosis [33]. Accordingly, positively charged nanoparticles were shown to cause increased toxicity on local and systemic level after intratracheal administration [166]. Further, in case of nanospheres translocating across the alveolar barrier,

clearance mechanisms are known to lead to rapid excretion of hydrophobic and/or highly charged substances [16, 15]. Having a closer look on the data presented in Figure V.2 A, this trend can be recognised for the investigated system with different PEG shell thickness: For the hydrophobic carrier, knockdown-efficiency *in vivo* slightly decreases as compared to the *in vitro* experiment, whereas the *vice versa* effect was seen for the more hydrophilic vector. Nevertheless, the results from *in vitro* and *in vivo* transfection experiments demonstrated excellent agreement, whereas nano-carriers prepared from PEG500-PCL10,000-PEI2500 turned out to be more effective under both experimental conditions. Therefore, this ratio of hydrophilic and hydrophobic polymer blocks results in a yet active vector with advantageous toxicity as compared to PEI homopolymers [118]. Fluorescence after instillation of PEG500-PCL10,000-PEI2500 carriers was primarily observed in the alveolar region of the lung tissue, whereas no emission was found in the vascular endothelium (Figure V.2 B). This suggests that carrier complexes remained in the lung and no translocation through the air-blood barrier took place, at least in the observed time span of 4 h. This is in a good agreement with studies on nanoparticles of various sizes (20, 100, 1000 nm) by Sarlo *et al.*, where no extra-pulmonary translocation of particles ≥ 100 nm was detected [167]. Whereas the air-blood barrier was reported to be permeable to hydrophilic pharmaceuticals such as nucleic acids [168], no such effects were seen in our studies for AF-siRNA. Moreover, the micrograph of alveolar tissue after lavage and removal of macrophages, other mobile cells, and surface-bound particles confirms the internalisation of the siRNA containing nanocarriers into the epithelium, which is the prerequisite for gene knockdown. This is a great improvement in comparison to lipid siRNA carriers that were reported to be found only in macrophages after pulmonary administration [169]. These results are also in accordance with the efficient *in vivo* knock-down, which was obtained from the homogenised lung tissue of PEG500-PCL10,000-lPEI2500 carriers. Therefore, from a clinical point of view, the amphiphiles presented in this work represent a promising carrier system for local treatment of airway diseases due to their increased retention time in the lung which is subsequently leads to high local drug concentrations [170].

To prove the concept of utilising loading of hydrophobic PCL moieties for “theranostic” purposes, QDs were encapsulated during the solvent displacement process. For obtaining a co-loaded complex with FRET functionality, AF-siRNA was subsequently used for complexation (Figure V.3). This was performed as a prototype for the well performing PEG500-PCL10,000-lPEI2500 nano-carrier. QD605 (λ_{em} : 605 nm) and AF647 (λ_{ex} : 647 nm, λ_{em} : 679 nm) were chosen as a FRET donor-acceptor pair. QD-emission and AF-excitation spectra are well overlapping between

600 and 650 nm, which is one of the prerequisites for successful FRET occurrence. Furthermore, acceptor and donor are required to be in close proximity (<10 nm, [99]), which is generally feasible, because cationic PEI charges for nucleic acid complexation and hydrophobic PCL moieties for QD encapsulation are covalently tethered in the block-copolymer structure and hence in close contact upon following nano-carrier preparation [118]. Therefore, the distance of the fluorophores was within the range for the FRET-effect, whereas the energy transfer is supposed to take place at the interface between PCL core and PEG shell. Since QDs have a broad excitation window, an excitation wavelength of 450 nm was chosen in order to avoid direct acceptor excitation. Hence, it is strongly expected that intact complexes can emit FRET-induced red light at 679 nm wavelength upon excitation at 450 nm wavelength. By contrast, after unpacking and dissociation of the complex, emission wavelength is supposed to shift to 605 nm wavelength due to direct QD emission.

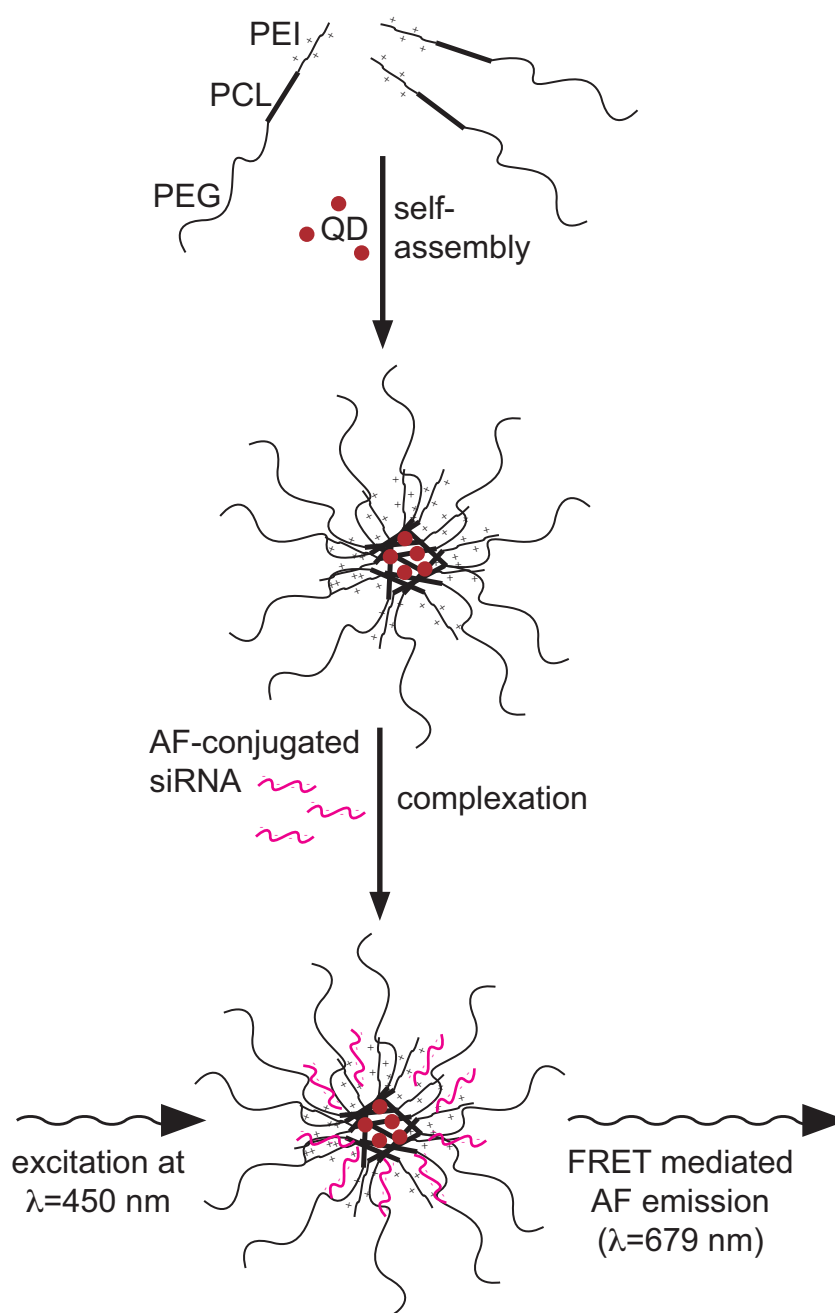


Figure V.3: Schematic illustration of the self-assembly process of QD-loaded nano-carriers by the solvent displacement method, followed by nano-carrier complexation with AF-siRNA. Intact FRET complexes emit at AF emission wavelength (679 nm) upon QD excitation (450 nm).

In a first step, loading capacity of the PCL core was evaluated. The hydrodynamic diameter was measured by DLS for various polymer/QD ratios (Table V.1). With increasing payload, carrier size and polydispersity increased from 94 nm (PDI=0.176) for unloaded carriers to a maximum diameter of 179 nm (PDI=0.392) for 10 pmol QD/mg polymer. To maintain sizes below the limit of endocytotic cell up-

take [131], 7.5 pmol QD/mg polymer yielding an average hydrodynamic diameter of 145 nm were used for further experiments.

Table V.1: Z-ave. and PDI of nano-carriers, loaded with various amounts of QDs; values are presented as mean values \pm standard deviation (n=3).

n(QD)/m(polymer) /pmol·mg ⁻¹	z-ave /nm	PDI
0.0	93.5±9.3	0.176±0.069
1.25	94.8±3.2	0.185±0.006
2.5	96.9±1.7	0.176±0.029
5.0	134.4±3.4	0.298±0.057
7.5	144.8±1.4	0.288±0.080
10.0	178.9±3.5	0.392±0.058

To test the hypothesis of FRET switching, QD-loaded carriers (7.5 pmol QD per mg polymer) were combined with AF-siRNA, whereas a mixture of labelled and unlabelled siRNA was employed for complexation to enable a constant N/P ratio at different QD/AF-ratios. Dose-dependent FRET induced AF signal emission at 679 nm was clearly identified upon QD excitation at 450 nm (Figure V.4). Rather weak AF intensity in comparison to the QD signal may be due to the self-quenching among a large number of AF molecules incorporated into a single complex [171, 172]. For the control samples, that are QD-loaded carriers with unlabelled siRNA (Figure V.4-(1)) and uncomplexed AF-siRNA (Figure V.4-(7)), no AF emission was noticed. Along with an increase in AF fluorescence, mitigating QD fluorescence intensity as a function of AF concentration was observed. This is supposed to be due to the transfer of energy from the donor to the acceptor, apparently leading to a decrease of donor fluorescence [99]. Hence, as shown in Figure V.4, detecting the ratio of donor and acceptor emission intensity can easily be employed for monitoring the degree of complex integrity in a sensitive manner.

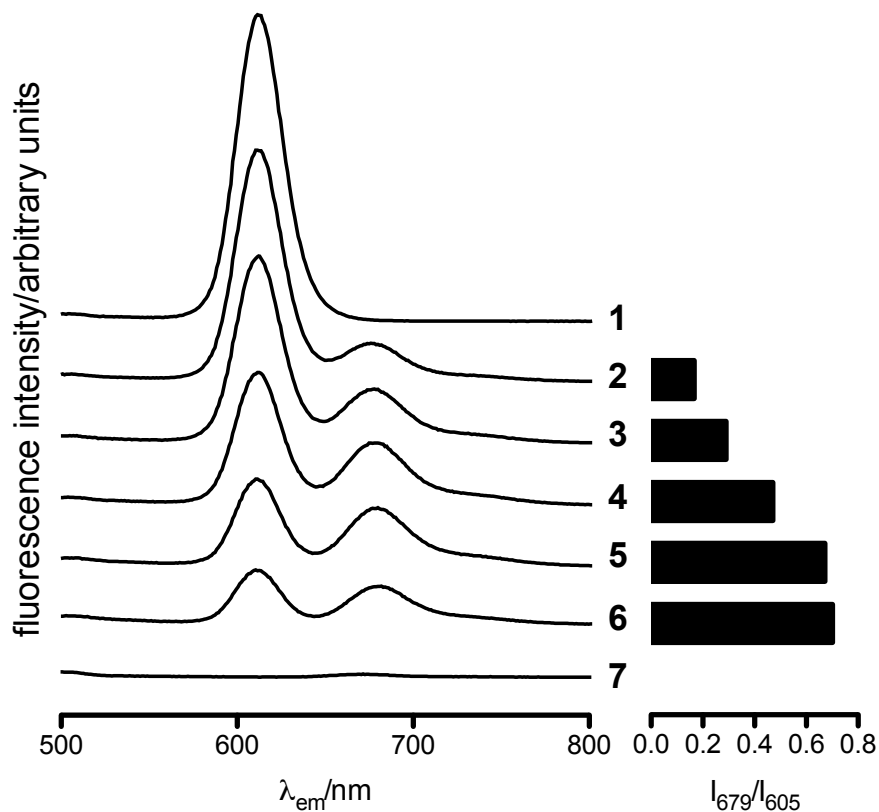


Figure V.4: Fluorescence emission spectra (λ_{ex} : 430 nm) of QD-loaded nano-carriers (7.5 pmol QD per mg polymer), complexed at N/P=10 with 0 (1), 0.25 (2), 0.5 (3), 1 (4), 2 (5) and 4 (6) mmol of AF-siRNA per mg polymer. The ratio of FRET induced AF (I_{679}) and QD (I_{605}) fluorescence intensity was used as a measure for FRET-efficiency. Uncomplexed AF-siRNA (7) was included for comparison reasons.

The concept of FRET monitoring was not only confirmed by fluorescence spectroscopy but also via fluorescence microscopy *in vitro* (SKOV3 cells). Upon excitation at 405 nm, QD (green channel) and AF fluorescence (red channel) were observed as an orange overlay in the cytosol (DAPI stained nuclei in blue channel) (Figure V.5). Presence of AF fluorescence upon QD excitation proved intact FRET complexes *in vitro*.

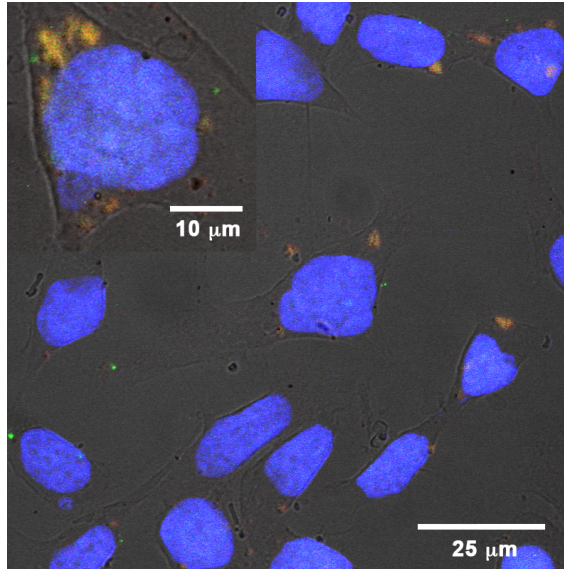


Figure V.5: Microscope image of QD-FRET complexes in SKOV3 cells; λ_{ex} : 405 nm; DAPI stained nuclei in blue; QD emission in green; Red FRET-induced AF emission proves complex integrity; orange colour indicates colocalisation.

Next, to test our design, we examined if AF emission could be quenched together with recovery of QD signal intensity (Figure V.6). Therefore, to mimic intracellular unpacking, polyanionic heparin was added to displace the majority of AF-siRNA from the carrier. As monitored by SYBRTM Gold assay, up to $81 \pm 2\%$ of the siRNA were displaced upon addition of the maximum amount of heparin. As expected, this resulted in a decrease in AF emission together with an increase in QD fluorescence emission intensity. After addition of heparin, the ratio of acceptor/donor fluorescence intensity decreased from 0.70 to 0.20. In line with SYBRTM Gold measurements this clearly indicates that most of the fluorescent dye was displaced from the carrier surface.

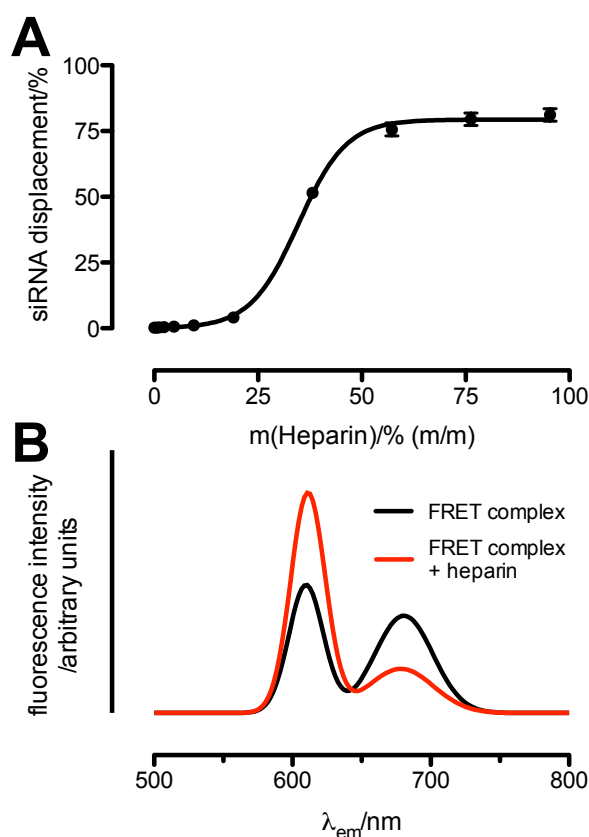


Figure V.6: The amount of siRNA displacement from the complex as a function of the competing polyanion heparin was measured via SYBRTM Gold assay; values are presented as mean values \pm standard deviation ($n=4$). B: Representative fluorescence spectrum ($\lambda_{ex}=430$ nm) of FRET-complexes (7.5 pmol QD and 4 mol AF-siRNA per g polymer) before and after displacement with heparin; decrease of acceptor/donor fluorescence intensity ratio (I_{679}/I_{605}) proves displacement of AF-siRNA from the carrier surface.

In the course of this work, the hydrophobic cores of amphiphilic nano-carriers that perform well *in vitro* and *in vivo* were successfully charged with fluorescent QDs and subsequently co-loaded with fluorescently labelled siRNA to provide FRET functionality. The resulting hybrid PEG-PCL-PEI QD-FRET gene carriers combine the benefits of cationic amphiphilic gene vectors such as high transfection efficiency, stability or low toxicity with bright QDs as imaging probes and FRET switching functionality for mechanistic investigations. QD-FRET studies in the literature commonly focus on a central QD scaffold with various functionalities grafted onto the surface [173]. On the basis of this principle, together with receptor binding functionality, biosensors for enzymes [161], dynamic biophysical processes [174] and various other organic molecules [175] have been studied. Carriers with central QD scaffolds have further been utilised in the field of gene delivery as multifunctional

“theranostic” vehicles [176, 177]. To elucidate the delivery process, those FRET capable systems have been employed for intracellular tracking of nucleic acid [178], drug [164] or combined nucleic acid/drug payloads [156]. In a different approach QDs have further been used to tag well-known carrier systems such as liposomes [95] or “polyplexes” based on PEI [95], PEG-PEI [165] or chitosan [99] to study their fate and unpacking behaviour. In these studies, however, carrier and nucleic acid were independently linked to fluorescent functionalities in a multi step process instead of physical entrapment. Whereas basic encapsulation of hydrophobic QDs into PLGA nanospheres [179] or micelles from PEG-PLGA, [180], Pluronic [181], or other types of block-copolymers [182] for therapeutic imaging and drug delivery [97] purposes represents a well known procedure, most of those systems are neither FRET capable, nor designed for gene delivery. Hence, physical entrapment of QDs for probing the fate of multifunctional amphiphilic gene-carriers has, to our knowledge, not yet been reported and may be applicable for various colloidal vector systems.

4 Conclusions

In summary, we reported herein the *in vitro* and *in vivo* evaluation of a PEG-PCL-PEI delivery system, which is capable of simultaneous delivery of nucleic acids plus hydrophobic substances such as drugs or dyes. In a first step, transfection performances of nano-carriers with different PEG shell thicknesses were not only determined *in vitro* but also *in vivo*. For the latter, siRNA loaded nano-carriers were pulmonary delivered to the lungs of balb/c mice. While nano-carriers constructed from rather hydrophobic amphiphiles (PEG500-PCL10,000-PEI2500) revealed good transfection efficiency ($61\pm 5\%$ knockdown *in vitro*, $55\pm 18\%$ knockdown *in vivo*), poor performance was found for their hydrophilic counterparts (PEG5000-PCL10,000-PEI2500) ($13\pm 6\%$ knockdown *in vitro*, $30\pm 17\%$ knockdown *in vivo*). This is in a good agreement with flow cytometry results, revealing 5-fold higher uptake of PEG500-carriers, possibly due to a thinner PEG shell and therefore an increased surface charge. Fluorescent microscopy images of murine lung tissue after instillation of AF-labeled carrier complexes revealed emission predominantly in the alveolar region, rendering this carrier system as promising for local treatment of airway diseases. Second, a well performing nano-carrier system was tested for its co-loading capability by charging the PCL reservoir with hydrophobic QDs. Subsequent complexation with fluorescently labelled AF-siRNA resulted in FRET capable carriers and energy transfer efficiency was optimised as a function of the ratio of acceptor/donor fluorophores. Fluorescence spectroscopy was further employed for *in vitro* FRET imaging. Fi-

nally, nucleic acid unpacking was mimicked by addition of heparin and thus the feasibility of FRET-switching functionality was approved (ratio of acceptor/donor fluorescence decreased from 0.70 to 0.20). As compared to QD-FRET systems in the literature based on covalent labelling or ligand strategies, the approach reported in this work offers the straightforward tagging of amphiphilic gene carriers with fluorescent QDs. In this versatile system the employed hydrophobic QDs could easily be exchanged by their analogues with varying optical characteristics (e.g. for non-invasive NIR detection *in vivo*), hydrophobic drugs or a mixture thereof to result in tailored vehicles for “theranostic” approaches and/or for co-delivery of drugs and nucleic acids. Subsequent studies deploying “theranostic” and FRET functionality of this delivery system *in vitro* and *in vivo* are believed to enlighten the basic principles of the delivery process.

Acknowledgments

We are grateful to Roland Hartmann and Dominik Helmecke (Institute of Pharmaceutical Chemistry, Philipps-Universität Marburg) for their assistance with fluorescence spectroscopy. Moreover we would like to thank Wolfgang Parak, Xiang Yu and Raimo Hartmann (Institute of Physics and WZMW, Philipps-Universität Marburg) for supporting us with fluorescence microscopy.

Part VI

Summary

Part I briefly reviews the most important aspects of non-viral gene delivery: Gene therapy offers the opportunity of directly introducing genetic material into cells for a causal therapy of yet incurable diseases. Gene carriers are required for formulation of nucleic acids, to enable cell internalisation and to prevent enzymatic degradation. Gradually, non-viral approaches have been considered as superior to viral ones and the discovery of RNAi enabled a new scope of transient gene therapy. Tailored polymeric carriers protect and guide the nucleic acid payload on its way into the target cell to tackle various challenges that arise *in vitro* and *in vivo*. Early non-viral gene delivery carriers such as PEI homopolymers have been constantly evolved to increasingly smart multifunctional delivery vehicles. In particular amphiphilic block copolymers, with their potential to self-assemble to various types of nano-carriers are regarded as suitable platforms for those sophisticated delivery systems. The modular designed PEG-PCL-PEI block copolymer platform, which has been established in the course of this thesis, represents a promising candidate of this new class of multifunctional, amphiphilic, cationic gene delivery vehicles.

It was the aim of **part II** to establish a set of carriers with varying hydrophilic/hydrophobic ratio and to derive a relationship between chemical structure and carrier characteristics. Therefore, a block copolymer library was synthesised, characterised and assembled into carriers. Subsequently, a non-invasive structural characterisation of the carrier assemblies in the liquid state was carried out. Carrier size was determined using DLS, cryoSEM and AFM. The core-corona structure of assemblies was elucidated via ζ -potential measurements and the PEG shell thickness was identified for different PEG segment lengths. Following, the impact of carrier structure on physicochemical and biological features was investigated: Colloidal stability and toxicity were found to depend on the length of the hydrophilic polymer block. Polymers hydrophilic in nature formed small (<40 nm) micelle-like carriers, whereas hydrophobic polymers aggregated to larger particle-like assemblies (>100 nm). Monitoring carrier size as a function of initial polymer concentration clarified different assembly mechanisms. The uncovering of a structure-function relationship allowed the systematic picking of representative compounds from each carrier class (particle and micelle) for further investigation. Contrary to screening

different polymers by trial and error, this systematic approach enables the selective manufacturing of tailor-made gene vectors.

It was the aim of **part III** to understand and optimise the assembly and loading process of previously picked polymer compounds. It is well known that polymer design and N/P ratio have a huge impact on carrier characteristics. The manufacturing process, however, had previously only roughly been investigated. Hence, for manufacturing compactly condensed carrier complexes at low N/P, it was hypothesised that a more homogeneous complexation procedure is supposed to lead to a more uniform distribution of charges and subsequently to increased colloidal stability, RNA protection and finally transfection efficiency. Microfluidic mixing techniques, bringing cationic polymer and nucleic acid together at a constant ratio during the entire mixing process, have the potential for a gentler complexation. In a first step, to elucidate complex formation and to narrow down suitable N/P ratios, size and ζ -potential were measured as a function of N/P. Then, the optimal timing for addition of siRNA was investigated. Therefore, complex diameters for addition of siRNA during (addition to the aqueous or the organic phase) or after (classical pipetting or microfluidic mixing) carrier assembly were monitored. Subsequently, for the most promising techniques (loading after assembly), colloidal stability, the ability to protect RNA as well as transfection efficiency *in vitro* were compared. Finally, parameters for the superior microfluidic mixing process were optimised with the help of a central composite design. It was noticed that the loading procedure is a predominantly charge controlled process and a discrepancy between stoichiometric and effective N/P was owed to the 3D-structure of the complex. As expected, a gentler loading leads to more homogeneous complexes. Hence, possibly due to a more consistent surface coating, loading after carrier assembly resulted in less aggregation. In comparison to bulk mixing, microfluidic assembly exhibited smaller diameters (179 ± 11 vs. 230 ± 97 nm), less heterogeneity ($\text{PDI}=0.205\pm 0.028$ vs. 0.353 ± 0.161), enhanced RNA protection (RNA recovery= 30.6 ± 1.0 vs. $15.4\pm 1.4\%$) as well as increased transfection performance (34.8 ± 1.5 vs. $24.5\pm 2.2\%$ knockdown *in vitro*). Hence, it was demonstrated that the Coulomb driven process can be controlled effectively by varying the basic conditions of charge fusion. This enables the manufacturing of carrier complex suspensions at high concentrations and low N/P ratios, which are prerequisites for *in vivo* usage. In particular the microfluidic complexation procedure represents a reproducible alternative for formulating gene delivery carriers with superior colloidal stability, RNA protection and transfection efficiency. The data collected in the central composite design enable the predic-

tion and fine-tuning of complex-size as a function of various intimately connected parameters.

It was the overall goal of **part IV** to transfer preassembled carriers and carrier-complexes to the dry state as ready-to-use formulations, which is a prerequisite for effective *in vivo* usage. Therefore, freshly-prepared nano-suspensions were lyophilised with glucose as lyoprotectant. Firstly, the required glucose concentration for sufficient stabilisation of unloaded carriers was determined via DLS. Morphology of fresh and rehydrated carriers was visualised by cryogenic scanning electron microscopy. Subsequently, the feasibility of siRNA loading before and after lyophilisation was investigated. For both strategies complex diameter and *in vitro* transfection efficiency were determined and correlated to freshly-prepared samples. Hydrodynamic diameter (95.2 ± 1.4 nm) and size distribution (0.132 ± 0.019) of unloaded nano-suspension were restored after rehydration by addition of $\geq 1.5\%$ of glucose before lyophilisation. Moreover, after loading of rehydrated carriers with siRNA, no significant difference in complex size was observed as compared to freshly-prepared ones. Stabilisation of pre-formed carrier/siRNA complexes during lyophilisation is feasible at elevated N/P (e.g. 20) and glucose concentrations above 5%. As determined via RT-PCR, lyophilised samples were as active as freshly-prepared ones regarding transfection efficiency. Therefore, lyophilisation is an effective technique to produce physically stable PEG-PCL-PEI formulations. These general findings may also be applicable to further particulate gene delivery systems to shelf ready-to-use formulations.

In the course of the previous parts, the polymer library was narrowed down to two paradigmatic compounds. It was the aim of **Part V** to investigate these polymers *in vitro* and *in vivo* to deduce a relationship between chemical composition and biological activity. Furthermore, it was the goal to prove the feasibility of dual carrier loading by charging the PCL cargo with hydrophobic fluorescent QDs followed by complexation of the resulting carriers with fluorescently labelled siRNA. Hence, a FRET pair for monitoring nucleic acid unpacking was to be established. *In vitro* transfection efficiencies of carriers with different PEG shell thickness were determined by RT-PCR and cell uptake was measured by flow cytometry. For *in vivo* experiments nano-carrier suspension was instilled into the lungs of four-week-old balb/c mice and transfection efficiency was determined after 5 d by RT-PCR. Well performing vectors were subsequently co-loaded with QDs and fluorescent siRNA and the resulting double-labelled complexes were analysed via fluorescence spectroscopy and fluorescence microscopy *in vitro*. Carriers constructed from rather hydrophobic block copolymers showed superior transfection efficiency ($61\pm 18\%$ knockdown *in*

vitro, $58\pm 20\%$ knockdown *in vivo*), whereas poor performance was found in case of predominantly hydrophilic ones ($13\pm 5\%$ knockdown *in vitro*, $32\pm 10\%$ knockdown *in vivo*) in a good correlation *in vitro* and *in vivo*. FACS studies revealed that this might possibly be due to reduced cell uptake of carriers with thicker PEG shell preventing cell interaction ($5\times$ extenuated uptake after 240 min). Double-labelled nano-carriers emitted light at the acceptor's emission wavelength upon donor excitation, proving successful FRET-effect and hence, complex integrity. Upon complex dissociation, which was simulated by addition of the polyanion heparin, a dose-dependent decrease in FRET-efficiency was observed, resulting in a shift to the donor emission wavelength. In the course of this part *in vitro* and *in vivo* delivery efficiency of different polymer compounds was investigated and correlated to chemical composition. The ability of double loading is especially useful for "theranostic" purposes or co-delivery of nucleic acids and drugs. FRET-switching functionality may be advantageous for monitoring complex stability and nucleic acid unpacking.

The five parts of this thesis comprehend the establishment of a multifunctional gene therapy platform. Across the scientific disciplines of chemistry, chemical physics, pharmacy and biomedicine the underlying work covers all aspects of non-viral gene delivery: In a first step, block copolymers were synthesised and characterised. Subsequently, the polymeric amphiphiles were assembled into carriers and their physicochemical properties were thoroughly investigated. Then, the nucleic acid loading process was optimised, carriers were transferred into stable ready-to-use formulations and finally tested for their *in vitro* and *in vivo* transfection efficiency. Furthermore, the feasibility of multifunctional carrier co-loading and FRET-monitored nucleic acid unpacking was approved. With the aim of deducing a structure-activity relationship, a library of block copolymers with systematically varying hydrophilic/hydrophobic ratio was built and, with advancing knowledge about the delivery system, confined to the most promising compounds. This refinement process resulted in the selection of two paradigmatic carriers with oppositional chemical composition, physicochemical characteristics and subsequently distinct *in vitro* and *in vivo* behaviour.

Zusammenfassung

Kapitel I fasst die wichtigsten Aspekte nicht-viraler Gentherapie zusammen: Im Gegensatz zu einer symptomatischen Behandlung schwerwiegender Erkrankungen ermöglicht die Gentherapie einen kausalen Therapieansatz durch direkte Manipulation

genetischen Materials. Trägersysteme werden im Rahmen dieser Therapie erforderlich, um Nucleinsäuren vor Abbau zu schützen und um eine Wechselwirkung negativ geladener Nucleinsäuren mit der Zellmembran überhaupt erst zu ermöglichen. Maßgeschneiderte Vektoren schützen hierbei genetisches Material und transportieren es spezifisch über die vielen Hindernisse biologischer Systeme hinweg zum Wirkort. Während anfangs vor allem virale Vektoren im Focus wissenschaftlicher Bemühungen standen, zeichnete sich in den letzten Jahren ein Umdenken hin zu nicht-viralen Ansätzen ab. Ferner eröffnete die Entdeckung der RNAi-Technologie neue Möglichkeiten zur vorübergehenden Abschaltung bestimmter Gene. Nicht-virale Trägersysteme der ersten Stunde bestanden hauptsächlich aus Homopolymeren wie PEI zur Komplexierung von Nucleinsäuren. Seitdem setzte jedoch eine rasante Weiterentwicklung dieser Systeme ein, welche bis zum heutigen Zeitpunkt immer wieder neue, ausgefeilte und multifunktionale Vektoren hervorgebracht hat. So finden selbstorganisierende Blockcopolymere als Nanoträger Anwendung und deren Eigenschaften können durch chemische Modifikation optimal angepasst werden. Die modular aufgebauten PEG-PCL-PEI Blockcopolymere, welche im Rahmen dieser Arbeit synthetisiert und untersucht wurden, bieten als vielversprechende Vertreter dieser Vektorklasse eine universale Basis für den Aufbau moderner, multifunktionaler Trägersysteme.

Ziel des **Kapitels II** war der Aufbau einer Vektorbibliothek aus PEG-PCL-PEI Blockcopolymeren. Das Verhältnis aus hydrophilen und hydrophoben Kettensegmenten wurde hierbei systematisch variiert, um einen Zusammenhang zwischen chemischer Struktur und den physikochemischen und biologischen Eigenschaften der Träger herzustellen. Die Blockcopolymere wurden in einer dreistufigen Synthese hergestellt, charakterisiert und zu Trägern verarbeitet. Eine nicht-invasive Charakterisierung dieser Systeme in ihrer wässrigen Umgebung beinhaltete die Bestimmung des hydrodynamischen Durchmessers mittels DLS, cryoSEM und AFM. LDA-Messungen des ζ -Potentials bestätigten die postulierte Kern-Hülle-Struktur der Träger und ermöglichten die Kalkulation der Schichtdicke der PEG-Hülle. Anschließend wurde der Einfluss der chemischen Trägerzusammensetzung auf die physikochemischen und biologischen Eigenschaften (Kolloidstabilität und Toxizität) untersucht. Überwiegend hydrophile Polymere bildeten kleine (<40 nm), mizellartige Träger, während eher hydrophobe Ketten sich zu größeren (>100 nm), partikelartigen Vektoren zusammenballten. Durch Messung des hydrodynamischen Durchmessers in Abhängigkeit der Polymerkonzentration während der Herstellung wurden unterschiedliche Mechanismen der Selbstorganisation nachgewiesen. Insbesondere wurde ein direkter Zusammenhang zwischen der Länge des hydrophilen Segments, PEG-

Schichtdicke, Kolloidstabilität und Toxizität eindeutig bewiesen. Geeignete Verbindungen aus der Vektorbibliothek wurden selektiert und in die nächste Projektphase überführt. Die Erforschung eines Zusammenhangs zwischen Polymerzusammensetzung und den Eigenschaften der Träger ermöglichte die selektive Auswahl repräsentativer Polymere einer jeden Vektorklasse (Partikel und Mizelle) mit dem Ziel der Herstellung maßgeschneiderter Therapiesysteme.

Ziel des **Kapitels III** dieser Arbeit war die Erforschung und Optimierung des Prozesses der Selbstorganisation von Polymeren zu Trägern und deren Beladung mit Nucleinsäuren. Es ist bekannt, dass das N/P-Verhältnis und die chemische Struktur des Polymers einen großen Einfluss auf die Trägereigenschaften haben. Der Herstellungsprozess und die Beladung von Trägern jedoch wurden bisher kaum untersucht. Dieses Kapitel basiert auf der Hypothese, dass ein gleichmäßigerer Komplexierungsvorgang zu einer homogeneren Verteilung von Ladungen und folglich zu verbesserter Kolloidstabilität, RNA-Einbettung und letztendlich auch Transfektionseffizienz führen sollte. Eine microfluidale Herstellungstechnik, bei der Träger und RNA während des gesamten Herstellungsprozesses gleichmäßig zusammengeführt werden, müsste folglich ideale Bedingungen zu garantieren. Für die Erforschung des Beladungsmechanismus und zur Evaluation geeigneter N/P-Verhältnisse wurden die Komplexdurchmesser und das ζ -Potential in Abhängigkeit des N/P-Verhältnisses ermittelt. Anschließend wurden Vektoren auf unterschiedliche Weise mittels einer Nanopräzipitationsmethode hergestellt. Ein Aspekt der Herstellung beinhaltete die Zugabe von RNA während des Selbstorganisationsprozesses des Trägers (durch Mischen von Nucleinsäure mit der wässrigen oder der organischen Phase). Andererseits wurde die nachträgliche Beladung von bereits gebildeten Trägern untersucht. Hier wiederum wurde die konventionelle Methode der Zugabe von RNA-Lösung mit einer kontinuierlichen, microfluidalen Technik verglichen. Die hydrodynamischen Durchmesser der auf unterschiedlichstem Wege hergestellten und beladenen Träger wurden anschließend mittels DLS erfasst. Für die vielversprechendste Methode der nachträglichen microfluidalen Beladung wurden die Prozessparameter im Rahmen eines statistischen Designs im Detail untersucht. Die Beladung von Trägern wurde als überwiegend ladungskontrollierter Vorgang identifiziert. Die Diskrepanz zwischen stöchiometrischem N/P-Verhältnis und Ladungsneutralität resultiert aus dem dreidimensionalen Aufbau der Trägerkomplexe. Eine nachträgliche Beladung führte wie erwartet zu kleineren und gleichmäßigeren Komplexen und die beiden Methoden der nachträglichen Beladung (konventionelle und microfluidale RNA-Zugabe) wurden daher genauer untersucht. Dies beinhaltete insbesondere einen direkten Vergleich von Kolloidstabilität, der Fähigkeit RNA vor Abbau zu schützen und der Transfektionseffi-

zienz *in vitro*. In Übereinstimmung mit der Hypothese der Verbesserung der Trägerqualität durch eine gleichmäßigere Beladung waren die durch nachträgliche Beladung entstandenen Komplexe wahrscheinlich deshalb weniger aggregiert, da diese Technik eine homogenere Anlagerung von Nucleinsäure an der Oberfläche des Trägers ermöglicht. Diese Annahme wurde durch Messergebnisse an microfluidal beladenen Trägern gestützt, welche sich durch kleinere Komplexdurchmesser (179 ± 11 vs. 230 ± 97 nm), gleichmäßigere Größenverteilungen ($\text{PDI} = 0.205 \pm 0.028$ vs. 0.353 ± 0.161), verbesserten Schutz der RNA vor Abbau (RNA-Wiedergewinnung = 30.6 ± 1.0 vs. $15.4 \pm 1.4\%$) sowie eine gesteigerte Transfektionseffizienz (34.8 ± 1.5 vs. $24.5 \pm 2.2\%$ knockdown) auszeichneten. Im Rahmen dieses Kapitels wurden Wege aufgezeigt, den Coulomb-kontrollierten Beladungsvorgang effektiv durch Variation der Rahmenbedingungen der Herstellung zu beeinflussen. Dies wiederum ermöglichte die Produktion von Nanokomplexsuspensionen hoher Konzentration bei niedrigem N/P-Verhältnis; beides vorteilhafte Bedingungen für einen effektiven Einsatz *in vivo*. Die automatisierte, microfluidale Komplexierungstechnik repräsentiert eine neuartige Variante, um Nanokomplexe gleichmäßiger, reproduzierbarer und mit verbesserten Eigenschaften herzustellen. Der Datensatz des statistischen Designs ermöglicht eine Vorhersage und Kontrolle der Komplexgröße in Abhängigkeit sich gegenseitig beeinflussender Herstellungsparameter.

Es war das Ziel von **Kapitel IV** Vektoren und Vektorkomplexe in eine lagerstabile, trockene Form zu überführen. Wasserfreie Träger könnten anschließend nach Rehydrierung schnell und reproduzierbar für *in vitro* und *in vivo* Experimente zur Verfügung stehen. Im Zuge der Untersuchungen wurden frisch hergestellte Trägersuspensionen unter Zugabe des Lyoprotektors Glucose gefriergetrocknet. In einem ersten Schritt wurde anhand von unbeladenen Trägern durch Größenmessung frischer und rehydrierter Träger die erforderliche Stabilisatormenge ermittelt. Im Zuge dessen wurde auch die Morphologie mittels cryoSEM direkt verglichen. Anschließend wurde evaluiert, ob auch beladene Träger durch Gefriertrocknung stabilisiert werden können. Für beladene und unbeladene Träger wurden daher nach Rehydrierung die hydrodynamischen Durchmesser und die Transfektionseffizienzen *in vitro* bestimmt und mit denen frisch hergestellter Vektoren verglichen. Bereits durch Zugabe von 1.5% Glucose konnten Durchmesser (95.2 ± 1.4 nm) und Größenverteilung (0.132 ± 0.019) unbeladener Träger nach Rehydrierung wiederhergestellt werden. Bei anschließender Beladung mit siRNA wurde im Vergleich zu frischen Trägern kein Unterschied bezüglich der Komplexgröße oder der Größenverteilung detektiert. Die Trocknung bereits beladener Trägerkomplexe gelingt bei erhöhten N/P-Verhältnissen (z. B. 20) ab einer Glucosekonzentration von 5%. Bezüglich ihrer

Transfektionseffizienz (durch RT-PCR ermittelt) unterscheiden sich weder getrocknete und anschließend beladene noch vor Trocknung beladene Träger von den frisch hergestellten Proben. Folglich eignet sich Gefriertrocknung hervorragend zur Überführung von Nanoträgern in einen lagerstabilen Zustand und diese Technik könnte auch für die Stabilisierung anderer amphiphiler Trägersysteme Anwendung finden.

Im Zuge der vorherigen Kapitel wurden letztendlich zwei Verbindungen mit spezifischen Eigenschaften aus der Vektorbibliothek ausgewählt. Diese sollten nun in **Kapitel V** zunächst auf ihre Transfektionsaktivität und Zellaufnahme *in vitro* hin untersucht werden. In einem nächsten Schritt wurde die Transfektionseffizienz *in vivo* ermittelt und mit den Ergebnissen der Zellkulturstudien korreliert. Ziel war hierbei die Ableitung eines spezifischen Zusammenhangs von chemischer Zusammensetzung und biologischer Aktivität. Ferner sollte die Möglichkeit einer doppelten Fluoreszenzmarkierung des Trägerkomplexes untersucht werden. Diese sollte durch Beladung des hydrophoben PCL-Kerns mit Quantenpunkten gefolgt von der Komplexierung mit fluoreszenzmarkierter siRNA realisiert werden. Ziel war folglich die Etablierung eines FRET-Paars, welches sich vor allem zur Detektion der Komplexintegrität eignet. Die *in vitro* Transfektionseffizienz der beiden Träger mit unterschiedlicher PEG-Schichtdicke wurde mittels RT-PCR, die Aufnahme in Zellen mittels FACS bestimmt. Im Rahmen der *in vivo* Experimente wurde eine Suspension aus Nanokomplexen in die Lungen von balb/c-Mäusen instilliert und die Transfektionseffizienz wurde nach fünf Tagen mittels RT-PCR quantifiziert. Der Vektor mit höherer biologischer Aktivität wurde im Anschluss wie beschrieben doppelt fluoreszenzmarkiert und mittels Fluoreszenzspektroskopie und Fluoreszenzmikroskopie *in vitro* untersucht. In guter Übereinstimmung der Ergebnisse *in vitro* und *in vivo* wurde bei hydrophoben Trägern eine hohe Transfektionseffizienz ($61\pm 18\%$ knockdown *in vitro*, $58\pm 20\%$ knockdown *in vivo*) ermittelt, wohingegen bei hydrophilen Vektoren kaum Aktivität detektiert wurde ($13\pm 5\%$ knockdown *in vitro*, $32\pm 10\%$ knockdown *in vivo*). Die Ergebnisse der FACS-Analyse zeigten, dass die geringe Aktivität hydrophiler Vektoren durch mangelnde zelluläre Wechselwirkung, höchstwahrscheinlich bedingt durch eine dickere PEG-Hülle, verursacht wird ($5\times$ niedrigere Aufnahme hydrophiler Komplexe nach 240 min). Die doppelt markierten hydrophoben Träger wurden mittels Fluoreszenzspektroskopie untersucht. Emission von Licht der Wellenlänge des Akzeptors bei Anregung des Donors lieferte den Beweis für den Energietransfer im intakten FRET-Komplex. Nach Entpacken der markierten siRNA (was durch Zugabe von Heparin simuliert wurde) veränderte sich erwartungsgemäß die Frequenz emittierten Lichts hin zu der des Donors. In diesem Kapitel wurde ein multifunktionales und biologisch aktives Vektorsystem geschaffen, welches sich her-

vorrangig für theragnostische Zwecke oder zu einer simultanen Verabreichung von Nucleinsäuren und Wirkstoffen eignet. Der FRET-induzierte Schalteffekt ermöglicht eine Echtzeituntersuchung von Komplexstabilität und Entladevorgang.

Gegenstand der vorliegenden Dissertation ist die Etablierung eines multifunktionalen Trägersystems für die Gentherapie. Hierfür erforderte das an der Schnittstelle unterschiedlichster wissenschaftlicher Disziplinen angesiedelte Thema fächerübergreifendes Arbeiten, um den chemischen, physikochemischen, pharmazeutischen und biomedizinischen Aspekten der Aufgabenstellung in vollem Umfang gerecht zu werden; notwendige Arbeiten reichten von der chemischen Polymersynthese und Charakterisierung über die physikochemische Charakterisierung selbst organisierender amphiphiler Strukturen, die optimale Formulierung dieser Verbindungen mit Nucleinsäuren, das Überführen der Träger in einen lagerfähigen festen Zustand bis hin zur Durchführung von Zellkultur- und Tierversuchen. Abschließend wurde das Trägersystem zusätzlich mit einem FRET-basierenden, sensitiven Mechanismus zur Detektion und Visualisierung intrazellulärer Vorgänge kombiniert. Zur Herleitung einer Kausalität zwischen chemischer Zusammensetzung mit physikochemischen und biologischen Eigenschaften entstand in der Synthesephase dieser Arbeit eine Bibliothek aus Blockcopolymeren mit variierender Hydrophilie. Im Zuge der Folgearbeiten wurden in jedem Arbeitsgang geeignete Verbindungen selektiert und genauer untersucht. Dieser Auswahlprozess endete in einer Gegenüberstellung zweier paradigmatischer Polymere mit unterschiedlicher chemischer Zusammensetzung, variierenden physikochemischen Eigenschaften und folglich auch voneinander abweichendem Verhalten *in vitro* und *in vivo*.

Part VII

Perspectives

One of the major hurdles of cationic non-viral delivery systems is the discrepancy between cell interaction and toxicity. Cationic surface charge from PEI amine functionalities increases the interaction with negatively charged cell membranes and the same time, however, this will inevitably increase unwanted interactions with blood components and tissue membranes in an unspecific manner. As a result membrane damage and cell necrosis lead to increased toxicity both on cellular and systemic level, making these highly charged polymers inapplicable for *in vivo* usage. Shielding of PEI charges by PEG can reduce toxicity but generally also leads to diminished activity. This basic relationship is the major reason for most active vectors just being also the most toxic ones. Therefore, to circumvent this charge-toxicity-relationship, carriers have to be taken up by the target tissue in a selective way, which can be achieved, up to a certain degree, via targeting ligands. A huge benefit of polymeric gene carriers is their ability to be optimally engineered by chemical modification. This also applies for the introduction of targeting functionalities such as transferrin, EGF or folic acid. Tailored PEG end groups may be utilised for coupling with targeting molecules e.g. by gentle click-chemistry reaction. Rather hydrophilic carriers with thicker PEG shells, increased colloidal stability and reduced toxicity represent the ideal candidates for this modification. This may possibly lead to increased affinity towards target tissue for an effective *in vivo* usage.

Part V includes a proof of concept study of encapsulating fluorescent QDs into the carrier PCL core. Whereas basic FRET functionality was shown by fluorescence studies, the potential of this multifunctional carrier system has not yet been fully exhausted. FRET based unpacking studies unveiling the kinetics of various carrier systems may contribute to clarify the mechanistic aspects of the delivery process and the intracellular fate of carrier and payload in a most sensitive manner. Bright and durable QDs may further be tracked for studying carrier biodistribution *in vivo*. Therefore, red-emitting QDs employed in this study may be exchanged by NIR emitting ones for non-invasive *in vivo* imaging.

In the long term, required work is evident: the development of more effective non-viral vectors and conquering the yet severe toxicity effects of current delivery systems mainly caused by host immune response. By a deeper understanding in the

mechanistic aspects of the gene delivery process plus a rational vector design we are on the right track to achieve that goal. Hopefully this work may contribute to the enormous scientific effort currently ongoing in the era of genomic medicine.

Ausblick

Zentrales Problem einer Vielzahl nicht-viraler Genvektoren ist noch immer die Diskrepanz zwischen zellulärer Wechselwirkung und Toxizität. Einerseits erhöhen die PEI-Kationen eine Aufnahme in die Zelle, andererseits führen genau diese positiven Ladungen auch zu unspezifischer Wechselwirkung. Daraus wiederum resultiert eine Schädigung von Membranen und Gewebe und somit eine Erhöhung der Toxizität auf zellulärer und systemischer Ebene, was eine *in vivo* Anwendung PEI-basierender Systeme mit hoher Ladungsdichte erschwert. PEGylierung ist zwar in der Lage, die Toxizität zu reduzieren, verringert aber aus genannten Gründen auch meist die Transfektionseffizienz. Diese Ambivalenz der positiven Ladung ist eine der Hauptursachen dafür, dass die Träger mit hoher biologischer Aktivität meist auch die mit erhöhter Toxizität sind. Die einzige Möglichkeit, diese Abhängigkeit zu durchbrechen, besteht in der Erhöhung der Selektivität des Trägersystems. Ziel ist letztendlich eine spezifische Aufnahme z. B. nur in erkrankte Zellen. Bis zu einem gewissen Grad ist das durch Einführung von geeigneten Rezeptoren in das Trägersystem heute bereits möglich. Eine der Stärken des in dieser Arbeit präsentierten Trägersystems ist dessen Möglichkeit der chemischen Modifikation. Dies schließt auch die Einführung neuer Funktionalitäten wie Folsäure, EGF oder Transferrin mit ein. So könnten beispielsweise die PEG-Endgruppen in einer Weise modifiziert werden, die eine anschließende Kupplung mit neuen Funktionalitäten, z. B. durch schonende „click-chemistry“-Reaktion, ermöglicht. Hydrophile Träger mit dicker PEG-Hülle, erhöhter Kolloidstabilität und geringer Toxizität wären die idealen Kandidaten für eine derartige Modifikation. Diese könnten dann effektiv *in vivo* Anwendung finden.

Kapitel V schließt mit einer Machbarkeitsstudie zur Verkapselung fluoreszierender Quantenpunkte. Hier wurde das FRET-basierte Schaltprinzip zwar grundsätzlich etabliert, dessen Potential hingegen noch nicht vollständig ausgeschöpft. Prospektive Kinetikstudien des Vorgangs der Dissoziation verschiedener Trägerkomplexe könnten dazu beitragen, die mechanistischen Zusammenhänge des Gentransfers besser zu verstehen und einen Einblick in intrazelluläre Prozesse während des Gentransfers zu erlangen. Ferner könnten Quantenpunkte auch dazu genutzt werden, die Bioverteilung *in vivo* zu untersuchen. Die in dieser Arbeit verwendeten roten Quan-

tenpunkte könnten dabei durch NIR-emittierende Quantenpunkte ersetzt werden, um eine nicht-invasive Detektion in Echtzeit zu ermöglichen.

Das Langzeitziel bei der Erforschung nicht-viraler Vektoren ist klar: Träger müssen einerseits effektiver, andererseits muss die Toxizität (welche maßgeblich durch eine nichtspezifische Immunantwort hervorgerufen wird) verringert werden. Durch rationales Vektordesign, welches wiederum systematische und intensive Grundlagenforschung bedingt, werden wir zukünftig hoffentlich in der Lage sein, sichere und effektive Trägersysteme zur kausalen Therapie gegenwärtig als unheilbar klassifizierter Krankheiten zu entwickeln.

References

- [1] M. A. Kay, State-of-the-art gene-based therapies: the road ahead, *Nat. Rev. Genet.* 12 (5) (2011) 316–328.
- [2] M. S. Shim, Y. J. Kwon, Acid-Responsive Linear Polyethylenimine for Efficient, Specific, and Biocompatible siRNA Delivery, *Bioconjugate Chem.* 20 (2009) 488–499.
- [3] T. Merdan, J. Kopecek, T. Kissel, Prospects for cationic polymers in gene and oligonucleotide therapy against cancer, *Adv. Drug Delivery Rev.* 54 (2002) 715–758.
- [4] O. M. Merkel, M. Zheng, H. Debus, T. Kissel, Pulmonary Gene Delivery Using Polymeric Nonviral Vectors, *Bioconjugate Chem.* 23 (1) (2012) 3–20.
- [5] R. Bertolotti, Editorial: Transient or long-term transgene expression and gene repair/ inactivation, *Gene Ther. Regul.* 1 (1) (2000) 1–8.
- [6] D. J. Gary, N. Puri, Y.-Y. Won, Polymer-based siRNA delivery: Perspectives on the fundamental and phenomenological distinctions from polymer-based DNA delivery, *J. Controlled Release* 121 (2007) 64–73.
- [7] M. Benfer, R. Reul, T. Betz, T. Kissel, Folic acid-decorated nanocomposites prepared by a simple solvent displacement method, *Macromol. Biosci.* 12 (4) (2012) 438–445.
- [8] L. Liu, M. Zheng, T. Renette, T. Kissel, Modular Synthesis of Folate Conjugated Ternary Copolymers: Polyethylenimine-graft-Polycaprolactone-block-Poly(ethylene glycol)-Folate for Targeted Gene Delivery, *Bioconjugate Chem.* 23 (6) (2012) 1211–1220.
- [9] C. Rudolph, U. Schillinger, C. Plank, A. Gessner, P. Nicklaus, R. H. Müller, J. Rosenecker, Nonviral gene delivery to the lung with copolymer-protected and transferrin-modified polyethylenimine, *Biochim. Biophys. Acta* 1573 (2002) 75–83.
- [10] R. Kircheis, L. Wightman, A. Schreiber, B. Robitza, V. Rössler, M. Kurs, E. Wagner, Polyethylenimine/DNA complexes shielded by transferrin target gene expression to tumors after systemic application, *Gene Ther.* 8 (2001) 28–40.
- [11] C.-L. Tseng, W.-Y. Su, K.-C. Yen, K.-C. Yang, F.-H. Lin, The use of biotinylated-EGF-modified gelatin nanoparticle carrier to enhance cisplatin accumulation in cancerous lungs via inhalation, *Biomaterials* 30 (20) (2009) 3476–3485.
- [12] Y. Matsumura, H. Maeda, A New Concept for Macromolecular Therapeutics in Cancer Chemotherapy: Mechanism of Tumoritropic Accumulation of Proteins and the Antitumor Agent Smancs, *Cancer Res.* 46 (1986) 6387–6392.

References

- [13] H. Cabral, K. Kataoka, Multifunctional nanoassemblies of block copolymers for future cancer therapy, *Sci. Technol. Adv. Mater.* 11 (1) (2010) 014109.
- [14] R. Tong, J. Cheng, Anticancer Polymeric Nanomedicines, *Polym. Rev. (Philadelphia, PA, U. S.)* 47 (3) (2007) 345–381.
- [15] S. Stolnik, L. Illum, S. S. Davis, Long circulating microparticulate drug carriers, *Adv. Drug Delivery Rev.* 16 (2-3) (1995) 195–214.
- [16] L. Illum, I. Hunneyball, S. Davis, The effect of hydrophilic coatings on the uptake of colloidal particles by the liver and by peritoneal macrophages, *Int. J. Pharm.* 29 (1) (1986) 53–65.
- [17] A. Beyerle, O. Merkel, T. Stoeger, T. Kissel, PEGylation affects cytotoxicity and cell-compatibility of poly(ethylene imine) for lung application: Structure-function relationships, *Toxicol. Appl. Pharmacol.* 242 (2) (2010) 146–154.
- [18] B. Shi, C. Fang, M. X. You, Y. Zhang, S. Fu, Y. Pei, Stealth MePEG-PCL micelles: effects of polymer composition on micelle physicochemical characteristics, in vitro drug release, in vivo pharmacokinetics in rats and biodistribution in tumor bearing mice, *Colloid Polym. Sci.* 283 (9) (2005) 954–967.
- [19] M. Zheng, D. Librizzi, A. Kilic, Y. Liu, H. Renz, O. M. Merkel, T. Kissel, Enhancing in vivo circulation and siRNA delivery with biodegradable polyethylenimine-graft-polycaprolactone-block-poly(ethylene glycol) copolymers, *Biomaterials* 33 (27) (2012) 6551–6558.
- [20] K. Avgoustakis, A. Beletsi, Z. Panagi, P. Klepetsanis, E. Livaniou, G. Evangelatos, D. Ithakissios, Effect of copolymer composition on the physicochemical characteristics, in vitro stability, and biodistribution of PLGA-mPEG nanoparticles, *Int. J. Pharm.* 259 (2003) 115–127.
- [21] H. Petersen, P. Fechner, D. Fischer, T. Kissel, Synthesis, Characterization, and Biocompatibility of Polyethylenimine-graft-poly(ethylene glycol) Block Copolymers, *Macromolecules (Washington, DC, United States)* 35 (18) (2002) 6867–6874.
- [22] H. Petersen, P. Fechner, A. Martin, K. Kunath, S. Stolnik, C. Roberts, D. Fischer, M. Davies, T. Kissel, Polyethylenimine-graft-Poly(ethylene glycol) Copolymers: Influence of Copolymer Block Structure on DNA Complexation and Biological Activities as Gene Delivery System, *Bioconjugate Chem.* 13 (4) (2002) 845–854.
- [23] K. Rihova, Receptor-mediated targeted drug or toxin delivery, *Adv. Drug Delivery Rev.* 29 (1998) 273–289.
- [24] W. T. Godbey, K. W. Kenneth, G. M. Antonios, PEI and its role in gene delivery, *J. Controlled Release* 60 (1999) 149–160.
- [25] D. W. Pack, A. S. Hoffman, S. Pun, P. S. Stayton, Design and development of polymers for gene delivery, *Nat. Rev. Drug Discovery* 4 (7) (2005) 581–593.

References

- [26] Z.-Y. Zhang, B. D. Smith, High-Generation Polycationic Dendrimers Are Unusually Effective at Disrupting Anionic Vesicles: Membrane Bending Model, *Bioconjugate Chem.* 11 (2000) 805–814.
- [27] I. Wörbel, D. Collins, Fusion of cationic liposomes with mammalian cells occurs after endocytosis, *Biochim. Biophys. Acta* 1235 (1994) 296–304.
- [28] Y. Lee, K. Miyata, M. Oba, T. Ishii, S. Fukushima, M. Han, H. Koyama, N. Nishiyama, K. Kataoka, Charge-Conversion Ternary Polyplex with Endosome Disruption Moiety: A Technique for Efficient and Safe Gene Delivery, *Angew. Chem., Int. Ed.* 47 (28) (2008) 5163–5166.
- [29] S. Sennato, F. Bordini, C. Cametti, M. Diociaiuti, P. Malaspina, Charge patch attraction and reentrant condensation in DNA-liposome complexes, *Biochim. Biophys. Acta, Biomembr.* 1714 (1) (2005) 11–24.
- [30] M. Neu, D. Fischer, T. Kissel, Recent advances in rational gene transfer vector design based on PEI and its derivatives, *J. Gene Med.* 7 (2005) 992–1009.
- [31] C. Plank, K. Mechtler, F. C. Szoka, E. Wagner, Activation of the Complement System by Synthetic DNA Complexes: A Potential Barrier for Intravenous Gene Delivery, *Hum. Gene Ther.* 7 (12) (2008) 1437–1446.
- [32] J. H. Choi, J. S. Choi, H. Suh, J. S. Park, Effect of Poly(ethylene glycol) Grafting on Polyethylenimine as a Gene Transfer Vector in vitro, *Bull. Korean Chem. Soc.* 22 (1) (2001) 46–52.
- [33] D. Fischer, Y. Li, B. Ahlemeyer, J. Kriegelstein, T. Kissel, In vitro cytotoxicity testing of polycations: influence of polymer structure on cell viability and hemolysis, *Biomaterials* 24 (2003) 1121–1131.
- [34] V. Incani, A. Lavasanifar, H. Uludag, Lipid and hydrophobic modification of cationic carriers on route to superior gene vectors, *Soft Matter.* 6 (2010) 2124–2138.
- [35] M. Breunig, U. Lungwitz, R. Liebl, J. Klar, B. Obermayer, T. Blunk, A. Goepferich, Mechanistic insights into linear polyethylenimine-mediated gene, *Biochim. Biophys. Acta, Gen. Subj.* 1770 (2007) 196–205.
- [36] M. Breunig, U. Lungwitz, R. Liebl, C. Fontanari, J. Klar, A. Kurtz, T. Blunk, A. Goepferich, Gene delivery with low molecular weight linear polyethylenimines, *J. Gene Med.* 7 (10) (2005) 1287–1298.
- [37] B. Brissault, C. Leborgne, C. Guis, O. Danos, H. Cheradame, A. Kichler, Linear topology confers in vivo gene transfer activity to polyethylenimines, *Bioconjugate Chem.* 17 (2006) 759–765.
- [38] Z. Zhong, J. Feijen, M. C. Lok, W. E. Hennink, L. V. Christensen, J. W. Yockman, Y.-H. Kim, S. W. Kim, Low Molecular Weight Linear Polyethylenimine-b-poly(ethylene glycol)-b-polyethylenimine Triblock Copolymers: Synthesis,

References

- Characterization, and in Vitro Gene Transfer Properties, *Biomacromolecules* 6 (6) (2005) 3440–3448.
- [39] L. Wightman, R. Kircheis, V. Rösser, S. Carotta, R. Ruzicka, M. Kursa, E. Wagner, Different behavior of branched and linear polyethylenimine for gene delivery in vitro and in vivo, *J. Gene Med.* 3 (4) (2001) 362–372.
- [40] N. Zhao, S. Roesler, T. Kissel, Synthesis of a new potential biodegradable disulfide containing poly(ethylene imine)-poly(ethylene glycol) copolymer cross-linked with click cluster for gene delivery, *Int. J. Pharm.* 411 (1-2) (2011) 197–205.
- [41] M. Ou, R. Xu, S. H. Kim, D. A. Bull, S. W. Kim, A family of bio-reducible poly(disulfide amine)s for gene delivery, *Biomaterials* 30 (2009) 5804–5814.
- [42] M. L. Adams, A. Lavasanifar, G. S. Kwon, Amphiphilic Block Copolymers for Drug Delivery, *J. Pharm. Sci.* 92 (7) (2003) 1343–1355.
- [43] Y. Zhang, S. Guo, C. Lu, L. Liu, Z. Li, J. Gu, Poly(ϵ -caprolactone)-*b*-Poly(ethylene glycol)-*b*-Poly(ϵ -caprolactone) Triblock Copolymers: Synthesis and Self-Assembly in Aqueous Solutions, *J. Polym. Sci., Part A: Polym. Chem.* 45 (2007) 605–613.
- [44] S. Zhou, X. Deng, H. Yang, Biodegradable poly(ϵ -caprolactone)-poly(ethylene glycol) block copolymers: characterization and their use as drug carriers for a controlled delivery system, *Biomaterials* 24 (20) (2003) 3563–3570.
- [45] C. Allen, Y. Yu, D. Maysinger, A. Eisenberg, Polycaprolactone-*b*-poly(ethylene Oxide) Block Copolymer Micelles as a Novel Drug Delivery Vehicle for Neurotrophic Agents FK506 and L-685,818, *Bioconjugate Chem.* 9 (5) (1998) 564–572.
- [46] H. Ge, Y. Hu, X. Jiang, D. Cheng, Y. Yuan, H. Bi, C. Yang, Preparation, Characterization, and Drug Release Behaviors of Drug Nimodipine-Loaded Poly(ϵ -caprolactone)-Poly(ethylene oxide)-Poly(ϵ -caprolactone) Amphiphilic Triblock Copolymer Micelles, *J. Pharm. Sci.* 91 (6) (2002) 1463–1473.
- [47] I. G. Shin, S. Y. Kim, Y. M. Lee, C. S. Cho, Y. K. Sung, Methoxy poly(ethylene glycol)/ ϵ -caprolactone amphiphilic block copolymeric micelle containing indomethacin.: I. Preparation and characterization, *J. Controlled Release* 51 (1) (1998) 1–11.
- [48] S. Y. Kim, Y. M. Lee, H. J. Shin, J. S. Kang, Indomethacin-loaded methoxy poly(ethylene glycol)/poly(ϵ -caprolactone) diblock copolymeric nanosphere: pharmacokinetic characteristics of indomethacin in the normal Sprague-Dawley rats, *Biomaterials* 22 (14) (2001) 2049 – 2056.
- [49] R. Rastogi, S. Anand, V. Koul, Polymerosomes of PCL and PEG Demonstrate Enhanced Therapeutic Efficacy of Insulin, *Curr. Nanosci.* 5 (2009) 409–416.

References

- [50] A. M. Master, M. E. Rodriguez, M. E. Kenney, N. L. Oleinick, A. S. Gupta, Delivery of the Photosensitizer Pc 4 in PEG–PCL Micelles for In Vitro PDT Studies, *J. Pharm. Sci.* 99 (5) (2010) 2386–2398.
- [51] F. Ahmed, D. E. Discher, Self-porating polymersomes of PEG-PLA and PEG-PCL: hydrolysis-triggered controlled release vesicles, *J. Controlled Release* 96 (1) (2004) 37–53.
- [52] A. Richter, C. Olbrich, M. Krause, J. Hoffmann, T. Kissel, Polymeric Micelles for parenteral delivery of Sagopilone: Physicochemical characterization, novel formulation approaches and their toxicity assessment in vitro as well as in vivo, *Eur. J. Pharm. Biopharm.* 75 (2) (2010) 80–89.
- [53] A. Richter, C. Olbrich, M. Krause, T. Kissel, Solubilization of Sagopilone, a poorly water-soluble anticancer drug, using polymeric micelles for parenteral delivery, *Int. J. Pharm.* 389 (1-2) (2010) 244–253.
- [54] F. Meng, C. Hiemstra, G. H. M. Engbers, J. Feijen, Biodegradable Polymersomes, *Macromolecules* (Washington, DC, United States) 36 (9) (2003) 3004–3006.
- [55] Y.-C. Chang, I.-M. Chu, Methoxy poly(ethylene glycol)-b-poly(valerolactone) diblock polymeric micelles for enhanced encapsulation and protection of camptothecin, *Eur. Polym. J.* 44 (12) (2008) 3922–3930.
- [56] S. Stolnik, C. R. Heald, J. Neal, M. C. Garnett, S. S. Davis, L. Illum, S. C. Purkis, R. J. Barlow, P. R. Gellert, Polylactide-poly(ethylene Glycol) Micellar-like Particles as Potential Drug Carriers: Production, Colloidal Properties and Biological Performance, *J. Drug Targeting* 9 (5) (2001) 361–378.
- [57] M. Vittaz, D. Bazile, G. Spenlehauer, T. Verrecchia, M. Veillard, F. Puisieux, D. Labarre, Effect of PEO surface density on long-circulating PLA-PEO nanoparticles which are very low complement activators, *Biomaterials* 17 (16) (1996) 1575–1581.
- [58] V. C. F. Mosqueira, P. Legrand, R. Gref, B. Heurtault, M. Appel, G. Barratt, Interactions between a Macrophage Cell Line (J774A1) and Surface-modified Poly(D,L-lactide) Nanocapsules Bearing Poly(ethylene glycol), *J. Drug Targeting* 7 (1) (1999) 65–78.
- [59] D. Bazile, C. Proud’homme, M.-T. Dassoullet, M. Marland, G. Spenlehauer, M. Veillard, Stealth Me.PEG-PLA Nanoparticles Avoid Uptake by the Mononuclear Phagocytes System, *J. Pharm. Sci.* 84 (4) (1995) 493–498.
- [60] C. R. Heald, S. Stolnik, K. S. Kujawinski, C. De Matteis, M. C. Garnett, L. Illum, S. S. Davis, S. C. Purkiss, R. J. Barlow, P. R. Gellert, Poly(lactic acid)–Poly(ethylene oxide) (PLA–PEG) Nanoparticles: NMR Studies of the Central Solidlike PLA Core and the Liquid PEG Corona, *Langmuir* 18 (9) (2002) 3669–3675.

References

- [61] H. S. Yoo, T. G. Park, Biodegradable polymeric micelles composed of doxorubicin conjugated PLGA-PEG block copolymer, *J. Controlled Release* 70 (1-2) (2001) 63–70.
- [62] T. Riley, T. Govender, S. Stolnik, C. D. Xiong, M. C. Garnett, L. Illum, S. S. Davis, Colloidal stability and drug incorporation aspects of micellar-like PLA-PEG nanoparticles, *Colloids Surf., B* 16 (1-4) (1999) 147–159.
- [63] E. Blanco, E. A. Bey, Y. Dong, B. D. Weinberg, D. M. Sutton, D. A. Boothman, J. Gao, beta-Lapachone-containing PEG-PLA polymer micelles as novel nanotherapeutics against NQO1-overexpressing tumor cells, *J. Controlled Release* 122 (3) (2007) 365–374.
- [64] T. Ameller, V. Marsaud, P. Legrand, R. Gref, G. Barratt, J.-M. Renoir, Polyester-Poly(Ethylene Glycol) Nanoparticles Loaded with the Pure Anti-estrogen RU 58668: Physicochemical and Opsonization Properties, *Pharm. Res.* 20 (2003) 1063–1070.
- [65] N. Bhattarai, S. R. Bhattarai, H. K. Yi, J. C. Lee, M. S. Khil, P. H. Hwang, H. Y. Kim, Novel Polymeric Micelles of Amphiphilic Triblock Copolymer Poly (p-Dioxanone-co-L-Lactide)-block-Poly (ethylene glycol), *Pharm. Res.* 20 (2003) 2021–2027.
- [66] G. Vandermeulen, L. Rouxhet, A. Arien, M. Brewster, V. Préat, Encapsulation of amphotericin B in poly(ethylene glycol)-block-poly(ϵ -caprolactone-co-trimethylenecarbonate) polymeric micelles, *Int. J. Pharm.* 309 (1-2) (2006) 234–240.
- [67] Y. Wang, C.-Y. Ke, C. W. Beh, S.-Q. Liu, S.-H. Goh, Y.-Y. Yang, The self-assembly of biodegradable cationic polymer micelles as vectors for gene transfection, *Biomaterials* 28 (35) (2007) 5358–5368.
- [68] S. C. Lee, H. S. Choi, T. Ooya, N. Yui, Block-Selective Polypseudorotaxane Formation in PEI-b-PEG-b-PEI Copolymers via pH Variation, *Macromolecules* (Washington, DC, United States) 37 (2004) 7464.
- [69] C. Zhu, S. Jung, S. Luo, F. Meng, X. Zhu, T. G. Park, Z. Zhong, Co-delivery of siRNA and paclitaxel into cancer cells by biodegradable cationic micelles based on PDMAEMA-PCL-PDMAEMA triblock copolymers, *Biomaterials* 31 (8) (2010) 2408–2416.
- [70] D. S. W. Benoit, S. M. Henry, A. D. Shubin, A. S. Hoffman, P. S. Stayton, pH-Responsive Polymeric siRNA Carriers Sensitize Multidrug Resistant Ovarian Cancer Cells to Doxorubicin via Knockdown of Polo-like Kinase 1, *Mol. Pharmaceutics* 7 (2) (2010) 442–455.
- [71] J. Akimoto, M. Nakayama, K. Sakai, T. Okano, Temperature-Induced Intracellular Uptake of Thermoresponsive Polymeric Micelles, *Biomacromolecules* 10 (6) (2009) 1331–1336.

References

- [72] D. Singh, S. Heinhorst, G. C. Cannon, S. E. Morgan, Synthesis and characterization of amphiphilic block copolymers for polymerosomes., *Polym. Prepr. (Am. Chem. Soc., Div. Polym. Chem.)* 51 (2) (2010) 561–562.
- [73] C.-Q. Mao, J.-Z. Du, T.-M. Sun, Y.-D. Yao, P.-Z. Zhang, E.-W. Song, J. Wang, A biodegradable amphiphilic and cationic triblock copolymer for the delivery of siRNA targeting the acid ceramidase gene for cancer therapy, *Biomaterials* 32 (11) (2011) 3124–3133.
- [74] T.-M. Sun, J.-Z. Du, L.-F. Yan, H.-Q. Maod, J. Wang, Self-assembled biodegradable micellar nanoparticles of amphiphilic and cationic block copolymer for siRNA delivery, *Biomaterials* 29 (2008) 4348–4355.
- [75] T.-M. Sun, J.-Z. Du, Y.-D. Yao, C.-Q. Mao, S. Dou, S.-Y. Huang, P.-Z. Zhang, K. W. Leong, E.-W. Song, J. Wang, Simultaneous Delivery of siRNA and Paclitaxel via a "Two-in-One" Micelleplex Promotes Synergistic Tumor Suppression, *ACS Nano* 5 (2) (2011) 1483–1494.
- [76] Y. Liu, T. Steele, T. Kissel, Degradation of Hyper-Branched Poly(ethylenimine)-graft-poly(caprolactone)-block-monomethoxypoly(ethylene glycol) as a Potential Gene Delivery Vector, *Macromol. Rapid Commun.* 31 (2010) 1509–1515.
- [77] X. Shuai, T. Merdan, F. Unger, M. Wittmar, T. Kissel, Novel biodegradable ternary copolymers hy-PEI-g-PCL-b-PEG, *Macromolecules (Washington, DC, United States)* 36 (2003) 5751–5759.
- [78] X. Shuai, T. Merdan, F. Unger, T. Kissel, Supramolecular Gene Delivery Vectors Showing Enhanced Transgene Expression and Good Biocompatibility, *Bioconjugate Chem.* 16 (2005) 322–329.
- [79] Y. Liu, J. Nguyen, T. Steele, O. Merkel, T. Kissel, A new synthesis method and degradation of hyper-branched polyethylenimine grafted polycaprolactone block mono-methoxyl poly (ethylene glycol) copolymers (hy-PEI-g-PCL-b-mPEG) as potential DNA delivery vectors, *Polymer* 50 (16) (2009) 3895–3904.
- [80] M. Zheng, Y. Liu, O. Samsonova, T. Endres, O. Merkel, T. Kissel, Amphiphilic and biodegradable hy-PEI-g-PCL-b-PEG copolymers efficiently mediate transgene expression depending on their graft density, *Int. J. Pharm.* 427 (1) (2011) 80–87.
- [81] T. Chandran, U. Katragadda, Q. Teng, C. Tan, Design and evaluation of micellar nanocarriers for 17-allylamino-17-demethoxygeldanamycin (17-AAG), *Int. J. Pharm.* 392 (1-2) (2010) 170–177.
- [82] L. Y. Qiu, Y. H. Bae, Self-assembled polyethylenimine-graft-poly(epsilon-caprolactone) micelles as potential dual carriers of genes and anticancer drugs, *Biomaterials* 28 (28) (2007) 4132–4142.

References

- [83] N. Cao, D. Cheng, S. Zou, H. Ai, J. Gao, X. Shuai, The synergistic effect of hierarchical assemblies of siRNA and chemotherapeutic drugs co-delivered into hepatic cancer cells, *Biomaterials* 32 (8) (2011) 2222–2232.
- [84] K. V. Butsele, S. Cajot, S. V. Vlierberghe, P. Dubruel, C. Passirani, J.-P. Benoit, R. Jerome, C. Jerome, pH-Responsive Flower-Type Micelles Formed by a Biotinylated Poly(2-vinylpyridine)-block-poly(ethylene oxide)-block-poly(ϵ -caprolactone) Triblock Copolymer, *Adv. Funct. Mater.* 19 (2009) 1416–1425.
- [85] Z. Guo, Y. Li, H. Tian, X. Zhuang, X. Chen, X. Jing, Self-Assembly of Hyperbranched Multiarmed PEG-PEI-PLys(Z) Copolymer into Micelles, Rings, and Vesicles, *Langmuir* 25 (17) (2009) 9690–9696.
- [86] J. Zhu, W. Jiang, Self-Assembly of ABC Triblock Copolymer into Giant Segmented Wormlike Micelles in Dilute Solution, *Macromolecules* (Washington, DC, United States) 38 (22) (2005) 9315–9323.
- [87] J.-F. Gohy, N. Willet, S. Varshney, J.-X. Zhang, R. Jerome, Core-Shell-Corona Micelles with a Responsive Shell, *Angew. Chem., Int. Ed.* 40 (17) (2001) 3214–3216.
- [88] H. Tian, C. Deng, H. Lin, J. Sun, M. Deng, X. Chen, X. Jing, Biodegradable cationic PEG-PEI-PBLG hyperbranched block copolymer: synthesis and micelle characterization, *Biomaterials* 26 (2005) 4209–4217.
- [89] H. Sun, L. Mei, C. Song, X. Cui, P. Wang, The in vivo degradation, absorption and excretion of PCL-based implant, *Biomaterials* 27 (9) (2006) 1735–1740.
- [90] S. Oh, S. Kang, J. Lee, Degradation behavior of hydrophilized PLGA scaffolds prepared by melt-molding particulate-leaching method: Comparison with control hydrophobic one, *J. Mater. Sci.: Mater. Med.* 17 (2006) 131–137.
- [91] J. Y. Cherng, H. Talsama, R. Verrijck, D. J. A. Crommelin, W. E. Hennink, The effect of formulation parameters on the size of poly-((2-dimethylamino)ethyl methacrylate)-plasmid complexes, *Eur. J. Pharm. Biopharm.* 47 (1998) 215–224.
- [92] H. Cho, I. Cheong, J. Lee, J. Kim, Polymeric nanoparticles, micelles and polymersomes from amphiphilic block copolymer, *Korean J. Chem. Eng.* 27 (2010) 731–740.
- [93] K. Letchford, H. Burt, A review of the formation and classification of amphiphilic block copolymer nanoparticulate structures: micelles, nanospheres, nanocapsules and polymersomes, *Eur. J. Pharm. Biopharm.* 65 (3) (2007) 259–269.
- [94] J. B. Delehanty, K. Boeneman, C. E. Bradburne, K. Robertson, I. L. Medintz, Quantum dots: a powerful tool for understanding the intricacies of nanoparticle-mediated drug delivery, *Expert Opin. Drug Delivery* 6 (10) (2009) 1091–1112.

References

- [95] Y. Wu, Y.-P. Ho, Y. Mao, X. Wang, B. Yu, K. W. Leong, L. J. Lee, Uptake and Intracellular Fate of Multifunctional Nanoparticles: A Comparison between Lipoplexes and Polyplexes via Quantum Dot Mediated Förster Resonance Energy Transfer, *Mol. Pharmaceutics* 8 (5) (2011) 1662–1668.
- [96] Y.-P. Ho, H. H. Chen, K. W. Leong, T.-H. Wang, Evaluating the intracellular stability and unpacking of DNA nanocomplexes by quantum dots-FRET, *J. Controlled Release* 116 (1) (2006) 83–89.
- [97] B. J. Nehilla, P. G. Allen, T. A. Desai, Surfactant-Free, Drug-Quantum-Dot Coloaded Poly(lactide-co-glycolide) Nanoparticles: Towards Multifunctional Nanoparticles, *ACS Nano* 2 (3) (2008) 538–544.
- [98] I. L. Medintz, H. Mattoussi, Quantum dot-based resonance energy transfer and its growing application in biology, *Phys. Chem. Chem. Phys.* 11 (2009) 17–45.
- [99] J. I. Lee, K.-S. Ha, H. S. Yoo, Quantum-dot-assisted fluorescence resonance energy transfer approach for intracellular trafficking of chitosan/DNA complex, *Acta Biomater.* 4 (4) (2008) 791–798.
- [100] Y. Lee, T. Ishii, H. Cabral, H. J. Kim, J.-H. Seo, N. Nishiyama, H. Oshima, K. Osada, K. Kataoka, Charge-Conversional Polyionic Complex Micelles-Efficient Nanocarriers for Protein Delivery into Cytoplasm, *Angew. Chem., Int. Ed.* 48 (29) (2009) 5309–5312.
- [101] M. Ferrari, Experimental therapies: Vectoring siRNA therapeutics into the clinic, *Nat. Rev. Clin. Oncol.* 7 (9) (2010) 485–486.
- [102] L. Zhang, A. Eisenberg, Multiple Morphologies of "Crew-Cut" Aggregates of Polystyrene-*b*-poly(acrylic acid) Block Copolymers, *Science* 268 (5218) (1995) 1728–1731.
- [103] T. Riley, S. Stolnik, C. R. Heald, C. D. Xiong, M. C. Garnett, L. Illum, S. S. Davis, S. C. Purkiss, R. J. Barlow, P. R. Gellert, Physicochemical Evaluation of Nanoparticles Assembled from Poly(lactic acid)–Poly(ethylene glycol) (PLA–PEG) Block Copolymers as Drug Delivery Vehicles, *Langmuir* 17 (11) (2001) 3168–3174.
- [104] P. R. Leroueil, S. Hong, A. Mecke, J. R. Baker, B. G. Orr, M. M. Holl, Nanoparticle interaction with biological membranes: Does nanotechnology present a Janus Face?, *Acc. Chem. Res.* 40 (5) (2007) 335–342.
- [105] T. D. Perrine, W. R. Landis, Analysis of polyethylenimine by spectrophotometry of Its copper chelate, *J. Polym. Sci., Part A-1: Polym. Chem.* 5 (1967) 1993–2003.
- [106] M. Beck-Broichsitter, M. Thieme, J. Nguyen, T. Schmehl, T. Gessler, W. Seeger, S. Agarwal, A. Greiner, T. Kissel, Novel 'Nano in Nano' Composites for Sustained Drug Delivery: Biodegradable Nanoparticles Encapsulated into Nanofiber Non-Wovens, *Macromol. Biosci.* 10 (12) (2010) 1527–1535.

References

- [107] K. Shimada, A. Miyagishima, Y. Sadzuka, Y. Nozawa, Y. Mochizuki, H. Ohshima, S. Hirota, Determination of the Thickness of the Fixed Aqueous Layer Around Polyethyleneglycol-coated Liposomes, *J. Drug Targeting* 3 (4) (1995) 283–289.
- [108] J. Nguyen, R. Reul, S. Roesler, E. Dayyoub, T. Schmehl, T. Gessler, W. Seeger, T. Kissel, Amine-Modified Poly(Vinyl Alcohol)s as Non-viral Vectors for siRNA Delivery: Effects of the Degree of Amine Substitution on Physicochemical Properties and Knockdown Efficiency, *Pharm. Res.* 27 (2010) 2670–2682.
- [109] A. Besheer, J. Vogel, D. Glanz, J. Kressler, T. Groth, K. Mäder, Characterization of PLGA Nanospheres Stabilized with Amphiphilic Polymers: Hydrophobically Modified Hydroxyethyl Starch vs Pluronics, *Mol. Pharmaceutics* 6 (2) (2009) 407–415.
- [110] W. G. Eversole, P. H. Lahr, Evidence for a Rigid Multilayer at a Solid-Liquid Interface, *J. Chem. Phys.* 9 (7) (1941) 530–534.
- [111] F. J. Carrión, A. D. L. Maza, J. L. Parra, The Influence of Ionic Strength and Lipid Bilayer Charge on the Stability of Liposomes, *J. Colloid Interface Sci.* 164 (1) (1994) 78–87.
- [112] Y. Sadzuka, A. Nakade, R. Hirama, A. Miyagishima, Y. Nozawa, S. Hirota, T. Sonobe, Effects of mixed polyethyleneglycol modification on fixed aqueous layer thickness and antitumor activity of doxorubicin containing liposome, *Int. J. Pharm.* 238 (1-2) (2002) 171–180.
- [113] A. D. S. Delgado, M. Leonard, E. Dellacherie, Surface modification of polystyrene nanoparticles using dextrans and dextran-POE copolymers: Polymer adsorption and colloidal characterization, *J. Biomater. Sci.* 11 (12) (2000) 1395–1410.
- [114] F. Podo, A. Ray, G. Nemethy, Structure and hydration of nonionic detergent micelles. High resolution nuclear magnetic resonance study, *J. Am. Chem. Soc.* 95 (19) (1973) 6164–6171.
- [115] G. Gaucher, M.-H. Dufresne, V. P. Sant, N. Kang, D. Maysinger, J.-C. Leroux, Block copolymer micelles: preparation, characterization and application in drug delivery, *J. Controlled Release* 109 (1-3) (2005) 169–188.
- [116] X. Zhang, S.-R. Pan, H.-M. Hu, G.-F. Wu, M. Feng, W. Zhang, X. Luo, Poly(ethylene glycol)-block-polyethylenimine copolymers as carriers for gene delivery: Effects of PEG molecular weight and PEGylation degree, *J. Biomed. Mater. Res., Part A* 84A (3) (2008) 795–804.
- [117] Y. Wang, S. Gao, W.-H. Ye, H. S. Yoon, Y.-Y. Yang, Co-delivery of drugs and DNA from cationic core-shell nanoparticles self-assembled from a biodegradable copolymer, *Nat. Mater.* 5 (10) (2006) 791–796.

References

- [118] T. K. Endres, M. Beck-Broichsitter, O. Samsonova, T. Renette, T. H. Kissel, Self-assembled biodegradable amphiphilic PEG-PCL-IPEI triblock copolymers at the borderline between micelles and nanoparticles designed for drug and gene delivery, *Biomaterials* 32 (2011) 7721–7731.
- [119] J. Jeong, T. Park, S. Kim, Self-assembled and nanostructured siRNA delivery systems, *Pharm. Res.* 28 (2011) 2072–2085.
- [120] J. C. Kasper, D. Schaffert, M. Ogris, E. Wagner, W. Friess, The establishment of an up-scaled micro-mixer method allows the standardized and reproducible preparation of well-defined plasmid/LPEI polyplexes, *Eur. J. Pharm. Biopharm.* 77 (1) (2011) 182–185.
- [121] F. Bordi, C. Cametti, M. Diociaiuti, D. Gaudino, T. Gili, S. Sennato, Complexation of anionic polyelectrolytes with cationic liposomes: Evidence of reentrant condensation and lipoplex formation, *Langmuir* 20 (13) (2004) 5214–5222.
- [122] Y. Ding, X. Bian, W. Yao, R. Li, D. Ding, Y. Hu, X. Jiang, Y. Hu, Surface-potential-regulated transmembrane and cytotoxicity of chitosan/gold hybrid nanospheres, *ACS Appl. Mater. Interfaces* 2 (5) (2010) 1456–1465.
- [123] J. Zhu, A. Tang, L. P. Law, M. Feng, K. M. Ho, D. K. L. Lee, F. W. Harris, P. Li, Amphiphilic core–shell nanoparticles with poly(ethylenimine) shells as potential gene delivery carriers, *Bioconjugate Chem.* 16 (1) (2004) 139–146.
- [124] Y. Wang, L.-S. Wang, S.-H. Goh, Y.-Y. Yang, Synthesis and characterization of cationic micelles self-assembled from a biodegradable copolymer for gene delivery, *Biomacromolecules* 8 (3) (2007) 1028–1037.
- [125] O. Zelphati, C. Nguyen, M. Ferrari, J. Felgner, Y. Tsai, P. L. Felgner, Stable and monodisperse lipoplex formulations for gene delivery, *Gene Ther.* 5 (9) (1998) 1272–1282.
- [126] J. Kim, I. Hwang, D. Britain, T. D. Chung, Y. Sun, D.-H. Kim, Microfluidic approaches for gene delivery and gene therapy, *Lab Chip* 11 (2011) 3941–3948.
- [127] Y.-P. Ho, C. L. Grigsby, F. Zhao, K. W. Leong, Tuning physical properties of nanocomplexes through microfluidics-assisted confinement, *Nano Lett.* 11 (5) (2011) 2178–2182.
- [128] J. Clement, K. Kiefer, A. Kimpfler, P. Garidel, R. Peschka-Süss, Large-scale production of lipoplexes with long shelf-life, *Eur. J. Pharm. Biopharm.* 59 (1) (2005) 35–43.
- [129] C. G. Koh, X. Kang, Y. Xie, Z. Fei, J. Guan, B. Yu, X. Zhang, L. J. Lee, Delivery of polyethylenimine/DNA complexes assembled in a microfluidics device, *Mol. Pharmaceutics* 6 (5) (2009) 1333–1342.

References

- [130] C. G. Koh, X. Zhang, S. Liu, S. Golan, B. Yu, X. Yang, J. Guan, Y. Jin, Y. Talmon, N. Muthusamy, K. K. Chan, J. C. Byrd, R. J. Lee, G. Marcucci, L. J. Lee, Delivery of antisense oligodeoxyribonucleotide lipopolyplex nanoparticles assembled by microfluidic hydrodynamic focusing, *J. Controlled Release* 141 (1) (2010) 62–69.
- [131] S. Hou, N. Ziebacz, S. A. Wieczorek, E. Kalwarczyk, V. Sashuk, T. Kalwarczyk, T. S. Kaminski, R. Holyst, Formation and structure of PEI/DNA complexes: quantitative analysis, *Soft Matter*. 7 (2011) 6967–6972.
- [132] M. Beck-Broichsitter, E. Rytting, T. Lehardt, X. Wang, T. Kissel, Preparation of nanoparticles by solvent displacement for drug delivery: A shift in the "ouzo region" upon drug loading, *Eur. J. Pharm. Sci.* 41 (2) (2010) 244–253.
- [133] M. Chen, X. Liu, A. Fahr, Skin penetration and deposition of carboxyfluorescein and temoporfin from different lipid vesicular systems: In vitro study with finite and infinite dosage application, *Int. J. Pharm.* 408 (1-2) (2011) 223–234.
- [134] O. M. Merkel, M. A. Mintzer, D. Librizzi, O. Samsonova, T. Dicke, B. Sproat, H. Garn, P. J. Barth, E. E. Simanek, T. Kissel, Triazine dendrimers as nonviral vectors for in vitro and in vivo RNAi: The effects of peripheral groups and core structure on biological activity, *Mol. Pharmaceutics* 7 (4) (2010) 969–983.
- [135] Y. Wang, K. Kimura, P. L. Dubin, W. Jaeger, Polyelectrolyte-Micelle Coacervation: Effects of micelle surface charge density, polymer molecular weight, and polymer/surfactant ratio, *Macromolecules* (Washington, DC, United States) 33 (9) (2000) 3324–3331.
- [136] F. Bordi, C. Cametti, S. Sennato, M. Diociaiuti, Direct evidence of multicompartment aggregates in polyelectrolyte-charged liposome complexes, *Biophys. J.* 91 (4) (2006) 1513–1520.
- [137] V. Milkova, K. Kamburova, I. Petkanchin, T. Radeva, Complexation of ferric oxide particles with pectins of different charge density, *Langmuir* 24 (17) (2008) 9495–9499.
- [138] D. Truzzolillo, F. Bordi, F. Sciortino, S. Sennato, Interaction between like-charged polyelectrolyte-colloid complexes in electrolyte solutions: A Monte Carlo simulation study in the Debye-Hückel approximation, *J. Chem. Phys.* 133 (2) (2010) 024901.
- [139] Y. Liu, O. Samsonova, B. Sproat, O. Merkel, T. Kissel, Biophysical characterization of hyper-branched polyethylenimine-graft- polycaprolactone-block-mono-methoxyl-poly(ethylene glycol) copolymers (hy-PEI-PCL-mPEG) for siRNA delivery, *J. Controlled Release* 153 (2011) 262–268.
- [140] O. M. Merkel, M. Zheng, M. A. Mintzer, G. M. Pavan, D. Librizzi, M. Maly, H. Höffken, A. Danani, E. E. Simanek, T. Kissel, Molecular modeling and in vivo imaging can identify successful flexible triazine dendrimer-based siRNA delivery systems, *J. Controlled Release* 153 (1) (2011) 23–33.

References

- [141] M. Ogris, P. Steinlein, M. Kursa, K. Mechtler, R. Kircheis, E. Wagner, The size of DNA/transferrin-PEI complexes is an important factor for gene expression in cultured cells, *Gene Ther.* 5 (1998) 1425–1433.
- [142] S.-W. Choi, I. W. Cheong, J.-H. Kim, Y. Xia, Preparation of uniform microspheres using a simple fluidic device and their crystallization into close-packed lattices, *Small* 5 (4) (2009) 454–459.
- [143] H. Kuramoto, Y.-S. Park, N. Kaji, M. Tokeshi, K. Kogure, Y. Shinohara, H. Harashima, Y. Baba, On-chip fabrication of multifunctional envelope-type nanodevices for gene delivery, *Anal. Bioanal. Chem.* 391 (2008) 2729–2733.
- [144] C. Brus, E. Kleemann, A. Aigner, F. Czubayko, T. Kissel, Stabilization of oligonucleotide-polyethylenimine complexes by freeze-drying: physicochemical and biological characterization, *J. Controlled Release* 95 (1) (2004) 119–131.
- [145] J. M. Chan, L. Zhang, K. P. Yuet, G. Liao, J.-W. Rhee, R. Langer, O. C. Farokhzad, PLGA-lecithin-PEG core-shell nanoparticles for controlled drug delivery, *Biomaterials* 30 (8) (2009) 1627–1634.
- [146] A. K. Kundu, P. K. Chandra, S. Hazari, G. Ledet, Y. V. Pramar, S. Dash, T. K. Mandal, Stability of lyophilized siRNA nanosome formulations, *Int. J. Pharm.* 432 (2) (2011) 525–534.
- [147] W. Abdelwahed, G. Degobert, S. Stainmesse, H. Fessi, Freeze-drying of nanoparticles: Formulation, process and storage considerations, *Adv. Drug Delivery Rev.* 58 (15) (2006) 1688–1713.
- [148] A. Wieber, T. Selzer, J. Kreuter, Physico-chemical characterisation of cationic DOTAP liposomes as drug delivery system for a hydrophilic decapeptide before and after freeze-drying, *Eur. J. Pharm. Biopharm.* 80 (2) (2011) 358–367.
- [149] C. Packhaeuser, K. Lahnstein, J. Sitterberg, T. Schmehl, T. Gessler, U. Bakowsky, W. Seeger, T. Kissel, Stabilization of aerosolizable nano-carriers by freeze-drying, *Pharm. Res.* 26 (2009) 129–138.
- [150] L. D. Hahn, H. Kong, D. J. Mooney, Polycation structure mediates expression of lyophilized polycation/pDNA complexes, *Macromol. Biosci.* 10 (10) (2010) 1210–1215.
- [151] S. W. Poxon, J. A. Hughes, The effect of lyophilization on plasmid DNA activity, *Pharm. Dev. Technol.* 5 (1) (2000) 115–122.
- [152] P. Yadava, M. Gibbs, C. Castro, J. Hughes, Effect of lyophilization and freeze-thawing on the stability of siRNA-liposome complexes, *AAPS PharmSciTech* 9 (2008) 335–341.
- [153] M. Reinisalo, A. Urtti, P. Honkakoski, Freeze-drying of cationic polymer DNA complexes enables their long-term storage and reverse transfection of post-mitotic cells, *J. Controlled Release* 110 (2) (2006) 437–443.

References

- [154] J. Yu, T. J. Anchordoquy, Synergistic effects of surfactants and sugars on lipoplex stability during freeze-drying and rehydration, *J. Pharm. Sci.* 98 (9) (2009) 3319–3328.
- [155] M. Å. Andersen, K. A. Howard, S. R. Paludan, F. Besenbacher, J. Kjems, Delivery of siRNA from lyophilized polymeric surfaces, *Biomaterials* 29 (4) (2008) 506–512.
- [156] J.-M. Li, Y.-Y. Wang, M.-X. Zhao, C.-P. Tan, Y.-Q. Li, X.-Y. Le, L.-N. Ji, Z.-W. Mao, Multifunctional QD-based co-delivery of siRNA and doxorubicin to HeLa cells for reversal of multidrug resistance and real-time tracking, *Biomaterials* 33 (9) (2012) 2780–2790.
- [157] M. Beck-Broichsitter, O. M. Merkel, T. Kissel, Controlled pulmonary drug and gene delivery using polymeric nano-carriers, *J. Controlled Release* 161 (2) (2012) 214–224.
- [158] T. Endres, M. Zheng, M. Beck-Broichsitter, O. Samsonova, H. Debus, T. Kissel, Optimising the self-assembly of siRNA loaded PEG-PCL-IPEI nano-carriers employing different preparation techniques, *J. Controlled Release* 160 (3) (2012) 583–591.
- [159] S. Chen, X.-Z. Zhang, S.-X. Cheng, R.-X. Zhuo, Z.-W. Gu, Functionalized Amphiphilic Hyperbranched Polymers for Targeted Drug Delivery, *Biomacromolecules* 9 (2008) 2578–2585.
- [160] T. Endres, M. Zheng, M. Beck-Broichsitter, T. Kissel, Lyophilised ready-to-use formulations of PEG-PCL-PEI nano-carriers for siRNA delivery, *International Journal of Pharmaceutics* 428 (1-2) (2012) 121–124.
- [161] C. Xu, B. Xing, J. Rao, A self-assembled quantum dot probe for detecting beta-lactamase activity, *Biochem. Biophys. Res. Commun.* 344 (3) (2006) 931–935.
- [162] H. H. Chen, Y.-P. Ho, X. Jiang, H.-Q. Mao, T.-H. Wang, K. W. Leong, Quantitative Comparison of Intracellular Unpacking Kinetics of Polyplexes by a Model Constructed From Quantum Dot-FRET, *Mol. Ther.* 16 (2) (2008) 324–332.
- [163] C.-H. Yang, K.-S. Huang, Y.-S. Lin, K. Lu, C.-C. Tzeng, E.-C. Wang, C.-H. Lin, W.-Y. Hsu, J.-Y. Chang, Microfluidic assisted synthesis of multifunctional polycaprolactone microcapsules: incorporation of CdTe quantum dots, Fe₃O₄ superparamagnetic nanoparticles and tamoxifen anticancer drugs, *Lab Chip* 9 (2009) 961–965.
- [164] V. Bagalkot, L. Zhang, E. Levy-Nissenbaum, S. Jon, P. W. Kantoff, R. Langer, O. C. Farokhzad, Quantum Dot–Aptamer Conjugates for Synchronous Cancer Imaging, Therapy, and Sensing of Drug Delivery Based on Bi-Fluorescence Resonance Energy Transfer, *Nano Lett.* 7 (10) (2007) 3065–3070.

References

- [165] A. V. Ulasov, Y. V. Khramtsov, G. A. Trusov, A. A. Rosenkranz, E. D. Sverdlov, A. S. Sobolev, Properties of PEI-based Polyplex Nanoparticles That Correlate With Their Transfection Efficacy, *Mol. Ther.* 19 (1) (2011) 103–112.
- [166] O. Harush-Frenkel, M. Bivas-Benita, T. Nassar, C. Springer, Y. Sherman, A. Avital, Y. Altschuler, J. Borlak, S. Benita, A safety and tolerability study of differently-charged nanoparticles for local pulmonary drug delivery, *Toxicol. Appl. Pharmacol.* 246 (1-2) (2010) 83–90.
- [167] K. Sarlo, K. L. Blackburn, E. D. Clark, J. Grothaus, J. Chaney, S. Neu, J. Flood, D. Abbott, C. Bohne, K. Casey, C. Fryer, M. Kuhn, Tissue distribution of 20 nm, 100 nm and 1000 nm fluorescent polystyrene latex nanospheres following acute systemic or acute and repeat airway exposure in the rat, *Toxicology* 263 (2-3) (2009) 117–126.
- [168] M. Bivas-Benita, S. Romeijn, H. E. Junginger, G. Borchard, PLGA-PEI nanoparticles for gene delivery to pulmonary epithelium, *Eur. J. Pharm. Biopharm.* 58 (1) (2004) 1–6.
- [169] U. Griesenbach, C. Kitson, S. Garcia, R. Farley, C. Singh, L. Somerton, H. Painter, R. Smith, D. Gill, S. Hyde, Y.-H. Chow, J. Hu, M. Gray, M. Edbrooke, V. Ogilvie, G. MacGregor, R. Scheule, S. Cheng, N. Caplen, E. Alton, Inefficient cationic lipid-mediated siRNA and antisense oligonucleotide transfer to airway epithelial cells in vivo, *Respiratory Research* 7 (1) (2006) 26.
- [170] H. H. Chen, Y.-P. Ho, X. Jiang, H.-Q. Mao, T.-H. Wang, , K. W. Leong, Simultaneous Non-invasive Analysis of DNA Condensation and Stability by Two-step QD-FRET, *Nano Today* 4 (2) (2009) 135–134.
- [171] R. Weissleder, C.-H. Tung, U. Mahmood, A. Bogdanov, In vivo imaging of tumors with protease-activated near-infrared fluorescent probes, *Nat. Biotechnol.* 17 (4) (1999) 375–378.
- [172] C. Bremer, C.-H. Tung, R. Weissleder, In vivo molecular target assessment of matrix metalloproteinase inhibition, *Nat. Med.* 7 (6) (2001) 743–748.
- [173] A. M. Derfus, A. A. Chen, D.-H. Min, E. Ruoslahti, S. N. Bhatia, Targeted Quantum Dot Conjugates for siRNA Delivery, *Bioconjugate Chem.* 18 (5) (2009) 1391–1396.
- [174] R. Freeman, R. Gill, I. Shweky, M. Kotler, U. Banin, I. Willner, Biosensing and Probing of Intracellular Metabolic Pathways by NADH-Sensitive Quantum Dots, *Angew. Chem., Int. Ed.* 48 (2) (2009) 309–313.
- [175] I. L. Medintz, A. R. Clapp, H. Mattoussi, E. R. Goldman, B. Fisher, J. M. Mauro, Self-assembled nanoscale biosensors based on quantum dot FRET donors, *Nat. Mater.* 2 (9) (2003) 630–638.
- [176] C. Liu, P. Zhang, X. Zhai, F. Tian, W. Li, J. Yang, Y. Liu, H. Wang, W. Wang, W. Liu, Nano-carrier for gene delivery and bioimaging based on carbon dots

References

- with PEI-passivation enhanced fluorescence, *Biomaterials* 33 (13) (2012) 3604–3613.
- [177] J.-M. Li, M.-X. Zhao, H. Su, Y.-Y. Wang, C.-P. Tan, L.-N. Ji, Z.-W. Mao, Multifunctional quantum-dot-based siRNA delivery for HPV18 E6 gene silencing and intracellular imaging, *Biomaterials* 32 (31) (2011) 7978–7987.
- [178] S. Li, Z. Liu, F. Ji, Z. Xiao, M. Wang, Y. Peng, Y. Zhang, L. Liu, Z. Liang, F. Li, Delivery of Quantum Dot-siRNA Nanoplexes in SK-N-SH Cells for BACE1 Gene Silencing and Intracellular Imaging, *Mol. Ther.* 1 (2012) 1–10.
- [179] J. S. Kim, K. J. Cho, T. H. Tran, M. Nurunnabi, T. H. Moon, S. M. Hong, Y. kyu Lee, In vivo NIR imaging with CdTe/CdSe quantum dots entrapped in PLGA nanospheres, *J. Colloid Interface Sci.* 353 (2) (2011) 363–371.
- [180] Y.-K. Lee, S. M. Hong, J. S. Kim, Encapsulation of CdSe/ZnS Quantum Dots in Poly(ethylene glycol)-Poly(D,L-lactide) Micelle for Biomedical Imaging and Detection, *Macromol. Res.* 15 (4) (2007) 330–336.
- [181] L. Liu, K.-T. Yong, I. Roy, W.-C. Law, L. Ye, J. Liu, J. Liu, R. Kumar, X. Zhang, P. N. Prasad, Bioconjugated Pluronic Triblock-Copolymer Micelle-Encapsulated Quantum Dots for Targeted Imaging of Cancer: In Vitro and In Vivo Studies, *Theranostics* 2 (7) (2012) 705–713.
- [182] M. Wang, M. Zhang, J. Li, S. Kumar, G. C. Walker, G. D. Scholes, M. A. Winnik, Self-Assembly of Colloidal Quantum Dots on the Scaffold of Triblock Copolymer Micelles, *ACS Appl. Mater. Interfaces* 2 (11) (2010) 3160–3169.

Appendices

List of figures

I.1	Vector mediated internalization of DNA	10
I.2	Steps in the RNAi process	12
I.3	Schematic illustration of the EPR effect	14
I.4	Schematic illustration of the proton sponge mechanism	16
I.5	Charge of cationic carrier upon complexation with siRNA as a function of N/P	18
I.6	Structures of commonly used homopolymer gene delivery vehicles	21
I.7	Micellisation model for an amphiphilic AB-diblock copolymer . .	28
I.8	Exemplaric illustration of FRET switching functionality	31
II.1	PEG-PCL-PEI synthesis in three steps	45
II.2	DSC thermograms of mPEG5k and mPCL10k homopolymers in comparison to mPEG5k-PCL10k diblock copolymer	47
II.3	¹ H NMR spectra of mPEG500-PCL10000 (A), mPEG500-PCL10000-linker (B) and mPEG500-PCL10k-IPEI2500 (C)	48
II.4	IR spectra of mPEG500-PCL2400 (A) and mPEG500-PCL2400-IPEI2500 (B)	49
II.5	Block copolymer composition by % (A) and MW (B)	50
II.6	CryoSEM images of PEG500-PCL10k-IPEI2500 carriers (A); AFM images in the liquid state of PEG500-PCL10k-IPEI2500 (B), PEG2k-PCL10k-IPEI2500 (C) and PEG5k-PCL10k-IPEI2500 (D) carriers	51
II.7	Carrier size as a function of initial polymer concentration in the organic phase during solvent displacement process	52
II.8	FALT-measurements: PEG shell thickness (A); dimensional sketch of carriers assembled from polymers bearing different PEG MWs (B)	53
II.9	¹ H NMR spectra of PEG5k-PCL10k-IPEI2500 dissolved in acetone-D ₆ (A) in comparison to carriers of the same polymer suspended in D ₂ O/acetone-D ₆ mixtures (B-F)	55
II.10	Temperature dependent ¹ H NMR spectra of PEG5k-PCL10k-IPEI2500 carriers suspended in D ₂ O	56
II.11	Size difference of mPEG5k-PCL10k-IPEI2500 carriers in comparison to mPCL10k particles as a function of T	57
II.12	Stability against NaCl (A) and albumin (B); values presented as means from at least three measurements ± standard deviation . .	58
II.13	Hydrodynamic diameter (A) and PDI (B) of nano-carriers with different PEG shell thickness as a function of NaCl concentration	58
II.14	Hydrodynamic diameter (A), PDI (B) and ζ-potential of nano-carriers with different PEG shell thickness as a function of albumin concentration	59

Appendices

II.15	CMC determination of hydrophilic copolymers mPEG500-PCL2400-IPEI2500 (A), mPEG2k-PCL2400-IPEI2500 (B) and mPEG5k-PCL10k-IPEI2500 (C)	60
II.16	Cytotoxicity of polymers bearing different PEG MWs in comparison to IPEI2500	61
III.1	CryoTEM images of blank carriers (A). Z-ave. and ζ -potential of loaded carriers (B)	76
III.2	Setup of the microfluidic mixing device (A). Microscope image of the mixing chip (B)	78
III.3	Z-ave. (A) and PDI (B) of unloaded carriers in comparison to those loaded with siRNA by different techniques at defined N/P ratios.	79
III.4	Z-ave. of carriers loaded via T1 (classical pipetting) and T2 (microfluidic mixing) at previously evaluated N/P ratios using three different siRNA concentrations (A). Detailed size distribution at N/P=9 using $c(\text{RNA})=100 \mu\text{M}$ (B).	80
III.5	z-ave and PDI after incubation in water	81
III.6	z-ave and PDI after incubation in bovine serum	82
III.7	Accessible siRNA concentration of carriers loaded via T1 (classical pipetting) and T2 (microfluidic mixing) at previously evaluated N/P ratios using three different siRNA concentrations . . .	83
III.8	Recovery of siRNA after RNase digestion.	83
III.9	Carriers were assembled via T1 (classical pipetting) and T2 (microfluidic mixing). Amount of recovered siRNA after incubation with RNase and different concentrations of heparin (A). Transfection efficiency <i>in vitro</i> (SKOV3 cells) was determined by RT-PCR. (B)	84
III.10	Standardised Pareto chart (A); main effect plots (B)	87
III.11	Surface plots	88
III.12	Surface plots	88
III.13	Surface plots	89
IV.1	Ratio of final and initial (f/i) z-ave and PDI of nano-carriers, lyophilised as a function of c_{glc} (A). Cryo-SEM images of freshly-prepared (B) and rehydrated (C) nano-carriers.	96
IV.2	Organisation chart of different formulation strategies (A); z-ave and PDI of carriers loaded at various N/P ratios and lyophilised by different strategies	98
IV.3	Transfection efficiency was determined <i>in vitro</i> by RT-PCR. Freshly-prepared complexes were compared to ones assembled after (L1) and before (L2) lyophilisation.	99
V.1	<i>In vitro</i> cell uptake of nano-complexes with different PEG shell-thickness determined by flow cytometry	111
V.2	A: <i>In vitro</i> and <i>in vivo</i> knockdown efficiency of nano-complexes with different PEG moiety; B: Fluorescence microscopy image of lung tissue instilled with carrier complexes from PEG500-PCL10,000-PEI2500 carriers and AF-siRNA after lavage	112

Appendices

V.3	Schematic illustration of the self-assembly and complexation procedure of QD-loaded nano-carriers by the solvent displacement method.	115
V.4	Fluorescence emission spectra of QD-loaded nano-carriers, complexed with various amounts of AF-siRNA	117
V.5	Microscope image of QD-FRET complexes in SKOV3 cells; λ_{ex} : 405 nm; DAPI stained nuclei in blue; QD emission in green; Red FRET-induced AF emission proves complex integrity; orange colour indicates colocalisation.	118
V.6	A: The amount of siRNA displacement from the complex as a function of the competing polyanion heparin; B: Representative fluorescence spectrum of FRET-complexes before and after displacement with heparin	119

List of tables

I.1	Literature overview of amphiphilic block copolymers used in drug- and gene-delivery	24
II.1	Composition of block copolymers with different hydrophilicity along with hydrodynamic diameters and PDIs	47
II.2	Shell thickness values of carriers with different PEG block length in comparison to calculated values and electrochemical characteristics	54
II.3	CMC and ΔG° values	60
III.1	Investigated factors and levels of the central composite design . .	86
IV.1	Ratio of final and initial (f/i) z-ave and PDI of complexes lyophilised (L2) at two different N/P ratios (10 and 20) as a function of c_{glc}	99
V.1	Z-ave. and PDI of nano-carriers, loaded with various amounts of QDs	116

List of commonly used abbreviations

a	<i>annum</i>
AF	Alexa Fluor
AFM	atomic force microscope
bPEI	branched PEI
BSA	bovine serum albumin
CMC	critical micelle concentration
c_p	heat flow capacity
cryoSEM	cryogenic scanning electron microscope
cryoTEM	cryogenic transmission electron microscope
d	<i>dies</i>
D	polydispersity
Da	Dalton
DAPI	4',6-diamidino-2-phenylindole
DLS	dynamic light scattering
DMAc	N,N-Dimethylacetamide
DMEM	Dulbecco's modified eagle's medium
DNA	deoxyribonucleic acid
DSC	differential scanning calorimetry
d_{shell}	PEG shell thickness determined via FALT
EGF	epidermal growth factor
EPR	enhanced permeation and retention
ϵ CL	ϵ -Caprolactone
ex	excitation
eq	stoichiometric equivalent
em	emission
f/i	ratio of final to initial z-ave.
FALT	fixed aqueous layer thickness
FCS	fetal calf serum
FR	flow rate
FRET	fluorescence (or Förster) resonance energy transfer
FT-IR	fourier transform infrared
G°	free energy
$\times g$	relative centrifugal force in multiples of gravitational acceleration
glc	glucose
GPC	gel permeation chromatography
h	hour
IC50	half minimal (50%) inhibitory concentration
k	Boltzmann constant
κ^{-1}	Debye length
λ	wavelength
LCST	lower critical solution temperature
LDA	laser doppler anemometry
LF	Lipofectamine TM

Appendices

IPEI	linear PEI
M	mol·L ⁻¹
\bar{M}_n	number average molecular weight
\bar{M}_w	weight average molecular weight
mPCL	monomethyl PCL
mPEG	monomethyl PEG
mRNA	messenger RNA
MTT	3-(4,5-dimethylthiazol-2-yl)-2,5-diphenyl tetrazolium bromide
MW	molecular weight
N/P	nitrogen per phosphate ratio
NIR	near infrared
NMR	nuclear magnetic resonance
NP	nanoparticle
NS	nanosuspension
ν	wave number
PAMAM	poly(amidoamine)
PCL	poly- ϵ -caprolactone
PCR	polymerase chain reaction
PDI	particle polydispersity index
pDMAEMA	poly((2-dimethylamino)ethyl methacrylate)
pDNA	plasmid DNA
PEG	polyethyleneglycol
PEI	polyethyleneimine
PLA	poly(lactic acid)
PLGA	poly(lactic-co-glycolic acid)
PPEEA	poly(2-aminoethyl ethylene phosphate)
ppm	parts per million
PS	polystyrene
Ψ_0	surface potential
QD	quantum dot
qRT-PCR	quantitative real-time-PCR
R	universal gas constant
R_g	radius of gyration
RISC	RNA-induced silencing complex
RNA	ribonucleic acid
RNAi	RNA interference
rpm	revolutions per minute
RT	room temperature
RT-PCR	real-time-PCR
σ_0	surface charge density
siRNA	small interfering RNA
SKOV3	folate receptor-positive SKOV3 ovarian carcinoma cells
Sn(Oct) ₂	Tin(II)-ethylhexanoate
T	temperature
T _g	glass transition temperature

Appendices

THF	Tetrahydrofuran
T_m	melting temperature
z-ave.	particle mean diameter
ζ	zeta-potential

List of publications

- ◇ T. Endres, M. Beck-Broichsitter, O. Samsonova, T. Renette, T. Kissel, Self-assembled biodegradable amphiphilic PEG-PCL-IPEI triblock copolymers at the borderline between micelles and nanoparticles designed for drug and gene delivery, *Biomaterials* 32 (2011), 7721–7731.
- ◇ T. Endres, M. Zheng, M. Beck-Broichsitter, O. Samsonova, H. Debus, T. Kissel, Optimising the self-assembly of siRNA loaded PEG-PCL-IPEI nano-carriers employing different preparation techniques, *J. Controlled Release* 160 (3), 583–591.
- ◇ T. Endres, M. Zheng, M. Beck-Broichsitter, T. Kissel, Lyophilised ready-to-use formulations of PEG-PCL-PEI nano-carriers for siRNA delivery, *Int. J. Pharm* 428 (1-2) (2012), 121–124.
- ◇ M. Zheng, Y. Liu, O. Samsonova, T. Endres, O. Merkel, T. Kissel, Amphiphilic and biodegradable hy-PEI-g-PCL-b-PEG copolymers efficiently mediate trans-gene expression depending on their graft density, *Int. J. Pharm.*, 427 (1) (2011) 80-87.
- ◇ T. Renette, D. Librizzi, T. Endres, O. Merkel, M. Beck-Broichsitter, N. Bege, H. Petersen, C. Curdy, T. Kissel, Poly(ethylene carbonate) Nanoparticles as Carrier System for Chemotherapy Showing Prolonged *in vivo* Circulation and Anti-Tumor Efficacy, *Macromol. Biosci.* 12 (7) (2012), 970-978.

In a nutshell

The great promise that gene therapy holds is the opportunity of directly introducing genetic material into cells for a causal therapy of yet incurable diseases. One promising way to achieve that goal is the usage of non-viral delivery vehicles, constructed from amphiphilic block copolymers.

This thesis presents the establishment of a multifunctional PEG-PCL-PEI block copolymer platform, designed for multifunctional gene delivery. Across the scientific disciplines of chemistry, chemical physics, pharmacy and biomedicine the underlying work covers all aspects of non-viral gene delivery:

In a first step, block copolymers were synthesised and characterised. In a systematic approach a library of compounds with varying hydrophilic/hydrophobic ratio was established. Subsequently, polymers were assembled into gene carriers followed by a non-invasive structural characterisation. Most importantly it was noticed, that polymers hydrophilic in nature formed smaller micelle-like carriers, whereas hydrophobic polymers aggregated to larger particle-like assemblies. In that vein, carrier features such as colloidal stability and toxicity were found to depend on chemical composition.

Second, the nucleic acid loading process was optimised. Herein it was the overall goal to manufacture compactly condensed carrier complexes by understanding the basic principles of the electrostatic loading procedure. It was hypothesised that a more homogeneous fusion of charges is supposed to lead to superior carrier complexes. In that line, a microfluidic mixing technique, bringing cationic polymer and nucleic acid together at a constant ratio during the entire mixing process, was found to be the most promising technique. Ultimately, gene delivery carriers with superior colloidal stability, RNA protection and transfection efficiency were manufactured and process parameters were optimised with the help of a central composite design.

Third, as a prerequisite for effective *in vivo* usage, carriers were transferred into stable ready-to-use formulations by lyophilisation with the help of glucose as a lyoprotectant. Unloaded nano-suspensions could be restored after rehydration by addition of small amounts of glucose. Upon loading of those rehydrated carriers, no significant difference in complex size or transfection efficiency was observed as compared to freshly-prepared ones. Moreover, the stabilisation of pre-formed carrier/siRNA complexes is feasible at elevated N/P and higher glucose concentrations.

Fourth, most promising carriers were tested for their *in vitro* and *in vivo* transfection efficiency. Vectors constructed from rather hydrophobic block copolymers showed superior transfection efficiency, whereas poor performance was found in case of predominantly hydrophilic ones in a good correlation *in vitro* and *in vivo*. FACS studies revealed that this might possibly be due to reduced cell uptake of carriers with thicker PEG shell preventing cell interaction. In that way a yet active vector with diminished toxicity as compared to PEI homopolymers was evaluated. Fluorescent microscopy images of murine lung tissue revealed emission predominantly in the alveolar region, rendering this carrier system as promising for local treatment of airway diseases.

Finally, the feasibility of multifunctional carrier co-loading and FRET-monitored nucleic acid unpacking was approved. Double-labelled nano-carriers emitted light at

the acceptor's emission wavelength upon donor excitation, proving successful FRET-effect and hence, complex integrity. The ability of dual loading is especially useful for "theranostic" purposes or co-delivery of nucleic acids and drugs. FRET-switching functionality may be advantageous for monitoring complex stability and nucleic acid unpacking.

In view of prospective experiments, to circumvent the observed charge-toxicity-relationship, carriers are supposed to be taken up by the target tissue in a selective way. This can be achieved, up to a certain degree, via targeting ligands. Rather hydrophilic carriers with thicker PEG shells, increased colloidal stability and reduced toxicity represent the ideal candidates for this modification.

In the long term, required work is evident: the development of more effective non-viral vectors and conquering the yet severe toxicity effects of current delivery systems. By a deeper understanding in the mechanistic aspects of the gene delivery process plus a rational vector design we are on the right track to achieve that goal.

Übersicht

Im Gegensatz zu einer symptomatischen Behandlung schwerwiegender Erkrankungen ermöglicht die Gentherapie einen kausalen Therapieansatz durch direkte Manipulation genetischen Materials. Eines der vielversprechendsten Trägersysteme zur Realisierung dieser Zielsetzung setzt sich aus amphiphilen Blockcopolymeren zusammen.

Gegenstand der vorliegenden Dissertation ist die Etablierung eines multifunktionalen PEG-PCL-PEI Blockcopolymer-Trägersystems für die Gentherapie. Hierfür erforderte das an der Schnittstelle unterschiedlichster wissenschaftlicher Disziplinen angesiedelte Thema fächerübergreifendes Arbeiten, um den chemischen, physikochemischen, pharmazeutischen und biomedizinischen Aspekten der Aufgabenstellung in vollem Umfang gerecht zu werden:

Der erste Schritt umfasste den Aufbau einer Vektorbibliothek aus PEG-PCL-PEI Blockcopolymeren. Das Verhältnis aus hydrophilen und hydrophoben Kettensegmenten wurde hierbei systematisch variiert. Anschließend wurden die Blockcopolymeren zu Trägern verarbeitet und deren Aufbau wurde mittels nicht-invasiver Methoden charakterisiert. Hierbei wurde beobachtet, dass sich überwiegend hydrophile Polymere zu kleineren, mizellartigen Trägern formierten, während eher hydrophobe Ketten zu größeren, partikelartigen Vektoren aggregierten. Die Erforschung eines Zusammenhangs zwischen Polymerzusammensetzung und den Eigenschaften der Träger (Kolloidstabilität und Toxizität) ermöglichte die selektive Auswahl repräsentativer Polymere einer jeden Vektorklasse.

Zweitens: Der Prozess der Selbstorganisation von Polymeren zu Trägern und deren Beladung mit Nucleinsäuren wurde erforscht und optimiert. Im Rahmen dieser Arbeiten war das Ziel die Grundzüge des elektrostatischen Ladungsprozesses besser zu verstehen und mit Hilfe dieser Erkenntnisse kompakte Nanokomplexe zu generieren. Dieses Kapitel basiert auf der Hypothese, dass ein gleichmäßigerer Komplexierungsvorgang zu einer homogeneren Verteilung von Ladungen und folglich zu Trägerkomplexen mit verbesserten Eigenschaften führen sollte. Folglich kristallisierte sich eine microfluidale Herstellungstechnik, bei der Träger und RNA während des

gesamten Herstellungsprozesses gleichmäßig zusammengeführt werden, als die am besten geeignete Beladungsmethode heraus. Durch diese Technik wurden Komplexe mit verbesserter Kolloidstabilität, RNA-Einbettung und letztendlich auch Transfektionseffizienz erzielt. Die Prozessparameter wurden anschließend im Rahmen eines statistischen Designs im Detail untersucht.

Drittens: Die Überführung von Nanoträgern in eine lagerstabile, trockene Form, stellt eine der Grundvoraussetzungen für die effektive Nutzung *in vivo* dar. Im Zuge der Untersuchungen wurden frisch hergestellte Trägersuspensionen unter Zugabe des Lyoprotektors Glucose gefriergetrocknet. Bereits durch geringe Glucosekonzentrationen konnten die Eigenschaften unbeladener Träger nach Rehydrierung wiederhergestellt werden. Bei anschließender Beladung mit siRNA wurde im Vergleich zu frischen Trägern kein Unterschied bezüglich der Komplexgröße, der Größenverteilung oder der Transfektionseffizienz detektiert. Darüber hinaus gelingt die Trocknung bereits beladener Trägerkomplexe bei erhöhten N/P-Verhältnissen sowie höheren Glucosekonzentrationen.

Viertens: Die vielversprechendsten Träger sollten nun auf ihre Transfektionsaktivität hin untersucht werden. In guter Übereinstimmung der Ergebnisse *in vitro* und *in vivo* wurde bei hydrophoben Trägern eine hohe Transfektionseffizienz ermittelt, wohingegen bei hydrophilen Vektoren kaum Aktivität detektiert wurde. Die Ergebnisse der FACS-Analyse zeigten, dass die geringe Aktivität hydrophiler Vektoren durch mangelnde zelluläre Wechselwirkung, höchstwahrscheinlich bedingt durch eine dickere PEG-Hülle, verursacht wird. Im Zuge dieser Arbeiten wurde folglich eine Verbindung ausgewählt, welche sich durch gute Transfektionseffizienz bei gleichzeitig geringerer Toxizität (im Vergleich zu PEI-Homopolymeren) auszeichnet. Fluoreszenzmikroskopische Aufnahmen des Lungengewebes untersuchter Mäuse zeigten vorrangig Emission im Alveolargewebe. Dieses Ergebnis prädestiniert das etablierte Trägersystem für eine zukünftige Anwendung zur lokalen Therapie von Lungenerkrankungen.

Schließlich wurde die Möglichkeit einer doppelten Fluoreszenzmarkierung von Trägerkomplexen untersucht. Durch Beladung des hydrophoben PCL-Kerns mit Quantenpunkten gefolgt von der Komplexierung mit fluoreszenzmarkierter siRNA wurde ein FRET-Paar etabliert, welches sich hervorragend zur Detektion der Komplexintegrität eignet. Die auf diese Weise doppelt markierten Träger zeichneten sich durch Emission von Licht der Wellenlänge des Akzeptors bei Anregung des Donors aus. Sie lieferten damit den Beweis für den Energietransfer im intakten FRET-Komplex. Es wurde folglich ein multifunktionales und biologisch aktives Vektorsystem geschaffen, welches sich hervorragend für theragnostische Zwecke oder für eine simultane Verabreichung von Nucleinsäuren und Wirkstoffen eignet. Der FRET-induzierte Schalteffekt ermöglicht eine Echtzeituntersuchung von Komplexstabilität und Entladevorgang.

Ein Durchbrechen des Zusammenhangs zwischen Ladung, Aktivität und Toxizität ist die wohl wichtigste Herausforderung zukünftiger Arbeiten. Dies könnte durch eine Erhöhung der Selektivität des Trägersystems im Zuge der Einführung von geeigneten Rezeptoren gelingen. Hydrophile Träger mit dicker PEG-Hülle, erhöhter Kolloidstabilität und geringer Toxizität wären die idealen Kandidaten für eine derartige Modifikation.

Appendices

Das Langzeitziel bei der Erforschung nicht-viraler Vektoren ist klar: Die Effektivität von Vektoren muss gesteigert, die Toxizität verringert werden. Durch rationales Vektordesign, welches wiederum systematische und intensive Grundlagenforschung bedingt, ist zu erhoffen, dass zukünftig sichere und effektive Trägersysteme zur kausalen Therapie gegenwärtig als unheilbar klassifizierter Krankheiten entwickelt werden können.

Curriculum vitæ

PERSÖNLICHE DATEN

<i>Geburtsdatum</i>	30.04.1982
<i>Geburtsort</i>	Dettelbach
<i>Staatsangehörigkeit</i>	deutsch
<i>Familienstand</i>	ledig
<i>Vater</i>	Dr. Josef Endres
<i>Mutter</i>	Christiane Endres (geb. Reinlein)

BERUFLICHER WERDEGANG

<i>Ab Feb 2012</i>	Evonik Industries Darmstadt Projektmanager im Bereich der Produktentwicklung von Pharma Polymeren
--------------------	--

SCHULISCHE AUSBILDUNG/STUDIUM/PROMOTION

<i>Jan 2009 - Feb 2012</i>	Institut für Pharm. Technologie und Biopharmazie Philipps-Universität Marburg Promotion
<i>Okt 2003 - Nov 2009</i>	Philipps-Universität Marburg Studium der Chemie Schwerpunkt: Polymerchemie Diplom
<i>Sep 1993 - Jun 2002</i>	Armin-Knab-Gymnasium Kitzingen Allgemeine Hochschulreife

GRUNDWEHRDIENST

<i>Jul 2002 - Mär 2003</i>	1./s Pionierbataillon Volkach
----------------------------	--------------------------------------

Marburg, 16.10.2012

Thomas Endres

Danksagung

An dieser Stelle möchte ich all jenen danken, die mich bei der Durchführung und Erstellung dieser Arbeit unterstützt haben.

Vor allem danke ich meinem Doktorvater Herrn Prof. Kissel für die interessante Aufgabenstellung, fachliche Anregungen und eine kompetente Unterstützung in allen Phasen dieser Arbeit. Seine hilfreichen Ideen, die Anregungen zu interdisziplinärem Arbeiten wie auch unsere interessanten und motivierenden Diskussionen haben zu großen Teilen zum Gelingen dieser Arbeit beigetragen.

Herrn Prof. Culmsee bin ich für die Übernahme des Vorsitzes der Prüfungskommission und seine Funktion als Nebenfachprüfer zu Dank verpflichtet.

Ebenso danke ich Herrn Prof. Kuschinsky für seine Rolle als Nebenfachprüfer, Herrn Prof. Greiner für die Übernahme der Funktion eines Nebenfachprüfer wie auch für die Erstellung des Zweitgutachtens.

Mein besonderer Dank geht an Dr. Moritz Beck-Broichsitter für interessante Diskussionen und Ideen.

Außerdem möchte ich mich bei Mengyao Zheng und Olga Samsonova für die Unterstützung bei Experimenten an biologischen Systemen bedanken.

Abschließend danke ich retrospektiv dem gesamten Arbeitskreis Kissel für eine inspirative und freundliche Atmosphäre. Es war mir zu jedem Zeitpunkt der vergangenen Jahre stets eine Freude, Teil dieser Arbeitsgruppe zu sein.

Erklärung

Ich versichere, dass ich meine Dissertation

”Biodegradable amphiphilic PEG-PCL-PEI
triblock copolymers designed for the self-assembly
of multifunctional gene carriers”

selbständig ohne unerlaubte Hilfe angefertigt und mich dabei keiner anderen als der von mir ausdrücklich gekennzeichneten Quellen bedient habe. Zu keinem Zeitpunkt wurde die vorliegende Arbeit in ihrer jetzigen oder einer ähnlichen Form bei einer anderen Hochschule eingereicht oder zu Prüfungszwecken verwendet.

Marburg, 16.10.2012

Thomas Endres